



U. Grundmann, U. Rohde,
S. Mittag, S. Kliem

DYN3D Version 3.2

Code for Calculation of Transients in
Light Water Reactors (LWR) with Hexagonal
or Quadratic Fuel Elements

- Description of Models and Methods -



Wissenschaftlich-Technische Berichte
FZR-434
August 2005

U. Grundmann, U. Rohde,
S. Mittag, S. Kliem

DYN3D Version 3.2

Code for Calculation of Transients in
Light Water Reactors (LWR) with Hexagonal
or Quadratic Fuel Elements

- Description of Models and Methods -

Bibliothek FZ Rossendorf



01288131



Forschungszentrum
Rossendorf

DYN3D Version 3.2

Code for Calculation of Transients in Light Water Reactors (LWR)

with Hexagonal or Quadratic Fuel Elements

- Description of Models and Methods -

U. Grundmann, U. Rohde, S. Mittag, S. Kliem

August 2005

Institute of Safety Research

NOTICE

The Code Documentation is associated to the DYN3D computer code. All sections of this documentation, like DYN3D itself, are protected as intellectual property of FZR. Any duplication or distribution, if complete or in part, are subject to the prior and express consent of FZR. Statements made within the documentation may be altered by FZR at any time.

FZR does not assume any liability or responsibility for damages arising out of the use of the Code Documentation.

The use of DYN3D will be licensed subject to the provisions of a Software License Agreement and shall be restricted to research and development in the field of reactor safety for peaceful purposes.

Abstract

DYN3D is a best estimate advanced code for the three-dimensional simulation of steady-states and transients in light water reactor cores with quadratic and hexagonal fuel assemblies. Burnup and poison-dynamic calculations can be performed. For the investigation of a wide range of transients, DYN3D is coupled with thermal-hydraulic system codes as ATHLET and RELAP5.

The neutron kinetic model is based on the solution of the three-dimensional two-group neutron diffusion equation by nodal expansion methods. The thermal-hydraulics comprises a one- or two-phase coolant flow model on the basis of four differential balance equations for mass, energy and momentum of the two-phase mixture and the mass balance for the vapour phase. Various cross section libraries are linked with DYN3D.

Systematic code validation is performed by FZR and independent organizations. A list of validation calculations is included.

Acknowledgements

The authors thank J. Hádek for his contribution to the development of the hexagonal flux reconstruction, E. Laggiard for the development of the decay heat model, D. Lucas for providing the algorithm of the PIC method and A. Manera for the improvement of the pressure drop/mass flow iteration.

Content

1	Introduction	3
2	Neutron Kinetics	5
2.1	Neutron Diffusion Equations	5
2.2	Homogeneous Steady State	8
2.2.1	Equations for the Node Averaged Fluxes	8
2.2.2	Nodal Expansion for Hexagonal-z Geometry	9
2.2.3	Nodal Expansion for Cartesian Geometry	19
2.2.4	Boundary Conditions	20
2.2.5	Assembly Discontinuity Factors (ADF)	23
2.3	Steady-State Case with External Source	26
2.4	Transient Case	26
2.6	The Poisoning in the Steady State	29
2.7	Nodal Flux Reconstruction	30
2.8	Reactivity Calculation and Adjoint Flux	35
2.8.1	Dynamic Reactivity	35
2.8.2	Adjoint Flux as Weighting Function	37
2.8.3	Calculation of the Different Reactivity Contributions	41
2.8.4	Calculation of Reactivity by Inverse Point Kinetics	41
	References Chapter 2	43
3	Treatment of Two-Group Neutronic Data	45
3.1	General Handling of Neutronic Data in DYN3D	45
3.2	Data Libraries for a KWU Konvoi Reactor	45
3.3	Parametrized Data Libraries for VVER Reactors	48
3.4	Multi-Dimensional-Table Libraries	49
3.5	Approximation-and-Interpolation Libraries	49
	References Chapter 3	52
4	Control Rod Description	53
4.1	Homogeneous Control Rods	53
4.2	Control Rods Consisting of Two or More Axial Segments	53
4.3	Control Assemblies in Russian VVER-440	54
5	Core Thermo-Hydraulics Model	55
5.1	Basic Assumptions and Equations	55
5.1.1	Basic Equations in Conservative Form	57
5.2	Constitutive Relations in the Thermo-Hydraulics Model	59
5.2.1	Hydraulics	59
5.2.2	Heat Transfer	60
5.2.3	Boiling Model	66
5.2.4	Thermo-physical Properties of Water and Steam	67
5.3	Core Thermohydraulic Boundary Conditions	68
5.4	Hot Channel Treatment	70
5.5	VVER-440 Coolant Mixing Model	71
5.6	Numerical Methods and Iterative Procedures in Thermohydraulics	77
5.6.1	Numerical Solution of the Energy and Vapour Mass Balance Equations	77

5.6.2	Numerical solution of the mass and momentum balance equations	79
5.6.3	Solution of the Boron Transport Equation	81
5.6.4	Iterative Procedures	86
	References Chapter 5	89
6	Fuel Rod Model	92
6.1	Fuel and Cladding Temperature Estimation.....	92
6.2	Thermo-physical Properties of Fuel and Cladding	92
6.3	Gas Gap Conductance	93
6.4	Thermo-mechanical Model	94
6.5	Fuel Rod Failure Estimation	96
6.6	Numerical methods for fuel rod behaviour calculations	97
6.7	Input data for the fuel rod model	97
	References Chapter 6	98
7	Neutron Kinetics - Thermal-Hydraulics Iterations and Time Step Control	99
7.1	Steady-State Iteration	100
7.2	Transient Iteration	101
8	Burnup Calculation	105
9	Reactor-Poison Dynamics	107
9.1	Xenon and Iodine	107
9.2	Promethium and Samarium	108
	References Chapter 9	109
10	Decay Heat Model	110
10.1	Basic Assumptions	110
10.2	Decay Heat Power Equations	110
	References Chapter 10	114
11	Coupling with Thermo-Hydraulic System Codes	115
11.1	Coupling DYN3D - ATHLET	115
11.1.1	Internal coupling	115
11.1.2	External coupling	117
11.1.3	Parallel coupling	118
11.1.4	Use of the different types of coupling	120
11.2	Coupling DYN3D - RELAP5	122
12	Verification and Validation of DYN3D and the Coupled Code DYN3D/ATHLET	124
12.1	Steady-State Problems	124
12.2	Transient Problems	124
	References Chapter 12	125
	List of Variables in Neutron Kinetics	129
	List of Variables in Thermal Hydraulics	138

1 Introduction

DYN3D is a **DY**Namical **3-D**imensional code for thermal reactor cores. The described versions 3.x of DYN3D are written in FORTRAN90. The three-dimensional neutronic model utilize nodal expansion methods (NEM) to solve the two-group neutron diffusion equation for Cartesian and hexagonal-z geometry. The steady-state with eigenvalue, the steady state with fixed source, the adjoint flux distribution, and the transient behaviour can be calculated. The core is divided in axial layers. The nodes are the parts of the fuel assemblies in the layers. Considering the Cartesian geometry each assembly can be subdivided in the radial direction by an even number of nodes.

Assembly discontinuity factors (ADF) can be taken into account for correction of homogenization errors. A flux reconstruction can be performed for chosen assemblies to calculate powers at given positions in the assembly. It can be used for hot channel calculation. Cross section libraries generated by different cell codes as CASMO, HELIOS or NESSEL are linked to DYN3D.

The thermal-hydraulic model of DYN3D is based on the solution of a four equation model for the two phase flow in parallel coolant channels. The balance equations for mass, momentum and energy of the mixture and the mass balance of the vapour phase are considered. Each coolant channel represents one or several fuel assemblies corresponding to the mapping scheme given by input. Additional hot channels can be considered which have no influence on the neutronic properties. One fuel pin belongs to each channel. The assembly feedback in an axial layer is calculated from the fuel and coolant properties of the coolant channel. Thermal-hydraulic boundary conditions for the core like coolant inlet temperature, pressure, coolant mass flow rate or pressure drop must be given as input for DYN3D.

Depletion calculations can be performed to determine the starting point of the transient. Steady state concentrations of the reactor poisons can be calculated. The transient behaviour of Xe and Sm can be analyzed. The decay heat can be taken into account based on power history and during the transient.

The neutron kinetic model is based on the solution of the three-dimensional two-group neutron diffusion equation by nodal expansion methods. It is assumed that the macroscopic cross sections are spatially constant in a node. Concerning Cartesian geometry three one-dimensional diffusion equations are solved for the transverse integrated fluxes of the nodes in the three directions x, y, z. In the case of hexagonal-z geometry, a two-dimensional diffusion equation in the hexagonal plane and a one-dimensional equation of the z-direction are solved for the transverse integrated fluxes. In each energy group, the one-dimensional equations are solved with the help of flux expansions in polynomials up to 2nd order and exponential functions being the solutions of the homogeneous equations. The fission source in the fast group and the scattering source in the thermal group as well as the leakage terms are approximated by the polynomials. Considering the 2-dimensional equation in the hexagonal plane, the side averaged values (HEXNEM1) or the side averaged and the corner point values (HEXNEM2) of flux and current are used for the coupling of nodes in the radial direction. In the steady state, the homogeneous eigenvalue problem or the heterogeneous problem with given source is solved. An inner and outer iteration strategy is applied. The outer iteration (fission source iteration) is accelerated by Chebychev extrapolation.

The steady-state iteration technique is applied for the calculation of the initial critical state, the depletion calculations and the Xe and Sm dynamics.

Concerning reactivity transients an implicit difference scheme with exponential transformation is used for the time integration over the neutronic time step. The exponents in each node are calculated from the previous time step or during the iteration process. The precursor equations are analytically solved, assuming the fission rate behaves exponential over the time step. The heterogeneous equations obtained for each time step are solved by an inner and outer iteration technique similar to the steady state.

Regarding thermal hydraulics the parallel channels are coupled hydraulically by the condition of equal pressure drop over all core channels. Additionally, so-called hot channels can be considered for the investigation of hot spots and uncertainties in power density, coolant temperature or mass flow rate. The module FLOCAL comprises an one- or two-phase coolant flow model on the basis of four differential balance equations for mass, energy and momentum of the two-phase mixture and the mass balance for the vapour phase allowing the description of thermodynamic non-equilibrium between the phases, a heat transfer regime map from one-phase liquid up to post-critical heat transfer regimes and superheated steam. A fuel rod model for the calculation of fuel and cladding temperatures is implemented. A thermal-mechanical fuel rod model allows the estimation of the relevant heat transfer behaviour of the gas gap during transients and the determination of some parameters for fuel rod failure estimation.

The two-phase flow model is closed by constitutive laws for heat mass and momentum transfer, e.g. vapour generation at the heated walls, condensation in the sub-cooled liquid, phase slip ratio, pressure drop at single flow resistances and due to friction along the flow channels as well as heat transfer correlations. Different packages of water and steam thermo-physical properties presentation can be used.

Concerning the coupling between neutron kinetics and thermal hydraulics a two time step scheme consisting of thermal-hydraulic and neutron kinetic time steps is used for the transient integration. One or several neutron kinetic steps are used within a thermal-hydraulic step. Iterations between neutron kinetics and thermal hydraulics are carried out in the steady state as well as for each thermal-hydraulic time step. Based on the changes of the main physical parameters of the transient process the time step size is controlled during the calculation.

The fundamental equations of the models used in DYN3D and the methods applied for the solution are described in the chapters 2 to 10. The basic principles of coupling of the core model DYN3D with the system codes ATHLET and RELAP are presented in chapter 11. The comprehensive work for the validation of DYN3D which exceeds the limit of this report is mentioned in chapter 12. The most work done for the verification and validation were performed in frame of international benchmark activities. Results and comparisons were published in the given references.

2 Neutron Kinetics

2.1 Neutron Diffusion Equations

The transient 3-dimensional neutron distribution is calculated by solving the time-dependent neutron diffusion equations for two energy groups and M groups of precursors of delayed neutrons with the help of nodal methods for hexagonal-z or Cartesian geometry [Gru95, Gru96b, Gru99a, Gru99b, Gru99c]. Dividing the reactor core into horizontal slices, the nodes n are the parts of the fuel assemblies in each slice. Considering the horizontal mesh in the Cartesian geometry the nodes can be subdivided, but not in hexagonal geometry. The thickness of the axial slices can be different. The neutron group constants are assumed to be spatially constant in each node n . The transient diffusion equation for the neutron fluxes in a node n is written by using standard notation

$$\begin{aligned} \frac{\partial \Phi_1^n(\mathbf{r}, t)}{v_1^n \partial t} + \nabla \mathbf{J}_1^n(\mathbf{r}, t) + \Sigma_r^n(t) \Phi_1^n(\mathbf{r}, t) &= \frac{1}{k_{eff}} \sum_{g=1}^2 (1 - \beta_g^n) v \Sigma_{f,g}^n(t) \Phi_g^n(\mathbf{r}, t) \\ &+ \sum_{j=1}^M \lambda_j^n C_j^n(\mathbf{r}, t) + S_{ext}^n(\mathbf{r}) \\ \frac{\partial \Phi_2^n(\mathbf{r}, t)}{v_2^n \partial t} + \nabla \mathbf{J}_2^n(\mathbf{r}, t) + \Sigma_a^n(t) \Phi_2^n(\mathbf{r}, t) &= \Sigma_s^n(t) \Phi_1^n(\mathbf{r}, t) \end{aligned} \quad (2.1.1)$$

$$\begin{aligned} \frac{\partial C_j^n(\mathbf{r}, t)}{\partial t} &= \frac{1}{k_{eff}} \sum_{g=1}^2 \beta_{g,j}^n v \Sigma_{f,g}^n(t) \Phi_g^n(\mathbf{r}, t) - \lambda_j^n C_j^n(\mathbf{r}, t) \\ &j = 1, 2, \dots, M. \end{aligned}$$

$$\beta_g^n = \sum_{j=1}^2 \beta_{g,j}^n \quad g = 1, 2.$$

The current $\mathbf{J}_g^n(\mathbf{r}, t)$ is connected with the flux gradient $\nabla \Phi_g^n(\mathbf{r}, t)$ by Fick's law

$$\mathbf{J}_g^n(\mathbf{r}, t) = -D_g^n(t) \nabla \Phi_g^n(\mathbf{r}, t) \quad (2.1.2)$$

with the diffusion coefficient $D_g^n(t)$.

An implicit finite difference scheme together with an exponential transformation technique is used for the time integration of equations (2.1.1).

The flux is represented by

$$\Phi_g^n(\mathbf{r}, t') = \exp[\Omega^n(t' - t + \Delta t)] \cdot \Phi_g^n(\mathbf{r}, t) \quad (2.1.3)$$

within the time step Δt

$$t - \Delta t \leq t' \leq t$$

with

$$\Phi_g^n(\mathbf{r}, t - \Delta t) = \Phi_g^n(\mathbf{r}, t - \Delta t) \quad (2.1.4)$$

Using an implicit difference scheme the time derivative of the neutron flux at the time t is replaced in equation (2.1.1) by

$$\frac{d\Phi_g^n(\mathbf{r}, t)}{dt} \approx \frac{1}{\Delta t} \cdot [(1 + \Omega^n \Delta t) \cdot \Phi_g^n(\mathbf{r}, t) - \exp(\Omega^n \Delta t) \cdot \Phi_g^n(\mathbf{r}, t - \Delta t)] \quad (2.1.5)$$

Ω^n can be estimated from the node-averaged fluxes $\bar{\Phi}_g^n$

$$\bar{\Phi}_g^n(t) = \frac{1}{V^n} \int_{V^n} \Phi_g^n(\mathbf{r}, t) dV \quad (2.1.6)$$

by

$$\Omega^n = \frac{1}{\Delta t} \cdot \ln \frac{\sum_{g=1}^2 \bar{\Phi}_g^n(t)}{\sum_{g=1}^2 \bar{\Phi}_g^n(t - \Delta t)} \quad (2.1.7)$$

V_n being the volume of the node n . At the beginning of the iteration for a time step, the previous step is used for the estimation of Ω^n . During the iteration process, Ω^n can be recalculated by using the $\bar{\Phi}_g^n(t)$ of the actual iteration step.

Assuming an exponential behaviour for $\Phi_g^n(\mathbf{r}, t)$ and $\nu \Sigma_{f,g}^n(t)$ being constant within the interval Δt the equations of precursors are integrated approximately

$$C_j^n(\mathbf{r}, t) = C_j^n(\mathbf{r}, t - \Delta t) \cdot \exp(-\lambda_j^n \Delta t) + \quad (2.1.8)$$

$$\frac{1 - \exp[-(\lambda_j^n + \Omega^n) \Delta t]}{(\lambda_j^n + \Omega^n)} \cdot \frac{1}{k_{eff}} \cdot \sum_{g=1}^2 \beta_{g,j}^n \nu \Sigma_{f,g}^n(t) \Phi_g^n(\mathbf{r}, t)$$

Inserting (2.1.5) and (2.1.8) in the equations for the fluxes in (2.1.1) the following inhomoge-

neous equation system is obtained

$$\begin{aligned} \nabla \mathbf{J}_1^n(\mathbf{r}, t) + \left[\Sigma_r^n(t) + \frac{1 + \Omega^n \Delta t}{v_1^n \Delta t} \right] \Phi_1^n(\mathbf{r}, t) &= \frac{1}{k_{eff}} \sum_{g=1}^2 \left(1 - \sum_{j=1}^M \beta_{g,j}^n \delta_j^n \right) v_{\Sigma_{f,g}}^n(t) \Phi_g^n(\mathbf{r}, t) \\ &+ \sum_{j=1}^M \lambda_j^n C_j^n(\mathbf{r}, t - \Delta t) \exp(-\lambda_j^n \Delta t) + \frac{\exp(\Omega^n \Delta t)}{v_1^n \Delta t} \cdot \Phi_1^n(\mathbf{r}, t - \Delta t) + S_{ext}^n(\mathbf{r}) \end{aligned} \quad (2.1.9)$$

$$\nabla \mathbf{J}_2^n(\mathbf{r}, t) + \left[\Sigma_a^n(t) + \frac{1 + \Omega^n \Delta t}{v_2^n \Delta t} \right] \Phi_2^n(\mathbf{r}, t) = \Sigma_s^n(t) \Phi_1^n(\mathbf{r}, t) + \frac{\exp(\Omega^n \Delta t)}{v_2^n \Delta t} \cdot \Phi_2^n(\mathbf{r}, t - \Delta t)$$

with

$$\delta_j^n = \frac{\Omega^n + \lambda_j^n \exp[-(\lambda_j^n + \Omega^n) \cdot \Delta t]}{\lambda_j^n + \Omega^n} \quad (2.1.10)$$

The equation system for the two groups can be written in a more concise form

$$\nabla \mathbf{J}_g^n(\mathbf{r}, t) + \tilde{\Sigma}_g^n(t) \Phi_g^n(\mathbf{r}, t) = S_g^n(\mathbf{r}, t) \quad (2.1.11)$$

with

$$\begin{aligned} \tilde{\Sigma}_1^n(t) &= \Sigma_r^n(t) + \frac{1 + \Omega^n \Delta t}{v_1^n \Delta t} \\ \tilde{\Sigma}_2^n(t) &= \Sigma_a^n(t) + \frac{1 + \Omega^n \Delta t}{v_2^n \Delta t} \end{aligned} \quad (2.1.12)$$

and

$$\begin{aligned} S_1^n(\mathbf{r}, t) &= \frac{1}{k_{eff}} \sum_{g=1}^2 \left(1 - \sum_{j=1}^M \beta_{g,j}^n \delta_j^n \right) v_{\Sigma_{f,g}}^n(t) \Phi_g^n(\mathbf{r}, t) \\ &+ \sum_{j=1}^M \lambda_j^n C_j^n(\mathbf{r}, t - \Delta t) \exp(-\lambda_j^n \Delta t) + \frac{\exp(\Omega^n \Delta t)}{v_1^n \Delta t} \cdot \Phi_1^n(\mathbf{r}, t - \Delta t) + S_{ext}^n(\mathbf{r}) \end{aligned} \quad (2.1.13)$$

$$S_2^n(\mathbf{r}, t) = \Sigma_s^n(t) \Phi_1^n(\mathbf{r}, t) + \frac{\exp(\Omega^n \Delta t)}{v_2^n \Delta t} \cdot \Phi_2^n(\mathbf{r}, t - \Delta t)$$

Integration of equation (2.1.11) over the node volume V^n gives the nodal balance equations for the node-averaged values:

$$\sum_m \frac{F^{n,m}}{V^n} (\mathbf{e}^{n,m} \mathbf{J}_g^n(t)) + \tilde{\Sigma}_g^n(t) \bar{\Phi}_g^n(t) = \bar{S}_g^n(t) \quad (2.1.14)$$

with

$$\begin{aligned} \bar{S}_1^n(t) &= \frac{1}{k_{eff}} \sum_{g=1}^2 \left(1 - \sum_{j=1}^M \beta_{g,j}^n \delta_j^n \right) v \Sigma_{f,g}^n(t) \bar{\Phi}_g^n(t) \\ &+ \sum_{j=1}^M \lambda_j^n \bar{C}_j^n(t - \Delta t) \exp(-\lambda_j^n \Delta t) + \frac{\exp(\Omega^n \Delta t)}{v_1^n \Delta t} \cdot \bar{\Phi}_1^n(t - \Delta t) + \bar{S}_{ext}^n \end{aligned} \quad (2.1.15)$$

$$\bar{S}_2^n(t) = \Sigma_s^n(t) \bar{\Phi}_1^n(t) + \frac{\exp(\Omega^n \Delta t)}{v_2^n \Delta t} \cdot \bar{\Phi}_2^n(t - \Delta t)$$

with

- \bar{S}_{ext}^n - averaged value of the fast neutron source in the node n
- $\bar{C}_j^n(t)$ - averaged value of the density of precursors of type j in the node
- $F^{n,m}$ - size of interface between node n and neighbouring node m
- $\mathbf{e}^{n,m}$ - unit vector from node n to node m (perpendicular to the interface $F^{n,m}$)
- $\mathbf{J}_g^{n,m}(t)$ - averaged net current of group g at the interface $F^{n,m}$

The different nodal methods which are used for the calculation of the node-averaged fluxes in hexagonal-z and Cartesian geometry are described for the homogeneous steady-state case in the following section. They are applied with small modifications for the steady-state calculation with source and the transient problem.

2.2 Homogeneous Steady State

2.2.1 Equations for the Node Averaged Fluxes

It is assumed that at the beginning of a transient calculation the steady state is determined. Applying the equations (2.1.11) and (2.1.13) for the steady state without external source $S_{ext}^n(\mathbf{r})$ leads to

$$\nabla \mathbf{J}_1^n(\mathbf{r}) + \Sigma_r^n \Phi_1^n(\mathbf{r}) = \frac{1}{k_{eff}} \sum_{g=1}^2 \nu \Sigma_{f,g}^n \Phi_g^n(\mathbf{r}) \quad (2.2.1)$$

$$\nabla \mathbf{J}_2^n(\mathbf{r}) + \Sigma_a^n \Phi_2^n(\mathbf{r}) = \Sigma_s^n \Phi_1^n(\mathbf{r})$$

Considering the node-averaged values for the fluxes as in (2.1.14) yields the simpler expression

$$\sum_m \frac{F^{n,m}}{V^n} (\mathbf{e}^{n,m} \mathbf{J}_1) + \Sigma_r^n \bar{\Phi}_1^n = \frac{1}{k_{eff}} \sum_{g=1}^2 \nu \Sigma_{f,g}^n \bar{\Phi}_g^n \quad (2.2.2)$$

$$\sum_m \frac{F^{n,m}}{V^n} (\mathbf{e}^{n,m} \mathbf{J}_2) + \Sigma_a^n \bar{\Phi}_2^n = \Sigma_s^n \bar{\Phi}_1^n$$

The solutions of the equation system requires relations between the averaged currents ($\mathbf{e}^{n,m} \mathbf{J}_g$) at the surfaces of the nodes and the node-averaged fluxes $\bar{\Phi}_g^n$. These are obtained in a simple way in finite-difference methods, but the loss of accuracy is too large for the used mesh size. More detailed flux expansions inside the nodes are used in nodal methods, leading to improved accuracy. The nodal expansion methods of DYN3D for hexagonal-z and rectangular geometry are outlined in the next sections.

2.2.2 Nodal Expansion for Hexagonal-z Geometry

In most of the nodal methods applied for Cartesian geometry, one-dimensional equations are derived by transverse integration over two directions. It leads to non regular terms for the transversal leakage in hexagonal-z geometry. These terms were neglected by Wagner [Wag89]. Other authors use a conformal mapping to transform the hexagonal problem to rectangular geometry [Cha95a]. In the nodal method implemented in the previous hexagonal version of the code DYN3D [Gru89], a flux factorization in the hexagonal plane and the axial direction was used. The two-dimensional diffusion equation in the hexagonal plane was solved by an expansion into Bessel functions. The solution of the two-dimensional problem in the hexagonal plane avoids the non regular terms of transversal leakage. In the HEXNEM1 and HEXNEM2 methods applied in the present DYN3D version, transverse integration is used for splitting the three-dimensional problem into a two-dimensional problem in the hexagonal plane and a one-dimensional problem

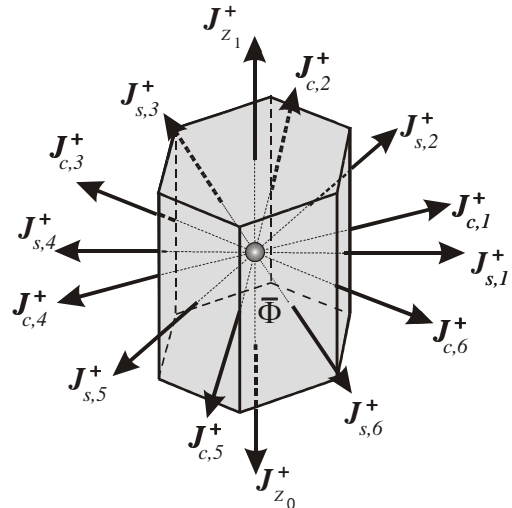


Fig. 2.1: Hexagonal node with directions of outgoing partial currents

lem in axial direction. In the hexagonal plane, the flux is expanded into two-dimensional polynomials up to the second order and into exponential functions being the solutions of the homogeneous Helmholtz equation. Leakage, fission and scattering terms are approximated by the polynomials. In the hexagonal plane, the nodes are coupled not only by the side-averaged fluxes and currents (HEXNEM1 method) but also by the corner values (HEXNEM2 method). A similar flux expansion is used for the one-dimensional problem in the axial direction. The method HEXNEM2 is described in the following for the solution of the steady-state homogeneous equation in hexagonal nodes of Fig. 2.1. In the hexagonal-z geometry, the node volume V^n is given by $V^n = F_{hex} \cdot a_z^n$ with the area of the hexagon $F_{hex} = \frac{\sqrt{3}}{2}d^2$. d is the distance

between parallel sides of the hexagons and a_z^n the height of the node n . Any node n will be considered and the index n of the node is omitted. Axially, the node is situated between the coordinates $z_0 = z_i - \frac{a_z}{2}$ and $z_1 = z_i + \frac{a_z}{2}$. Firstly, we integrate equations (2.2.1) over the axial directions z and obtain the two-dimensional equations for each energy group g

$$-D_g \left(\frac{\partial^2}{\partial x^2} + \frac{\partial^2}{\partial y^2} \right) \hat{\Phi}_g(x, y) + \Sigma_g \hat{\Phi}_g(x, y) = \hat{Q}_g(x, y) \quad (2.2.3)$$

with

$$\hat{Q}_g(x, y) = \hat{S}_g(x, y) - \hat{L}_g(x, y) \quad (2.2.4)$$

The average values of flux, source and leakage terms are defined by

$$\hat{\Phi}_g(x, y) = \frac{1}{a_z} \int_{z_0}^{z_1} \Phi_g(\mathbf{r}) dz \quad (2.2.5)$$

$$\hat{S}_g(x, y) = \frac{1}{a_z} \int_{z_0}^{z_1} S_g(\mathbf{r}) dz \quad (2.2.6)$$

with

$$S_1(\mathbf{r}) = \frac{1}{k_{eff}} \sum_{g=1}^2 \nu \Sigma_{f,g} \Phi_g(\mathbf{r}) \quad (2.2.7)$$

and

$$S_2(\mathbf{r}) = \Sigma_s \cdot \Phi_1(\mathbf{r}) \quad (2.2.8)$$

The transverse integrated leakage term $\hat{L}_g(x, y)$ is given by

$$\hat{L}_g(x, y) = -\frac{D_g}{a_z} \int_{z_0}^{z_1} \frac{d^2}{dz^2} \Phi_g(\mathbf{r}) dz \quad (2.2.9)$$

The integration of equations (2.2.1) over the hexagon F_{hex} provides the one-dimensional equation for the radial averaged flux $\hat{\Phi}_g(z)$ along the direction z

$$-D_g \frac{d^2}{dz^2} \hat{\Phi}_g(z) + \Sigma_g \hat{\Phi}_g(z) = \hat{Q}_g(z) \quad (2.2.10)$$

with

$$\hat{Q}_g(z) = \hat{S}_g(z) - \hat{L}_g(z) \quad (2.2.11)$$

and

$$\hat{\Phi}_g(z) = \frac{1}{F_{hex}} \int_{F_{hex}} \Phi_g(\mathbf{r}) dF \quad (2.2.12)$$

$$\hat{S}_g(z) = \frac{1}{F_{hex}} \int_{F_{hex}} S_g(\mathbf{r}) dF \quad (2.2.13)$$

The transverse integrated leakage term $\hat{L}_g(z)$ is given by

$$\hat{L}_g(z) = -\frac{D_g}{F_{hex}} \int_{F_{hex}} \left(\frac{\partial^2}{\partial x^2} + \frac{\partial^2}{\partial y^2} \right) \Phi_g(\mathbf{r}) dF \quad (2.2.14)$$

The methods applied for the approximate calculation of the integrated neutron fluxes $\hat{\Phi}_g(x, y)$ in the hexagonal plane and $\hat{\Phi}_g(z)$ in the z -direction are described in the following.

Hexagonal Plane

First, the following transformation is carried out to get simpler expressions

$$x' = \frac{x}{a}, y' = \frac{y}{a}, D' = \frac{D}{a}, \Sigma' = \Sigma \cdot a, \hat{S}' = \hat{S} \cdot a, \hat{L}' = \hat{L} \cdot a, \hat{Q}' = \hat{Q} \cdot a \quad (2.2.15)$$

with

$$a = \frac{d}{2}$$

The flux in the hexagonal plane is expanded by using polynomials up to the 2nd order and exponential functions being the solutions to the homogeneous equation (2.2.3). The energy-group subscript g will be omitted in the following, because each energy group can be considered in the same way. With the notation (2.2.15), the HEXNEM2 flux expansion can be written as

$$\hat{\Phi}(x', y') \approx \sum_{i=0}^5 c_i \cdot h_i(x', y') + \sum_{k=1}^6 a_{s,k} \cdot \exp[B'(\mathbf{e}_{s,k} \cdot \mathbf{r}'_{x,y})] + \sum_{k=1}^6 a_{c,k} \cdot \exp[B'(\mathbf{e}_{c,k} \cdot \mathbf{r}'_{x,y})] \quad (2.2.16)$$

with the vector $\mathbf{r}'_{x,y} = (x', y')$. The unit vectors $\mathbf{e}_{s,k}$ point from the hexagon centre to the midpoints of the sides and $\mathbf{e}_{c,k}$ from the centre to the corners of the hexagon, respectively (see Fig. 2.2). The buckling B' is given by

$$B' = \sqrt{\frac{\Sigma'}{D'}} \quad (2.2.17)$$

The polynomials $h_i(x', y')$ are given by

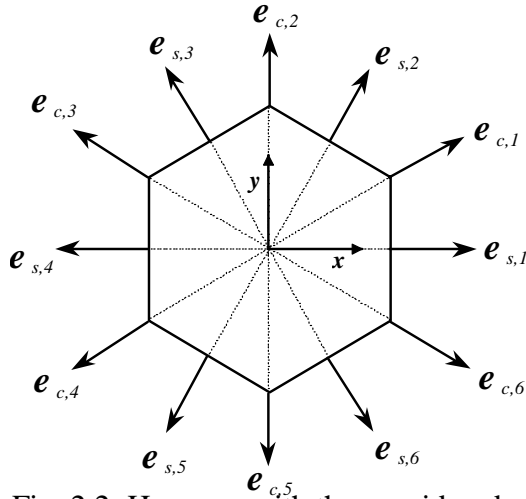


Fig. 2.2: Hexagon with the considered directions $\mathbf{e}_{s,i}$ and $\mathbf{e}_{c,i}$

$$\begin{aligned} h_0 &= \frac{1}{N_0} \\ h_1 &= \frac{x'}{N_1} \\ h_2 &= \frac{y'}{N_2} \\ h_3 &= \frac{1}{N_3} \left(x'^2 + y'^2 - \frac{5}{9} \right) \\ h_4 &= \frac{x'^2 - y'^2}{N_4} \\ h_5 &= \frac{x'y'}{N_5} \end{aligned} \quad (2.2.18)$$

with the hexagonal fuel assembly pitch d . The polynomials $h_i(x', y')$ together with the normalization factors N_i satisfy the orthogonality relation (δ_{ij} Kroneckers symbol):

$$\int_{F'_{hex}} h_i(x', y') h_j(x', y') dy' dx' = \delta_{ij} \quad (2.2.19)$$

F'_{hex} is the area of the transformed hexagon.

The normalization constants are given by

$$\begin{aligned}
 N_0^2 &= 2\sqrt{3} \\
 N_1^2 &= N_2^2 = \frac{5}{9}\sqrt{3} \\
 N_3^2 &= \frac{86}{405}\sqrt{3} \\
 N_4^2 &= N_5^2 = \frac{56}{135}\sqrt{3}
 \end{aligned} \tag{2.2.20}$$

The source $\hat{Q}'_g(x', y')$ is approximated by the polynomials

$$\hat{Q}'(x', y') \approx \sum_{i=0}^5 q_i \cdot h_i(x', y') \tag{2.2.21}$$

Inserting the flux approximation (2.2.16) and the source term (2.2.21) in the diffusion equation (2.2.3) with (2.2.4), the coefficients of the polynomial expansion are obtained

$$c_0 = \frac{1}{\Sigma'} q_0 + \frac{36}{B'^2} \sqrt{\frac{5}{43}} c_3 \tag{2.2.22}$$

and

$$c_i = \frac{q_i}{\Sigma'} \quad \text{for } i = 1, 2, \dots, 5 \tag{2.2.23}$$

The coefficients to the exponential functions in (2.2.16) are obtained from the inter-nodal interface conditions or the boundary conditions for nodes located at the outer boundary of the system. In the frame of diffusion approximation, the current of neutrons, which are going in or coming from a half space with the direction \mathbf{e} are represented by the outgoing J^+ and the incoming J^- partial currents. The side-averaged or corner point values of the partial currents are given by

$$J^\pm = \frac{1}{2} \left(\frac{1}{2} \Phi \pm (\mathbf{e} \mathbf{J}) \right) \tag{2.2.24}$$

with the side-averaged or corner point fluxes Φ and the side-averaged or corner point net currents \mathbf{J} . The directions \mathbf{e} can be seen in Fig. 2.2. Using the flux expansion (2.2.16) and (2.1.2) the partial currents for all sides and corners can be represented by the equations

$$\begin{aligned}
 \mathbf{J}_s^\pm &= \mathbf{P}_s^\pm \mathbf{C} + \mathbf{Q}_{ss}^\pm \mathbf{A}_s + \mathbf{Q}_{sc}^\pm \mathbf{A}_c \\
 \mathbf{J}_c^\pm &= \mathbf{P}_c^\pm \mathbf{C} + \mathbf{Q}_{cs}^\pm \mathbf{A}_s + \mathbf{Q}_{cc}^\pm \mathbf{A}_c
 \end{aligned} \tag{2.2.25}$$

with the vectors $\mathbf{C}, \mathbf{A}_s, \mathbf{A}_c$ of the coefficients $c_i, a_{s,k}$ and $a_{c,k}$ of the expansion (2.2.16), respectively. The side-averaged partial currents $J_{s,k}^\pm$ form the vector \mathbf{J}_s^\pm and the partial currents

at the corners $J_{c,k}^{\pm}$ the vector J_c^{\pm} . Due to the symmetry of the problem each of the 6x6 matrices has only a few different elements, i. e. the matrices (P_s^{\pm}, P_c^{\pm}) , $(Q_{ss}^{\pm}, Q_{cc}^{\pm})$, $(Q_{sc}^{\pm}, Q_{cs}^{\pm})$ consist of 6, 4 and 3 different elements, respectively [Gru99a]. The A_s, A_c are determined by analytical matrix inversion for the (12x12) equation system (2.2.25), with the incoming partial currents J_s^-, J_c^- and the coefficients C given. Thus eliminating the vectors A_s, A_c in the equations (2.2.25), the outgoing partial currents J_s^+, J_c^+ can be expressed in terms of the incoming partial currents J_s^-, J_c^- and the coefficients C of the polynomial expansion:

$$J_s^+ = V_s C + W_{ss} J_s^- + W_{sc} J_c^- \quad (2.2.26)$$

$$J_c^+ = V_c C + W_{cs} J_s^- + W_{cc} J_c^-$$

The matrices in (2.2.26) have the same structure as those of (2.2.25). The different elements can be calculated at the beginning of the iteration. If the fluxes and currents are assumed to be continuous at the interface between two hexagons, the side-averaged incoming partial currents J^- are equal to the outgoing currents J^+ from the adjacent nodes. Continuous fluxes and currents at the corners of three hexagons 1, 2 and 3 in Fig. 2.3 lead to the following interface condition (number of hexagons in parentheses):

$$\{J_{c,1}^+(1) - J_{c,1}^-(1)\} + \{J_{c,3}^+(2) - J_{c,3}^-(2)\} + \{J_{c,5}^+(3) - J_{c,5}^-(3)\} = 0 \quad (2.2.27)$$

Based on these relations the outgoing partial currents for all nodes are calculated. Using the interface and boundary conditions, the incoming currents for the next run (inner iteration step) are thus determined. Assembly discontinuity factors (ADF) can be taken into account by modifying the interface conditions. The equations of the axial direction, described in the next section, are integrated in the iteration process of the 3-dimensional problem.

In the HEXNEM1 method, which is a simplification of HEXNEM2, only the first of equations (2.2.25) with $A_c = 0$ exists. Instead of the two equations (2.2.26) the simpler equation

$$J_s^+ = V_s C + W_{ss} J_s^- \quad (2.2.28)$$

is obtained.

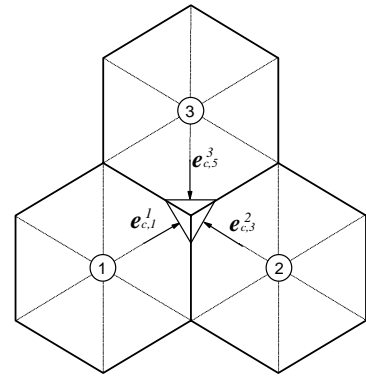


Fig. 2.3: Directions at the corner of 3 hexagons

Axial Direction

A procedure analogous to the 2-dimensional case above is used for the solution of equation (2.2.10) in the axial layer between $z_0 = z_i - \frac{a_z}{2}$ and $z_1 = z_i + \frac{a_z}{2}$, i. e. the flux $\Phi(z)$ is expanded by polynomials until the second order and exponential functions. A co-ordinate transformation is performed for the variables in equation (2.2.10), too:

$$z'' = \frac{z}{a_z}, D'' = \frac{D}{a_z}, \Sigma'' = \Sigma \cdot a_z, \hat{S}'' = \hat{S} \cdot a_z, \hat{L}'' = \hat{L} \cdot a_z, \hat{Q}'' = \hat{Q} \cdot a_z \quad (2.2.29)$$

$$\hat{\Phi}(z'') = \sum_{i=1}^2 c_i^z h_i(z'') + a_1^z \exp(B'' z'') + a_2^z \exp(-B'' z'') \quad (2.2.30)$$

with

$$B'' = \sqrt{\frac{\Sigma''}{D''}} \quad (2.2.31)$$

The polynomials are

$$h_0(z'') = 1, h_1(z'') = 2\sqrt{3}z'', h_2(z'') = \sqrt{5}\left(\frac{1}{2} - 6z''^2\right) \quad (2.2.32)$$

The functions $h_i(z'')$ satisfy the orthogonality relation

$$\int_{z'' = -\frac{1}{2}}^{z'' = \frac{1}{2}} h_i(z'') h_j(z'') dz'' = \delta_{ij} \quad (2.2.33)$$

The source terms $\hat{Q}(z)$ are approximated as

$$\hat{Q}''(z'') \approx \sum_{i=0}^2 q_i^z \cdot h_i(z'') \quad (2.2.34)$$

with the coefficients q_i^z . After inserting the flux expansion (2.2.30) and the source term expansion (2.2.34) in the diffusion equation (2.2.10) the polynomial coefficients of the flux expansion are given

$$c_0^z = \frac{1}{\Sigma''} q_0^z - \frac{12}{B''^2} \sqrt{5} c_2^z \quad (2.2.35)$$

$$c_i^z = \frac{1}{\Sigma''} q_i^z \quad (2.2.36)$$

Using a similar procedure as for the 2-dimensional case yields for the outgoing $J_{z_0}^+$, $J_{z_1}^+$ and incoming $J_{z_0}^-$, $J_{z_1}^-$ partial currents at the bottom (z_0) and top (z_1) of node

$$\mathbf{J}_z^\pm = \mathbf{P}^{z\pm} \mathbf{C}^z + \mathbf{Q}^{z\pm} \mathbf{A}^z \quad (2.2.37)$$

After eliminating the a_1^z, a_2^z in this (2x2) equation system, the outgoing partial currents are expressed in terms of incoming partial currents in axial direction:

$$\mathbf{J}_z^+ = \mathbf{V}^z \mathbf{C}^z + \mathbf{W}^z \mathbf{J}_z^- \quad (2.2.38)$$

With (2.2.26) and (2.2.38) the equations for the inner iteration process of the 3-dimensional problem are complete. The coefficients of the source terms consisting of fission, scattering and transversal leakage are updated in the outer iteration step.

Calculation of the Transversal-Leakage Terms

The transversal leakage terms are approximated by applying the polynomials in the hexagonal plane and the axial direction.

First consider the transversal leakage of the hexagonal plane, using the polynomials (2.2.18):

$$\hat{L}'(x', y') \approx a \sum_{i=0}^5 l_i h_i(x', y') \quad (2.2.39)$$

The coefficients l_i of the transversal leakage in the axial direction have to be calculated from the averaged values of the transversal leakage of the node and the neighbouring nodes. The averaged value of a considered node n is obtained from equation (2.2.9) with the help of the partial currents

$$L_0 = \frac{1}{a_z} (J_{z_1}^+ - J_{z_1}^- + J_{z_0}^+ - J_{z_0}^-) \quad (2.2.40)$$

Within the nodes, a linear change of the transversal leakage is assumed to approximate the 6 averaged values L_k of the transversal leakage at the sides of the hexagon from the average of the node L_0 and $L_{0,k}$ of the 6 neighbouring nodes $k = 1, 2, \dots, 6$

$$L_k = \frac{D(L_0 + L_{0,k})}{(D + D_k)} \quad \text{for } k = 1, 2, \dots, 6 \quad (2.2.41)$$

D, D_k being the representative diffusion coefficients. This approximation is obtained from the assumption that the second derivative of the flux in the direction of z at the interface between

two assemblies perpendicular to x fulfills the same conditions as the flux itself. That is for the nodes n and $n + 1$ being the upper neighbour of the node n

$$\frac{1}{D^n} L_k^n = \frac{1}{D^{n+1}} L_{k'}^{n+1} \quad (2.2.42)$$

$$\frac{\partial L_k^n}{\partial x} = \frac{\partial L_{k'}^{n+1}}{\partial x} \quad (2.2.43)$$

k and k' are the sides of node n and $n + 1$ which have the same interface. If the derivative of the flux at the boundary of the node n is approximated by

$$\frac{\partial L_k^n}{\partial x} \approx \frac{(L_k^n - L_0^n)}{a} \quad (2.2.44)$$

the expression (2.2.41) is obtained. The coefficients l_i of polynomial expansion (2.2.39) $\hat{L}'(x', y')$ follow from

$$\sum_{k=0}^6 \left[\sum_{i=0}^5 l_i h_{i,k} - L_k \right]^2 \rightarrow \min \quad (2.2.45)$$

The index n of the L_k is omitted. The $h_{i,k}$ are the values of the polynomials averaged over the hexagon ($k = 0$) or its sides ($k > 0$). The leakage coefficients are obtained from (2.2.45)

$$\begin{aligned} l_0 &= N_0 L_0 \\ l_1 &= \frac{N_1}{6} (2L_1 + L_2 - L_3 - 2L_4 - L_5 + L_6) \\ l_2 &= \frac{N_2}{2\sqrt{3}} (L_2 + L_3 - L_5 - L_6) \\ l_3 &= \frac{3N_3}{10} (L_1 + L_2 + L_3 + L_4 + L_5 + L_6 - 6L_0) \\ l_4 &= \frac{3N_4}{16} (2L_1 - L_2 - L_3 + 2L_4 - L_5 - L_6) \\ l_5 &= \frac{3\sqrt{3}N_5}{16} (L_2 - L_3 + L_5 - L_6) \end{aligned} \quad (2.2.46)$$

The leakage term in radial direction is approximated by the polynomials (2.2.32):

$$\hat{L}''(z) \approx a_z \sum_{i=0}^2 l_i^z h_i(z'') \quad (2.2.47)$$

The coefficients l_i^z can be calculated by using the averaged values L_0^z given by

$$L_0^z = \frac{2}{3d} \sum_{k=1}^6 (J_{s,k}^+ - J_{s,k}^-) \quad (2.2.48)$$

The values L_0^z of the considered node together with the values L_0^l, L_0^u of the lower and upper node are applied for the determination of the coefficients l_i^z in a similar way as above. Using (2.2.42) and (2.2.43) with the linear approximation for the derivative at the bottom and top node boundaries, the leakage values are obtained

$$L_{z_l} = \frac{D(L_0^l a_z + L_0^z a_z^l)}{D^l a_z + D a_z^l} \quad (2.2.49)$$

$$L_{z_u} = \frac{D(L_0^z a_z^u + L_0^u a_z)}{D a_z^u + D^u a_z}$$

The polynomial coefficients of (2.2.47) are then

$$\begin{aligned} l_0^z &= L_0^z \\ l_1^z &= \frac{L_{z_u} - L_{z_l}}{2\sqrt{3}} \\ l_2^z &= \frac{L_0 - \frac{1}{2}(L_{z_u} + L_{z_l})}{\sqrt{5}} \end{aligned} \quad (2.2.50)$$

2.2.3 Nodal Expansion for Cartesian Geometry

The described method is based on the transverse integration over all combinations of two directions of the rectangular node (see Fig. 2.4). It is applied in most of the nodal codes for rectangular geometry, see e.g. Ref. [Raj89, Wag89].

The transverse integration leads to one-dimensional equations for x, y, and z-direction. Therefore this method is much simpler than for hexagonal-z geometry and the methods used for the axial direction z can be applied for any of the directions x, y, and z. Considering the direction x, the transverse integration over y and z leads to the equation

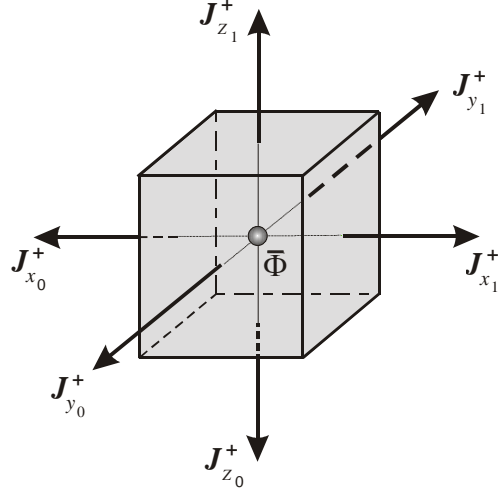


Fig. 2.4: Cartesian node with directions and outgoing partial currents

$$-D_g \frac{d^2}{dx^2} \hat{\Phi}_g(x) + \Sigma_g \hat{\Phi}_g(x) = \hat{Q}_g(x) \quad (2.2.51)$$

with

$$\hat{Q}_g(x) = \hat{S}_g(x) - \hat{L}_g(x) \quad (2.2.52)$$

and

$$\hat{\Phi}_g(x) = \frac{1}{a_y a_z} \int_{y_j - \frac{a_y}{2}}^{y_j + \frac{a_y}{2}} \int_{z_k - \frac{a_z}{2}}^{z_k + \frac{a_z}{2}} \Phi(x, y, z) dz dy \quad (2.2.53)$$

$$\hat{S}_g(x) = \frac{1}{a_y a_z} \int_{y_j - \frac{a_y}{2}}^{y_j + \frac{a_y}{2}} \int_{z_k - \frac{a_z}{2}}^{z_k + \frac{a_z}{2}} S(x, y, z) dz dy \quad (2.2.54)$$

The transverse integrated leakage term is given by

$$\hat{L}_g(x) = -\frac{D_g}{a_y a_z} \int_{y_j - \frac{a_y}{2}}^{y_j + \frac{a_y}{2}} \int_{z_k - \frac{a_z}{2}}^{z_k + \frac{a_z}{2}} \left(\frac{\partial^2}{\partial y^2} + \frac{\partial^2}{\partial z^2} \right) \Phi_g(x, y, z) dz dy \quad (2.2.55)$$

The average leakage is obtained by

$$L_0^x = \frac{1}{a_y} (J_{y_1}^+ - J_{y_1}^- + J_{y_0}^+ - J_{y_0}^-) + \frac{1}{a_z} (J_{z_1}^+ - J_{z_1}^- + J_{z_0}^+ - J_{z_0}^-) \quad (2.2.56)$$

The method described in the previous section for the axial direction of the hexagonal-z method is applied here for each of the directions x, y, and z.

2.2.4 Boundary Conditions

Albedo conditions are assumed for partial currents at the outer boundary of the system, i.e. the core or the core with radial and/or axial reflector. The boundary conditions at all outer faces i of the system are generally described for the two energy groups by

$$J_{s,i,1}^- = R_{11}^s J_{s,i,1}^+ \quad (2.2.57)$$

$$J_{s,i,2}^- = R_{21}^s J_{s,i,1}^+ + R_{22}^s J_{s,i,2}^+$$

The albedo coefficients $R_{gg'}^s$ are input data to the problem. If the reactor is calculated without reflector, the albedos can be estimated from a previous steady-state calculation with reflector. The first term of the right hand side of the second relation in (2.257) represents the incoming thermal neutrons that originate from leaving fast neutrons slowed down outside and re-entering the system as thermal neutrons. The relations

$$R_{21}^s = 0, R_{gg}^s \cong 0 \quad (2.2.58)$$

can be assumed for the case of vacuum boundary conditions, whereas

$$R_{21}^s = 0, R_{gg}^s = -1 \quad (2.2.59)$$

describe the zero-flux boundary conditions.

When the HEXNEM2 method is applied, boundary conditions are required for the corner points. It is not quite clear what sort of boundary condition has to be used at the corners, when certain boundary conditions are applied to the sides. The concept of extrapolation length in diffusion theory is based on the requirement that the diffusion theory results give a flux distribution inside of the system close to the transport solution. Therefore, the extrapolation lengths cannot be derived from diffusion theory alone. For example, the vacuum extrapolation length derived from the transport theory at plane surfaces is somewhat different from the vacuum boundary condition that is obtained from the diffusion theory expression [Bel70]

$$\Psi(\mathbf{r}, \Omega) = \frac{1}{4\pi} [\Phi(\mathbf{r}) + 3\Omega\mathbf{J}(\mathbf{r})] \quad (2.2.60)$$

under the assumption of vanishing incoming current. Nevertheless, equation (2.2.60) is used in the reference [Gru99a] to estimate boundary conditions at the corners from the given boundary conditions of the sides. There are two types of corners at the outer boundary. If there are no nodes at the two sides of the considered corner, this corner is called of type I. If one side has an adjacent node, the corner is of type II

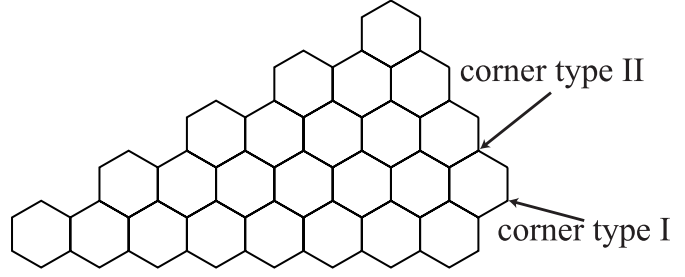


Fig. 2.5: Different types of outer corners in case of hexagonal geometry.

(see Fig. 2.5). The boundary conditions of the partial currents at the corner type II depend on the behaviour of the partial currents at the common corner of the two neighbouring assemblies.

Considering corners of type I the following boundary conditions are used for the partial currents

$J_{c,i,g}^+$, $J_{c,i,g}^-$ at the corner i

$$J_{c,i,1}^- = R_{11}^{c,t11} J_{c,i,1}^+ \quad (2.2.61)$$

$$J_{c,i,2}^- = R_{21}^{c,t1p} J_{c,i,1}^+ - R_{21}^{c,t1m} J_{c,i,1}^- + R_{22}^{c,t11} J_{c,i,2}^+$$

$R_{gg}^{c,t11}$ is derived from the diffusion approximation of the angular flux. If the albedo boundary conditions of the sides R_{gg}^s are given, the albedos of the partial currents at the corner point are calculated. Instead of 180 degree, we have to consider in the case of corner type I or II an outer angle of 240 degree or 120 degree, respectively.

It leads to

$$R_{gg}^{c,t11} = \frac{(K_1 - 1) + R_{gg}^s \cdot (K_2 + 1)}{(K_1 + 1) + R_{gg}^s \cdot (K_2 - 1)} \quad (2.2.62)$$

and

$$R_{12}^{c,t1p} = \frac{R_{21}^s \cdot (K_2 + 1)}{(K_1 + 1) + R_{22}^s \cdot (K_2 - 1)}$$

$$R_{12}^{c,t1m} = \frac{R_{21}^s \cdot (K_2 - 1)}{(K_1 + 1) + R_{22}^s \cdot (K_2 - 1)}$$

with

$$K_1 = \frac{4}{3\sqrt{3}} + \frac{1}{\pi} \quad \text{and} \quad K_2 = \frac{8}{3\sqrt{3}} - \frac{1}{\pi}$$

The boundary conditions are simplified in the case of outer vacuum

$$J_{c,i,g}^- = R_{gg}^{c,t11} J_{c,i,g}^+ \quad (2.2.63)$$

Considering the corner points of type II, the partial currents of the neighbouring hexagon j in-

fluence the incoming partial currents

$$J_{c,i,1}^- = R_{11}^{c,t21} J_{c,i,1}^+ + R_{11}^{c,t22} (J_{c,j,1}^+ - J_{c,j,1}^-) \quad (2.2.64)$$

$$J_{c,i,1}^- = R_{21}^{c,t2p} J_{c,i,1}^+ + R_{21}^{c,t2m} J_{c,i,1}^- + R_{21}^{c,t22} (J_{c,j,1}^+ - J_{c,j,1}^-) \\ + R_{22}^{c,t21} J_{c,i,2}^+ + R_{22}^{c,t22} (J_{c,j,2}^+ - J_{c,j,2}^-)$$

with the coefficients

$$R_{11}^{c,t21} = \frac{(K_2 - 1) + R_{11}^s \cdot (K_1 + 1)}{(K_2 + 1) + R_{11}^s \cdot (K_1 - 1)}$$

$$R_{11}^{c,t22} = \frac{K_2 + R_{11}^s \cdot K_1}{(K_2 + 1) + R_{11}^s \cdot (K_1 - 1)} \quad (2.2.65)$$

$$R_{21}^{c,t2p} = \frac{R_{21}^s \cdot (K_1 + 1)}{(K_2 + 1) + R_{22}^s \cdot (K_2 - 1)}$$

$$R_{21}^{c,t2m} = -R_{21}^{c,t2p}$$

$$R_{21}^{c,t22} = \frac{R_{21}^s \cdot K_1}{(K_2 + 1) + R_{22}^s \cdot (K_2 - 1)}$$

and

$$R_{22}^{c,t21} = \frac{(K_2 - 1) + R_{22}^s \cdot (K_1 + 1)}{(K_2 + 1) + R_{22}^s \cdot (K_2 - 1)} \quad (2.2.66)$$

$$R_{22}^{c,t22} = \frac{K_2 + R_{22}^s \cdot K_1}{(K_2 + 1) + R_{22}^s \cdot (K_2 - 1)}$$

If we have outer vacuum simpler expressions are obtained:

$$J_{c,i,g}^- = R_{gg}^{c,t21} J_{c,i,g}^+ + R_{gg}^{c,t22} (J_{c,j,g}^+ - J_{c,j,g}^-) \quad (2.2.67)$$

Using these conditions a good agreement of the results with references was obtained for benchmark problems with radial reflector [Gru99a]. If the reflector is removed, the boundary values for both sides and corners can be determined by a previous steady-state calculation with reflector. The boundary conditions at each outer side and corner are different. There exists the possibility to use these values as input data for calculations without radial reflector. Values can be generated for each side and corner between core and reflector. In most cases, it is sufficient to use axially averaged values.

2.2.5 Assembly Discontinuity Factors (ADF)

Generating homogenized cross sections for the assemblies by cell calculations, the diffusion equation for the homogenized assembly is not completely equivalent to the original heterogeneous problem. It leads to some deviations of the results obtained with homogenized cross sections against the results of heterogeneous cell calculation. The introduction of assembly discontinuity factors (ADF) improves the homogenized results [Smi86]. If the group constants for the homogenized diffusion equation are derived from the heterogeneous equation, the interface conditions between two homogenized areas are not defined. The continuity of the heterogeneous fluxes is given. Therefore the conditions of the homogeneous fluxes are given by the ratios of heterogeneous and homogeneous fluxes at both sides of the interface. The so-called ADF of each energy group are defined as the ratio of the average values of heterogeneous and homogeneous neutron fluxes $\bar{\Phi}_{het}^s, \bar{\Phi}_{hom}^s$ at the radial fuel assembly boundaries

$$f^s = \frac{\bar{\Phi}_{het}^s}{\bar{\Phi}_{hom}^s} \quad (2.2.68)$$

The energy group index is omitted in all equations. There are different possibilities to determine the ADF in the cell calculations. A detailed heterogeneous calculation of the whole system is too expensive in most cases. Therefore approximations of the fluxes are used for the determination of the ADF. If the cell calculation is performed with reflecting boundary conditions, $\bar{\Phi}_{het}^s$ can be obtained as average value of the considered side and $\bar{\Phi}_{hom}^s$ is the assembly averaged value of the neutron flux. If the surrounded assemblies are taken into account, better approximation should be obtained.

If $f^s \approx 1$ the ADF can be neglected in homogenized diffusion theory. The effect of the ADF on the results is more important, if the assembly has larger heterogeneities near the boundary. Therefore the ADF should be taken into account, if absorbing pins or absorber plates near to the boundary of the fuel assemblies are present. The ADF can have an effect, if the fuel assembly consists of different fuel pins (enrichment or MOX).

The ADF are taken into account in DYN3D by modified interface conditions between the nodes. So far it has been assumed that the side-averaged neutron fluxes are continuous at the sides. It leads to continuous partial currents at the interfaces. Modified interface conditions are derived for the partial currents, if the ADF are taken into account. Considering two neighbouring assemblies i and j the following equation is obtained

$$\begin{aligned} J_s^-(i) &= (1 + \Theta^s(ij))J_s^+(j) + \Theta^s(ij) J_s^-(j) \\ \Theta^s(ij) &= \frac{1}{2} \left(\frac{f^s(j)}{f^s(i)} - 1 \right) \end{aligned} \quad (2.2.69)$$

In the HEXNEM2 method for hex-z geometry corner ADF f^c can also be considered.

Using the equation (2.2.27), the incoming corner partial current of the assembly 1 (Fig. 2.3)

$$J_{c,1}^-(1) = \frac{1}{(1+f^c(1))} \left\{ (1-f^c(1))J_{c,1}^+(1) + (2+\Theta^c(2))J_{c,3}^+(2) + \Theta^c(2)J_{c,3}^-(2) \right. \\ \left. + (2+\Theta^c(3))J_{c,5}^+(3) + \Theta^c(3)J_{c,5}^-(3) \right\}$$

with (2.2.70)

$$\Theta^c(i) = \left(\frac{f^c(i)}{2} - 1 \right)$$

The outer boundary of the system can be treated in a similar way.

In the iteration process, the ADF can be considered by using these modified interface and boundary conditions.

2.2.6 Iteration Procedure

An inner and outer iteration scheme is applied to solve the equation system for all nodes of the core. The inner iterations are performed separately for the radial plane and the axial direction in hexagonal-z geometry or for each direction x, y, z in the case of square geometry. It is assumed in the inner iteration process that the fission and scattering sources and the transversal leakage are approximated only by the polynomials. Considering the hexagonal-z geometry as example in the following, the polynomial coefficients of the right hand side of (2.2.3) and (2.2.10) are given from the last outer iteration ($k-1$). Those are used to calculate the polynomial coefficients of the fluxes from equations (2.2.22), (2.2.23), (2.2.35) and (2.2.36). First, inner iterations are performed for the fast group. Then, the polynomial coefficients of scattering source are upgraded to perform the inner iterations of the thermal group by the same procedure.

After finishing the inner iterations upgraded polynomial coefficients of the group fluxes $C^{*(k)}$, $C^{z*(k)}$ were obtained by integrating the flux expansion (2.2.16) with the polynomials as weighting functions and the orthogonality relation (2.2.19). Eliminating the contributions of the A_s, A_c vectors by the relations (2.2.25) for the incoming partial currents, the following equations are obtained:

$$C^{*(k)} = C^{(k)} + H_s J_s^{-(k)} + H_c J_c^{-(k)} \quad (2.2.71)$$

In the same way, (2.2.30) is applied for z direction. Together with (2.2.33) and (2.2.37) the following expression for the axial direction is given:

$$C^{z*(k)} = C^{z(k)} + H^z J_z^{-(k)} \quad (2.2.72)$$

Finishing the inner iterations of the fast group the upgraded coefficients of the scattering source are used for the inner iterations of the thermal group.

The polynomial coefficients c_i and c_i^z of the flux expansion are calculated from (2.2.23) and (2.2.36) for $i > 0$. Therefore they are not changed during inner iterations. Instead of calculating the coefficients c_0 and c_0^z by (2.2.22) and (2.2.35) they are calculated in each inner iteration from the node-averaged fluxes, which were upgraded from the integrated balance equations:

$$\sum_{l=1}^{nos} (J_{1,l}^{+n(k)} - J_{1,l}^{-n(k)}) + \sum_r^n \bar{\Phi}_1^{n(k)} = \frac{1}{k_{eff}^{(k-1)}} \sum_{g=1}^2 v \Sigma_{f,g}^n \bar{\Phi}_g^{n*(k-1)} \quad (2.2.73)$$

$$\sum_{l=1}^{nos} (J_{2,l}^{+(k)} - J_{2,l}^{-(k)}) + \sum_a^n \bar{\Phi}_2^{n(k)} = \sum_s^n \bar{\Phi}_1^{n*(k)}$$

Based on $\bar{\Phi}_g^{n(k)}$ the coefficients c_0 and c_0^z were obtained by integration of the flux expansions (2.2.16) over the hexagon and (2.2.30) over the z-interval. The coefficients A_s, A_c and A^z can be eliminated by the incoming partial currents and the higher coefficients c_3 and c_2^z of the symmetrical polynomials by using the relations (2.2.25) and (2.2.37) for the incoming partial currents.

The outgoing partial currents were calculated by (2.2.26) and (2.2.38) respectively. The incoming partial currents are determined from the outgoing currents of the neighbouring nodes using the interface conditions between the nodes with or without consideration of the ADF. The boundary conditions are used at the core border.

After few (3 - 5) inner iterations for the two groups the source terms are upgraded. The approximations of the fission sources for the radial and axial direction are given by

$$\hat{S}^{(k)}(x', y') \approx \sum_{i=0}^5 s_i^{(k)} h_i(x', y') \quad (2.2.74)$$

with

$$s_i^{(k)} = \frac{1}{k_{eff}^{(k)}} \sum_{g=1}^2 v \Sigma_{f,g} c_{i,g}^{*(k)} \quad (2.2.75)$$

and

$$\hat{S}^{(k)}(z'') \approx \sum_{i=0}^2 s_i^{z,(k)} h_i(z'') \quad (2.2.76)$$

with

$$s_i^{z,(k)} = \frac{1}{k_{eff}^{(k)}} \sum_{g=1}^2 v \Sigma_{f,g} c_{i,g}^{z,*(k)} \quad (2.2.77)$$

The coefficients $c_{i,g}^{*(k)}, c_{i,g}^{z,*(k)}$ are the updated coefficients $C^{*(k)}, C^{z*(k)}$ of (2.2.71) and (2.2.72) for each energy group g . The leakage coefficients were obtained from (2.2.46) and (2.2.50).

Using the node-averaged fluxes $\bar{\Phi}_1, \bar{\Phi}_2$ on the left hand side of (2.2.71) come from the end of the last outer iteration. The leakage terms are calculated from the *nos* surfaces of the node. The eigenvalue $k_{eff}^{(k)}$ of the outer iteration step (k) is estimated from

$$k_{eff}^{(k)} = \frac{\sum_{n=1}^N \left(\sum_{g=1}^2 v \Sigma_{f,g}^n \bar{\Phi}_g^{n,(k)} \right)^2}{\sum_{n=1}^N \left(\left[\sum_{g=1}^2 v \Sigma_{f,g}^n \bar{\Phi}_g^{n,(k)} \right] \cdot \left[\sum_{g=1}^2 v \Sigma_{f,g}^n \bar{\Phi}_g^{n,(k-1)} \right] \right)} \quad (2.2.78)$$

with the total number of nodes N .

A Chebychev extrapolation scheme is applied to accelerate the outer iteration in all cases.

In the case of Cartesian geometry, the solution technique is the same. Instead of the equations for the hexagonal plane and the axial direction, respective equations have to be applied for each direction x, y, z , which are of the same type as for the axial direction z in the hexagonal- z geometry.

2.3 Steady-State Case with External Source

If a steady-state distribution is to be calculated for a given source, the eigenvalue k_{eff} of the homogeneous equation has to be calculated first. The solution of the inhomogeneous equation exists in the case $k_{eff} < 1$. If this condition is fulfilled, the inhomogeneous problem can be solved. The following option for an external neutron source is implemented in the code. It is assumed that only fast neutrons are emitted. The distribution of the neutrons inside the nodes is assumed to be spatially constant. It varies only from node to node. Thus the source contributes to the right hand side of first equation (2.2.73) with $k_{eff} = 1$:

$$\sum_{l=1}^{nos} (J_{1,l}^{+n(k+1)} - J_{1,l}^{-n(k+1)}) + \Sigma_r^n \bar{\Phi}_1^{n(k+1)} = \sum_{g=1}^2 v \Sigma_{f,g}^n \bar{\Phi}_g^{n*(k)} + S_{ext}^n \quad (2.3.1)$$

The other equations have the same form as (2.2.71) to (2.2.77) of the homogeneous problem with $k_{eff} = 1$. Thus the solution procedure of this problem is slightly modified compared to the homogeneous case.

2.4 Transient Case

In the transient case the precursor distributions inside a node are described by polynomial expansions. The node-averaged precursors and the coefficients of their polynomial expansion at the initial state at $t = 0$ are obtained from the coefficients $c_{g,i}$ of the flux expansions.

$$\bar{C}_j^n(0) = \frac{1}{k_{eff}} \sum_{g=1}^2 \beta_{g,j} v_{\Sigma_{f,g}}^n(0) \bar{\Phi}_g^n(0) \quad (2.4.1)$$

$$c_{pre,j,i}^n(0) = \frac{1}{k_{eff}} \sum_{g=1}^2 \beta_{g,j} v_{\Sigma_{f,g}}^n(0) c_{g,i}^n(0) \quad \text{for } i=1,\dots,5. \quad (2.4.2)$$

$$c_{pre,j,i}^{z,n}(0) = \frac{1}{k_{eff}} \sum_{g=1}^2 \beta_{g,j} v_{\Sigma_{f,g}}^n(0) c_{g,i}^{z,n}(0) \quad \text{for } i=1,2. \quad (2.4.3)$$

$$j = 1, 2, \dots, M$$

Based on the results at the time $t - \Delta t$ the following outer-iteration scheme of the node-averaged fluxes is obtained from equations (2.1.14) and (2.1.15) for the $(k+1)$ outer iteration step:

$$\begin{aligned} \sum_{l=1}^{nos} (J_{1,l}^{+n(k+1)}(t) - J_{1,l}^{-n(k+1)}(t)) + \left[\Sigma_r^n(t) + \frac{1 + \Omega^n \Delta t}{v_1^n \Delta t} \right] \bar{\Phi}_1^{n(k+1)}(t) = \\ \frac{1}{k_{eff}} \sum_{g=1}^2 \left(1 - \sum_{j=1}^M \beta_{g,j} \delta_j^n \right) v_{\Sigma_{f,g}}^n(t) \bar{\Phi}_g^{n*(k)}(t) + \sum_{j=1}^M \lambda_j^n \bar{C}_j^n(t - \Delta t) \exp(-\lambda_j^n \Delta t) \\ + \frac{\exp(\Omega^n \Delta t)}{v_1^n \Delta t} \cdot \bar{\Phi}_1^n(t - \Delta t) + \bar{S}_{ext}^n \end{aligned} \quad (2.4.4)$$

and

$$\begin{aligned} \sum_{l=1}^{nos} (J_{2,l}^{+(k+1)}(t) - J_{2,l}^{-(k+1)}(t)) + \left[\Sigma_a^n(t) + \frac{1 + \Omega^n \Delta t}{v_2^n \Delta t} \right] \bar{\Phi}_2^{n(k+1)}(t) = \\ \Sigma_s^n(t) \bar{\Phi}_1^{n*(k+1)}(t) + \frac{\exp(\Omega^n \Delta t)}{v_2^n \Delta t} \cdot \bar{\Phi}_2^n(t - \Delta t) \end{aligned} \quad (2.4.5)$$

The terms of right hand sides of equations (2.4.4) and (2.4.5) are expanded only by the polynomials. Therefore $\bar{\Phi}_g^{n*(k)}(t)$ is described by the updated polynomial coefficients of the last outer iteration k and $\bar{\Phi}_1^{n*(k+1)}(t)$ is represented by the updated coefficient of the fast group of the outer iteration $(k+1)$.

The equations (2.4.4) and (2.4.5) represent the equations for all coefficients. As in the steady state, the node-averaged fluxes are considered instead of the coefficients c_0 and c_0^z . Like the steady state, the respective equations of the higher coefficients are obtained by transverse integration on the equations (2.1.9). In the case of hexagonal fuel assemblies, two-dimensional equations are derived for the hexagonal plane and an one-dimensional equation for the axial direction. In the case of Cartesian geometry three one-dimensional equations were obtained for

the three directions x, y, z . For the higher coefficients of the polynomial expansion, the assumption of an exponential behaviour within the time interval Δt is applied instead of the time step integration. This approach reduces the computer-memory size occupied by the code.

$$\begin{aligned}
-D_1^n(t) \left(\frac{\partial^2}{\partial x^2} + \frac{\partial^2}{\partial y^2} \right) \hat{\Phi}_1^n(x, y, t) + \left(\Sigma_r^n(t) + \frac{\Omega^n}{v_1} \right) \hat{\Phi}_1^n(x, y, t) = \sum_{j=1}^M \lambda_j^n \hat{C}_j^n(x, y, t - \Delta t) \exp(-\lambda_j^n \Delta t) \\
+ \frac{1}{k_{eff}} \sum_{g=1}^2 \left(1 - \sum_{j=1}^M \beta_{g,j}^n \delta_j^n \right) v_{\Sigma_{f,g}^n}(t) \hat{\Phi}_g^n(x, y, t) - \hat{L}_1^n(x, y, t)
\end{aligned}$$

and (2.4.6)

$$-D_2^n(t) \left(\frac{\partial^2}{\partial x^2} + \frac{\partial^2}{\partial y^2} \right) \hat{\Phi}_2^n(x, y, t) + \left(\Sigma_a^n(t) + \frac{\Omega^n}{v_2} \right) \hat{\Phi}_2^n(x, y, t) = \Sigma_s(t) \hat{\Phi}_1^n(x, y, t) - \hat{L}_2^n(x, y, t)$$

The one-dimensional equations for the radial-averaged flux $\hat{\Phi}(z)$ along the axial direction z are analogous

$$\begin{aligned}
-D_1^n(t) \frac{d^2}{dz^2} \hat{\Phi}_1^n(z, t) + \left(\Sigma_r^n(t) + \frac{\Omega^n}{v_1} \right) \hat{\Phi}_1^n(z, t) = \\
\frac{1}{k_{eff}} \sum_{g=1}^2 \left(1 - \sum_{j=1}^M \beta_{g,j}^n \delta_j^n \right) v_{\Sigma_{j,i}^n}(t) \hat{\Phi}_g^n(z, t) + \sum_{j=1}^M \lambda_j^n \hat{C}_j^n(z, t - \Delta t) \exp(-\lambda_j^n \Delta t) - \hat{L}_1^{z,n}(z, t)
\end{aligned}$$

(2.4.7)

$$-D_2^n(t) \frac{d^2}{dz^2} \hat{\Phi}_2^n(x, y, t) + \left(\Sigma_a^n(t) + \frac{\Omega^n}{v_2} \right) \hat{\Phi}_2^n(z, t) = \Sigma_s(t) \hat{\Phi}_1^n(z, t) - \hat{L}_2^{z,n}(z, t)$$

The following equations depend only on the higher order coefficients c , which are functions of time t .

$$\begin{aligned}
\left(\Sigma_r^n(t) + \frac{\Omega^n}{v_1} \right) c_{1,i}^n(t) = \sum_{j=1}^M \lambda_j^n c_{pre,j,i}^n(t - \Delta t) \exp(-\lambda_j^n \Delta t) + \\
\frac{1}{k_{eff}} \sum_{g=1}^2 \left(1 - \sum_{j=1}^M \beta_{g,j}^n \delta_j^n \right) v_{\Sigma_{f,g}^n}(t) c_{g,i}^n(t) - l_{1,i}^n(t)
\end{aligned}$$

(2.4.8)

$$\left(\Sigma_a^n(t) + \frac{\Omega^n}{v_2} \right) c_{2,i}^n(t) = \Sigma_s(t) c_{1,i}^n(t) - l_{2,i}^n(t)$$

and

$$\left(\Sigma_r^n(t) + \frac{\Omega^n}{v_1} \right) c_{1,i}^{z,n}(t) = \sum_{j=1}^M \lambda_j^n c_{pre,j,i}^{z,n}(t - \Delta t) \exp(-\lambda_j^n \Delta t) + \frac{1}{k_{eff}^n} \sum_{g=1}^2 \left(1 - \sum_{j=1}^M \beta_{g,j}^n \delta_j^n \right) v \Sigma_{f,g}^n(t) c_{g,i}^{z,n}(t) - l_{1,i}^{z,n}(t) \quad (2.4.9)$$

$$\left(\Sigma_2^n(t) + \frac{\Omega^n}{v_2} \right) c_{2,i}^{z,n}(t) = \Sigma_s^n(t) c_{1,i}^{z,n}(t) - l_{2,i}^{z,n}(t)$$

The inhomogeneous equations (2.4.4) through (2.4.9) are solved by fission-source iteration, in a similar way as the homogeneous steady-state equations described in chapter 2.2, which were also transformed into inhomogeneous equations.

2.5 Calculation of Power Densities

The feedback is caused by the dependency of neutron group constants by the thermal-hydraulic state of the reactor. It is calculated from the average values of power densities in each node. The average values of nuclear power densities at time t in a node n is given by

$$P^n(t) = \sum_{g=1}^2 \varepsilon_g^n \Sigma_{f,g}^n(t) \bar{\Phi}_g^n(t) \quad (2.5.1)$$

The energy release per fission ε_g^n is nearly independent from the energy of the incident neutron. Most part of the nuclear power is released in the fuel, but the so-called gamma heating of coolant in the LWR reactors can be considered by a portion of nuclear power which is released directly in the coolant. This splitting is considered in the thermal-hydraulic model.

2.6 The Poisoning in the Steady State

The contributions of the fission products ^{135}Xe and ^{149}Sm to the absorption cross sections $\Sigma_{c,g}^n$ in each node are calculated from their concentrations c_{Xe}^n and c_{Sm}^n

$$\Sigma_{c,g}^{n,pois} = \Sigma_{c,g}^n + c_{Xe}^n \sigma_{Xe,g}^n + c_{Sm}^n \sigma_{Sm,g}^n \quad (2.6.1)$$

and

$\sigma_{Xe,g}^n, \sigma_{Sm,g}^n$ - the effective microscopic cross sections of ^{135}Xe and ^{149}Sm .

Assuming equilibrium conditions in the steady state, the concentrations c_{Xe}^n and c_{Sm}^n of the fission product ^{135}Xe and ^{149}Sm together with the concentrations c_I^n and c_{Pm}^n of their precursors ^{135}I and ^{149}Pm are calculated by

$$c_I^n = \frac{\gamma_I^n \sum_{g=1}^2 \Sigma_{f,g}^n \bar{\Phi}_g^n}{\lambda_I}; \quad c_{Xe}^n = \frac{(\gamma_I^n + \gamma_{Xe}^n) \sum_{g=1}^2 \Sigma_{f,g}^n \bar{\Phi}_g^n}{\lambda_{Xe} + \sum_{g=1}^2 \sigma_{Xe,g}^n \bar{\Phi}_g^n} \quad (2.6.2)$$

and

$$c_{Pm}^n = \frac{\gamma_{Pm}^n \sum_{g=1}^2 \Sigma_{f,g}^n \bar{\Phi}_g^n}{\lambda_{Pm}}; \quad c_{Sm}^n = \frac{\gamma_{Pm}^n \sum_{g=1}^2 \Sigma_{f,g}^n \bar{\Phi}_g^n}{\sum_{g=1}^2 \sigma_{Sm,g}^n \bar{\Phi}_g^n} \quad (2.6.3)$$

with

$\gamma_I^n, \gamma_{Xe}^n, \gamma_{Pm}^n$ - effective yields of $^{135}I, ^{135}Xe$ and ^{149}Pm .

$\lambda_I, \lambda_{Xe}, \lambda_{Pm}$ - decay constants of $^{135}I, ^{135}Xe$ and ^{149}Pm .

The microscopic cross sections $\sigma_{Xe,g}^n, \sigma_{Sm,g}^n$ have to be included in the cross section library. Absorption cross sections of the thermal group exist only in some libraries, because the much lower microscopic cross section of the fast group may be neglected.

There are different possibilities for considering the fission product poisons in the calculations. The equilibrium concentrations of poisons can be written on files. Thus it is possible to read them from the file generated in a previous calculation. If this calculation was made before the shut-down of the reactor and a new calculation is to be performed for the next start-up phase, the decay of ^{149}Pm to ^{149}Sm can be taken into account.

2.7 Nodal Flux Reconstruction

To calculate the pin with the maximum power in selected assemblies, a two-dimensional flux reconstruction of the nodal flux can be made on the basis of the node homogenized cross sections. A superposition of this solution with the node pin powers obtained from the cell calculations can be performed.

The method of successive smoothing is applied for the reconstruction of the neutron flux in chosen assemblies [Fin90]. The neutron flux is reconstructed by an analytical solution of the two-dimensional diffusion equation in each layer of the assembly which is obtained by the following assumptions

- exponential behaviour of neutron fluxes during the time step
- distribution of delayed neutrons proportional to the prompt neutrons
- axial leakage described by the transversal buckling.

$$-D_1^n(t) \left(\frac{\partial^2}{\partial x^2} + \frac{\partial^2}{\partial y^2} \right) \Phi_{r,1}^n(x, y, t) + \left(\Sigma_1^n(t) + \frac{\Omega^n}{v_1} \right) \Phi_{r,1}^n(x, y, t) = \sum_{g=1}^2 v \Sigma_{f,g}^* \Phi_{r,g}^n(x, y, t) \quad (2.7.1)$$

$$-D_2^n(t) \left(\frac{\partial^2}{\partial x^2} + \frac{\partial^2}{\partial y^2} \right) \Phi_{r,2}^n(x, y, t) + \left(\Sigma_2^n(t) + \frac{\Omega^n}{v_2} \right) \Phi_{r,2}^n(x, y, t) = \Sigma_s(t) \Phi_{r,1}^n(x, y, t)$$

with

$$v \Sigma_{f,g}^{n*} = (1 - \beta_g^n) \frac{v \Sigma_{f,g}^n}{k_{eff}} + \sum_{j=1}^M \frac{\lambda_j^n \beta_{g,j}^n v \Sigma_{f,g}^n}{2 \sum_{g'=1} \beta_{g',j}^n v \Sigma_{f,g'}^n} C_j^n(t) \quad (2.7.2)$$

and

$$\Sigma_1^n(t) = \Sigma_r^n(t) + D_1^n(t) B_{z,1}^{n,2}$$

$$\Sigma_2^n(t) = \Sigma_a^n(t) + D_2^n(t) B_{z,2}^{n,2}$$

The transversal buckling of the node n between the axial co-ordinates z_0, z is given by

$$B_{z,g}^{n,2} = \frac{1}{D_g^n(t) \Phi_g^n a_z} (J_{g,z_1}^{+n} - J_{g,z_1}^{-n} + J_{g,z_0}^{+n} - J_{g,z_0}^{-n}) \quad (2.7.3)$$

Omitting the node index n and the time t , the solution of the two-dimensional diffusion equation is given by the approach

$$\Phi_{r,g}(\mathbf{r}_{xy}) = \chi_g^f \sum_{i=1}^{nop} [a_{c,i}^f \cos(\mathbf{B}_i^f \mathbf{r}_{xy}) + a_{s,i}^f \sin(\mathbf{B}_i^f \mathbf{r}_{xy})] + \chi_g^t \sum_{i=1}^{nop} [a_{c,i}^t \cosh(\mathbf{B}_i^t \mathbf{r}_{xy}) + a_{s,i}^t \sinh(\mathbf{B}_i^t \mathbf{r}_{xy})]. \quad (2.7.4)$$

The unknown coefficients $a_{c,i}^f, a_{s,i}^f, a_{c,i}^t, a_{s,i}^t$ have to be determined from the boundary conditions. Therefore the number of unknown coefficients depends on the number of conditions at the node boundary, which are taken into account. If the side-averaged fluxes and the corner point fluxes are used, $nop = 4$ for Cartesian geometry and $nop = 6$ for hexagonal geometry.

The magnitude of the vectors $\mathbf{B}_i^f, \mathbf{B}_i^t$ are obtained from the equations

$$\begin{aligned} (D_1 B^2 + \Sigma_1) \chi_1 &= v \Sigma_{f,1}^* \chi_1 + v \Sigma_{f,2}^* \chi_2 \\ (D_2 B^2 + \Sigma_2) \chi_2 &= \Sigma_s \chi_1 \end{aligned} \quad (2.7.5)$$

which were obtained by inserting the (2.7.4) in the equations (2.7.1).

The superscripts of the bucklings in equation (2.7.4) describe the two solutions of (2.7.5) with (f) for the fundamental solution and (t) for the transient mode. Considering fuel assemblies we obtain the fundamental solution with

$$B^2 \geq 0$$

described by the cos and sin functions. The transient mode is obtained from the solution with

$$B^2 < 0$$

and it is described by the cosh and sinh functions. In some cases the two solutions can have bucklings with $B^2 < 0$. The bucklings are calculated from the quadratic equation

$$B^2 = \frac{K_3}{2} \left(\pm \sqrt{1 + 4 \frac{K_4}{K_3}} - 1 \right) \quad (2.7.6)$$

with

$$\begin{aligned} K_3 &= \left(\frac{\Sigma_2}{D_2} + \frac{\Sigma_1 - v \Sigma_{f,1}^*}{D_1} \right)^2 \\ K_4 &= \frac{v \Sigma_{f,2}^* \Sigma_s - (\Sigma_1 - v \Sigma_{f,1}^*) \Sigma_2}{D_1 D_2} \end{aligned} \quad (2.7.7)$$

or

$$\begin{aligned} K_4 &= \frac{k_{r,\infty} - 1}{\frac{D_1}{\Sigma_1} \cdot \frac{D_2}{\Sigma_2}} \\ k_{r,\infty} &= \frac{v \Sigma_{f,1}^* + v \Sigma_{f,2}^* \frac{\Sigma_s}{\Sigma_2}}{\Sigma_1} \end{aligned} \quad (2.7.8)$$

The estimation of $k_{r,\infty}$ is similar to that of k-infinity, but it is done with the modified fission cross sections and the axial leakage is taken into account as an additional absorption in the cross sections Σ_1, Σ_2 . $k_{r,\infty}$ defines the type of the function in equation (2.7.4) via the buckling B^2 :

$$B^2 \geq 0 \quad \text{for} \quad k_{r,\infty} \geq 1$$

and

$$B^2 < 0 \quad \text{for} \quad k_{r,\infty} < 1 \quad (2.7.9)$$

Assuming $\chi_2 = 1$ for the two eigenvalues χ_1 is given by

$$\chi_1 = \frac{(D_2 B^2 + \Sigma_1)}{\Sigma_s} \quad (2.7.10)$$

Each direction of the bucklings B between 0 and 180 degrees gives a possible solution of the equation system. In the numerical estimation of bucklings, $B^2 = 0$ is avoided.

If $nop = 4$ (Cartesian geometry) or $nop = 6$ (hexagonal geometry) is used, the angles $0^\circ, 45^\circ, 90^\circ, 135^\circ$ or $0^\circ, 30^\circ, 60^\circ, 90^\circ, 120^\circ, 150^\circ$, respectively, are chosen to obtain continuously distributed directions within the node.

In the case of Cartesian geometry the corner-point values can be obtained by the application of a formula derived by Fischer and Finnemann in Ref. [Fis81]. Considering a corner in the middle of 4 nodes numbered by $i = 1, \dots, 4$ the corner-point flux of each node is obtained by assuming a linear expression for the flux in each one

$$\Phi_c(i) = \Phi_{s,1}(i) + \Phi_{s,2}(i) - \bar{\Phi}(i) \quad (2.7.11)$$

with $\Phi_{s,1}(i), \Phi_{s,2}(i)$ being the side-averaged fluxes of the assembly sides defining the corner.

The corner-point flux is determined as the average of the corner-point fluxes of the 4 assemblies:

$$\Phi_c = \frac{1}{4} \sum_{i=1}^4 \Phi_c(i) \quad (2.7.12)$$

In case of hexagonal geometry three assemblies are situated around a corner. The corner flux of one assembly is obtained by

$$\Phi_c(i) = \frac{1}{3} [2\Phi_{s,1}(i) + 2\Phi_{s,2}(i) - \bar{\Phi}(i)] \quad (2.7.13)$$

and

$$\Phi_c = \frac{1}{3} \sum_{i=1}^3 \Phi_c(i) \quad (2.7.14)$$

If the HEXNEM2 method is applied, the corner fluxes are given from the partial currents at the corners. Instead of geometrical weighting in equations (2.7.12) or (2.7.14) sometimes the diffusion coefficients are used. If the ADF are considered, the continuity of the heterogeneous fluxes has to be taken into account at the corners by slightly modified formulas.

Based on the flux expansion for $\Phi_{r,g}(\mathbf{r}_{xy})$ in equation (2.7.4) the reconstructed power distribution is computed for each axial layer by calculating the expansion coefficients from the

boundary conditions. A more detailed description of the method for hexagonal geometry developed by Hádék can be found in reference [Hád97].

The power distribution in each layer of the considered assembly (node n) is estimated from the flux distribution

$$P_r^n(\mathbf{r}_{xy}) = \sum_{g=1}^2 \varepsilon_g^n \Sigma_{f,g}^n \Phi_{r,g}^n(\mathbf{r}_{xy}) \quad (2.7.15)$$

The local power peak factor $f_{r,p}^{z_k}$ of each axial layer between z_{k-1} and z_k is given by

$$f_{r,p}^{z_k} = \frac{\max P_r^n(\mathbf{r}_{xy})}{\bar{P}_r^n} \quad (2.7.16)$$

where $\max P_r^n(\mathbf{r}_{xy})$ is the maximum value and \bar{P}_r^n the average value of the reconstructed power distribution. For the calculation of the hot channel of the assembly, described in section 5.4 the peak factor $f_{r,p}^{z_k}$ is multiplied by the nodal power and additional peak factors describing the peak factor of the pin powers of the cell calculation and/or technical uncertainties. It is also possible to multiply the normalized pin powers of the cell calculation with the pin powers of (2.7.15) and to estimate the maximum (2.7.16) by using these results. This option depends on whether these data are present in the used cross section library.

2.8 Reactivity Calculation and Adjoint Flux

2.8.1 Dynamic Reactivity

The dynamic reactivity during a transient is based on the description of the time-dependent neutron flux distribution $\Phi_g^n(\mathbf{r}, t)$ by a shape function $\Psi_g^n(\mathbf{r}, t)$ depending on space, energy group and time multiplied with an amplitude function $N(t)$ which depends on time only.

$$\Phi_g^n(\mathbf{r}, t) = N(t) \cdot \Psi_g^n(\mathbf{r}, t) \quad (2.8.1)$$

By inserting this approach in the time-dependent multigroup neutron diffusion equation (2.1.1), using (2.1.2), the following equations are obtained

$$\begin{aligned} \frac{\partial \Psi_1^n(\mathbf{r}, t)}{v_1^n \partial t} - \nabla D_1^n(t) \nabla \Psi_1^n(\mathbf{r}, t) + \left(\Sigma_r^n(t) + \frac{1}{v_1^n N(t)} \cdot \frac{dN(t)}{dt} \right) \Psi_1^n(\mathbf{r}, t) = \\ = \frac{1}{k_{eff}} \sum_{g=1}^2 (1 - \beta_g^n) v \Sigma_{f,g}^n(t) \Psi_g^n(\mathbf{r}, t) + \frac{1}{N(t)} \cdot \sum_{j=1}^M \lambda_j^n C_j^n(\mathbf{r}, t) + \frac{1}{N(t)} \cdot S_{ext}^n(\mathbf{r}) \end{aligned} \quad (2.8.2)$$

$$\frac{\partial \Psi_2^n(\mathbf{r}, t)}{v_2^n \partial t} - \nabla D_2^n(t) \nabla \Psi_2^n(\mathbf{r}, t) + \left(\Sigma_a^n(t) + \frac{1}{v_2^n N(t)} \cdot \frac{dN(t)}{dt} \right) \Psi_2^n(\mathbf{r}, t) = \Sigma_s^n(t) \Psi_1^n(\mathbf{r}, t)$$

$$\frac{\partial C_j^n(\mathbf{r}, t)}{\partial t} = \frac{N(t)}{k_{eff}} \sum_{g=1}^2 \beta_g^n v \Sigma_{f,g}^n(t) \Psi_g^n(\mathbf{r}, t) - \lambda_j^n C_j^n(\mathbf{r}, t)$$

The decay constants λ_j^n of the delayed neutron precursors do not strongly depend on the material in the different nodes n , so that core-averaged values $\bar{\lambda}_j$, as defined in section 2.8.4, can be used:

$$\frac{\partial C_j^n(\mathbf{r}, t)}{\partial t} = \frac{N(t)}{k_{eff}} \sum_{g=1}^2 \beta_{g,j}^n v \Sigma_{f,g}^n(t) \Psi_g^n(\mathbf{r}, t) - \bar{\lambda}_j C_j^n(\mathbf{r}, t) \quad (2.8.3)$$

The following procedure was used by A. F. Henry [Rad64] for deriving the point kinetic equations. Integration over space using weighting function $\mathbf{W}_g^n(\mathbf{r})$ and summation over the energy groups leads to.

$$\begin{aligned}
I \cdot \frac{dN(t)}{dt} = & N(t) \sum_{g=1}^2 \sum_n \int_{V_n} dV \cdot \mathbf{W}_g^n(\mathbf{r}) \left\{ \nabla D_g^n(t) \nabla \Psi_g^n(\mathbf{r}, t) - \Sigma_g^n(t) \Psi_g^n(\mathbf{r}, t) \right\} + \\
& N(t) \sum_n \int_{V_n} dV \cdot \left\{ \mathbf{W}_1^n(\mathbf{r}) \sum_{g'=1}^2 (1 - \beta_{g'}^n) \nu \Sigma_{f, g'}^n(t) \Psi_{g'}^n(\mathbf{r}, t) + \mathbf{W}_2^n(\mathbf{r}) \Sigma_s^n(t) \Psi_1^n(\mathbf{r}, t) \right\} + \\
& \sum_{j=1}^M \bar{\lambda}_j \sum_n \int_{V_n} dV \mathbf{W}_1^n(\mathbf{r}) C_j^n(\mathbf{r}, t) + \sum_n \int_{V_n} dV \mathbf{W}_1^n(\mathbf{r}) S_{ext}^n(\mathbf{r})
\end{aligned} \tag{2.8.4}$$

and

$$\sum_n \int_{V_n} \mathbf{W}_1^n(\mathbf{r}) \frac{\partial C_j^n(\mathbf{r}, t)}{\partial t} = N(t) \sum_n \int_{V_n} dV \mathbf{W}_1^n(\mathbf{r}) \sum_{g'=1}^2 \beta_{g'}^n \nu \Sigma_{f, g'}^n(t) \Psi_{g'}^n(\mathbf{r}, t) - \bar{\lambda}_j \sum_n \int_{V_n} \mathbf{W}_1^n(\mathbf{r}) C_j^n(\mathbf{r}, t)$$

$j = 1, \dots, M$

with

$$\Sigma_1^n(t) = \Sigma_r^n(t)$$

$$\Sigma_2^n(t) = \Sigma_a^n(t)$$

and the normalization integral I

$$I = \sum_{g=1}^2 \sum_n \int_{V_n} dV \cdot \mathbf{W}_g^n(\mathbf{r}) \frac{1}{\nu_g} \Psi_g^n(\mathbf{r}, t) \tag{2.8.5}$$

There is no restriction concerning the splitting the neutron flux in the amplitude and the shape function in (2.8.1). Therefore the additional requirement that the normalization integral I is constant during time evolution is introduced, i. e.

$$\frac{dI}{dt} = 0 \tag{2.8.6}$$

No physical assumption is required with (2.8.6), but considering the case that the shape function is independent on time, $N(t)$ represents the point kinetic amplitude. The following generalized point kinetic equations are obtained for $N(t)$

$$\frac{dN(t)}{dt} = \frac{\rho(t) - \beta_{eff}(t)}{\bar{l}(t)} N(t) + \sum_{j=1}^M \bar{\lambda}_j \bar{C}_j(t) + \bar{S} \tag{2.8.7}$$

$$\frac{d\bar{C}_j(t)}{dt} = \frac{\beta_{eff,j}(t)}{l(t)} N(t) - \bar{\lambda}_j \bar{C}_j(t) \quad \text{with} \quad \beta_{eff}(t) = \sum_{j=1}^M \beta_{eff,j}(t)$$

The averaged yields of delayed neutrons $\beta_{eff,j}(t)$, the averaged prompt neutron lifetime $l(t)$ are given by

$$\beta_{eff,j}(t) = \left[\sum_n \int_{V_n} dV \cdot \mathbf{W}_1^n(\mathbf{r}) \sum_{g'=1}^2 v \Sigma_{f,g'}^n(t) \Psi_{g'}^n(\mathbf{r}, t) \right]^{-1} \cdot \sum_n \int_{V_n} dV \mathbf{W}_1^n(\mathbf{r}) \sum_{g'=1}^2 \beta_{g'}^n v \Sigma_{f,g'}^n(t) \Psi_{g'}^n(\mathbf{r}, t)$$

$$l(t) = I \cdot \left[\sum_n \int_{V_n} dV \cdot \mathbf{W}_1^n(\mathbf{r}) \sum_{g'=1}^2 v \Sigma_{f,g'}^n(t) \Psi_{g'}^n(\mathbf{r}, t) \right]^{-1} \quad (2.8.8)$$

The dynamic reactivity $\rho(t)$ is obtained

$$\rho(t) = \left[\sum_n \int_{V_n} dV \cdot \mathbf{W}_1^n(\mathbf{r}) \sum_{g'=1}^2 v \Sigma_{f,g'}^n(t) \Psi_{g'}^n(\mathbf{r}, t) \right]^{-1} \left[\sum_{g=1}^2 \sum_n \int_{V_n} dV \cdot \mathbf{W}_g^n(\mathbf{r}) \left\{ \nabla D_g^n(t) \nabla \Psi_g^n(\mathbf{r}, t) \right\} \right.$$

$$\left. - \sum_n \int_{V_n} dV \left\{ \sum_{g=1}^2 \mathbf{W}_g^n(\mathbf{r}) \Sigma_g^n(t) \Psi_g^n(\mathbf{r}, t) - \mathbf{W}_1^n(\mathbf{r}) \sum_{g'=1}^2 v \Sigma_{f,g'}^n(t) \Psi_{g'}^n(\mathbf{r}, t) - \mathbf{W}_2^n(\mathbf{r}) \Sigma_s^n(t) \Psi_1^n(\mathbf{r}, t) \right\} \right] \quad (2.8.9)$$

The averaged precursor densities $\bar{C}_j(t)$ and the averaged source \bar{S} are defined by

$$\bar{C}_j(t) = \frac{1}{I} \sum_n \int_{V_n} \mathbf{W}_1^n(\mathbf{r}) C_j^n(\mathbf{r}, t)$$

$$\bar{S} = \frac{1}{I} \sum_n \int_{V_n} dV \mathbf{W}_1^n(\mathbf{r}) S_{ext}^n(\mathbf{r}) \quad (2.8.10)$$

2.8.2 Adjoint Flux as Weighting Function

Using the steady state adjoint group fluxes as weighting function, the reactivity can be calculated from changes of the neutron physical constants. Firstly the adjoint fluxes of the steady-state are calculated by the procedure used for the calculation of the normal flux. The adjoint equations are derived from the steady-state flux equations (2.2.1)

$$-\nabla D_1^n(0) \nabla \Phi_1^n(\mathbf{r}) + \Sigma_1^n(0) \Phi_1^n(\mathbf{r}) = \frac{1}{k_{eff}} \sum_{g=1}^2 v \Sigma_{f,g}^n(0) \Phi_g^n(\mathbf{r})$$

$$-\nabla D_2^n(0) \nabla \Phi_2^n(\mathbf{r}) + \Sigma_2^n(0) \Phi_2^n(\mathbf{r}) = \Sigma_s^n(0) \Phi_1^n(\mathbf{r}) \quad (2.8.11)$$

The adjoint equations have the following form

$$\begin{aligned} -\nabla D_1^n(0) \nabla \Phi_1^{\dagger n}(\mathbf{r}) + \Sigma_1^n(0) \Phi_1^{\dagger n}(\mathbf{r}) &= \frac{\nu \Sigma_{f,1}^n(0)}{k_{eff}} \Phi_1^{\dagger n}(\mathbf{r}) + \Sigma_s^n(0) \Phi_2^{\dagger n}(\mathbf{r}) \\ -\nabla D_2^n(0) \nabla \Phi_2^{\dagger n}(\mathbf{r}) + \Sigma_2^n(0) \Phi_2^{\dagger n}(\mathbf{r}) &= \frac{\nu \Sigma_{f,2}^n(0)}{k_{eff}} \Phi_1^{\dagger n}(\mathbf{r}) \end{aligned} \quad (2.8.12)$$

In the DYN3D code the adjoint equations are solved by the method used for the normal neutron flux. For this purpose, the cross sections are redefined

$$\begin{aligned} \nu \Sigma'_{f,1} &= \frac{\nu \Sigma_{f,1}^n(0)}{k_{eff}} \\ \nu \Sigma'_{f,2} &= \Sigma_s^n(0) \\ \Sigma'_s &= \frac{\nu \Sigma_{f,2}^n(0)}{k_{eff}} \end{aligned} \quad (2.8.13)$$

The adjoint equation is of the same type as the homogeneous steady-state equation with the artificial eigenvalue α instead of k_{eff}

$$\begin{aligned} -\nabla D_1^n(0) \nabla \Phi_1^{\dagger n}(\mathbf{r}) + \Sigma_1^n(0) \Phi_1^{\dagger n}(\mathbf{r}) &= \frac{1}{\alpha} (\nu \Sigma'_{f,1} \Phi_1^{\dagger n}(\mathbf{r}) + \nu \Sigma'_{f,2} \Phi_2^{\dagger n}(\mathbf{r})) \\ -\nabla D_2^n(0) \nabla \Phi_2^{\dagger n}(\mathbf{r}) + \Sigma_2^n(0) \Phi_2^{\dagger n}(\mathbf{r}) &= \Sigma'_s \Phi_1^{\dagger n}(\mathbf{r}) \end{aligned} \quad (2.8.14)$$

Instead of (2.2.57) the adjoint equations have to fulfil the adjoint boundary conditions

$$J_{s,i,1}^{\dagger-} = R_{11}^s J_{s,i,1}^{\dagger+} + R_{21}^s J_{s,i,2}^{\dagger+}$$

and

$$J_{s,i,2}^{\dagger-} = R_{22}^s J_{s,i,2}^{\dagger+} \quad (2.8.15)$$

Considering the HEXNEM2 method, adjoint boundary conditions at the corner points are derived in a similar way.

If assembly discontinuity factors are considered, the adjoint fluxes are continuous at the interfaces. The adjoint current is discontinuous like the relation between the currents of the adjoint heterogeneous $\bar{J}_{het}^{\dagger s}$ and the adjoint homogeneous calculation $\bar{J}_{hom}^{\dagger s}$

$$\frac{1}{f^s} = \frac{\bar{J}_{het}^{\dagger s}}{\bar{J}_{hom}^{\dagger s}} \quad (2.8.16)$$

with the same assembly discontinuity factor as in (2.2.68). The interface conditions of the adjoint nodal calculation are derived from the condition of continuous current of the heterogene-

ous case.

Solving the adjoint equation after the calculation of the normal steady-state flux and k_{eff} yields the adjoint eigenvalue α is near to 1.0. Deviations are the result of approximations made in the same way as in the normal flux calculation.

The steady-state adjoint flux $\Phi_g^{\dagger n}(\mathbf{r})$ is introduced for the weighting function $\mathbf{W}_g^n(\mathbf{r})$ in the expressions (2.8.5), (2.8.8), and (2.8.9). The shape function $\Psi_g^n(\mathbf{r}, t)$ occurring in the numerator and the denominator can be replaced by the flux $\Phi_g^n(\mathbf{r}, t)$ in (2.8.8) and (2.8.9). The following expression for the reactivity is obtained after substitution, integration and algebra

$$\begin{aligned} \rho(t) = & \left[\sum_n \int_{V_n} dV \cdot \Phi_1^{\dagger n}(\mathbf{r}) \sum_{g'=1}^2 v \Sigma_{f,g'}^n(t) \Phi_{g'}^n(\mathbf{r}, t) \right]^{-1} \left[- \sum_{g=1}^2 \sum_n \int_{V_n} dV \nabla \Phi_g^{\dagger n}(\mathbf{r}) \delta D_g^n(t) \nabla \Phi_g^n(\mathbf{r}, t) \right. \\ & - \sum_n \int_{V_n} dV \sum_{g=1}^2 \Phi_g^{\dagger n}(\mathbf{r}) \delta \Sigma_g^n(t) \Phi_g^n(\mathbf{r}, t) \\ & \left. + \sum_n \int_{V_n} dV \left\{ \Phi_1^{\dagger n}(\mathbf{r}) \cdot \sum_{g'=1}^2 \delta v \Sigma_{f,g'}^n(t) \Phi_{g'}^n(\mathbf{r}, t) + \Phi_2^{\dagger n}(\mathbf{r}) \delta \Sigma_s^n(t) \Phi_1^n(\mathbf{r}, t) \right\} \right] \end{aligned} \quad (2.8.17)$$

with the following changes of cross sections and diffusion constants

$$\begin{aligned} \delta \Sigma_g^n(t) &= \Sigma_g^n(t) - \Sigma_g^n(0) \\ \delta D_g^n(t) &= D_g^n(t) - D_g^n(0) \end{aligned} \quad (2.8.18)$$

The expression of reactivity known from perturbation theory is obtained, which is valid for small changes of the flux shape. In order to reduce computer memory needed by the code, the integrals are calculated approximately. Most of the terms in (2.8.17) are estimated by using node-averaged fluxes and adjoint fluxes. In the leakage term in (2.8.17), the gradients are replaced by the product of the node-averaged values

$$\nabla \Phi_g^{\dagger n}(\mathbf{r}) \cdot \nabla \Phi_g^n(\mathbf{r}, t) \approx \overline{\nabla \Phi_g^{\dagger n}(\mathbf{r})} \cdot \overline{\nabla \Phi_g^n(\mathbf{r}, t)} \quad (2.8.19)$$

Such node-averaged values are approximated by

$$\frac{1}{V_n} \int_{V_n} dV \nabla \Phi_g^{\dagger n}(\mathbf{r}) = \frac{1}{V_n} \oint_{A_n} dA \Phi_g^{\dagger n}(\mathbf{r}) \approx \frac{1}{V_n} \sum_i e_i A_i^n \Phi_{g,i}^{\dagger n}, \quad (2.8.20)$$

with the surfaces A_i^n of the nodes V_n and the normal vectors \mathbf{e}_i , $\Phi_{g,i}^{\dagger n}$ being the surface-averaged adjoint fluxes. Applying this procedure for the gradient of the time-dependent flux

$\nabla\Phi_g^n(\mathbf{r}, t)$, the leakage term can be approximated by

$$L = -\sum_{g=1}^2 \sum_n \int_{V_n} dV \nabla\Phi_g^{\dagger n}(\mathbf{r}) \delta D_g^n(t) \nabla\Phi_g^n(\mathbf{r}, t) \quad (2.8.21)$$

$$\approx -\sum_{g=1}^2 \sum_n \frac{1}{V_n} \delta D_g^n(t) \sum_i \sum_j (\mathbf{e}_i \cdot \mathbf{e}_j) A_i^n A_j^n \Phi_{g,i}^{\dagger n} \Phi_{g,j}^n(t) ,$$

with $\Phi_1^n(\mathbf{r}, t)$ representing the surface-averaged time-dependent fluxes.

The fluxes at the radial node faces are numbered counter clockwise starting with $i = 1$ in x -direction. The bottom and top of faces are specified by the indices z_0 and z_1 . Thus, the leakage term of a hexagonal node takes the form

$$L = -\sum_{g=1}^2 \sum_n \delta D_g^n \left\{ \frac{\sqrt{3} \cdot d^2}{2\Delta z} \cdot (\Phi_{g,z_1}^{\dagger n} - \Phi_{g,z_0}^{\dagger n}) \cdot (\Phi_{g,z_1}^n(t) - \Phi_{g,z_0}^n(t)) \quad (2.8.22)$$

$$+ \frac{\Delta z}{3\sqrt{3}} \cdot [(\Phi_{g,1}^{\dagger n} - \Phi_{g,4}^{\dagger n}) \cdot (2\Phi_{g,1}^n(t) + \Phi_{g,2}^n(t) - \Phi_{g,3}^n(t) - 2\Phi_{g,4}^n(t) - \Phi_{g,5}^n(t) + \Phi_{g,6}^n(t))$$

$$+ (\Phi_{g,2}^{\dagger n} - \Phi_{g,5}^{\dagger n}) \cdot (2\Phi_{g,2}^n(t) + \Phi_{g,3}^n(t) - \Phi_{g,4}^n(t) - 2\Phi_{g,5}^n(t) - \Phi_{g,6}^n(t) + \Phi_{g,1}^n(t))$$

$$+ (\Phi_{g,3}^{\dagger n} - \Phi_{g,6}^{\dagger n}) \cdot (2\Phi_{g,3}^n(t) + \Phi_{g,4}^n(t) - \Phi_{g,5}^n(t) - 2\Phi_{g,6}^n(t) - \Phi_{g,1}^n(t) + \Phi_{g,2}^n(t))] \right\}$$

In case of Cartesian geometry, the following expression is obtained

$$L = -\sum_{g=1}^2 \sum_n \delta D_g^n \left\{ \frac{\Delta x \cdot \Delta y}{\Delta z} \cdot (\Phi_{g,z_1}^{\dagger n} - \Phi_{g,z_0}^{\dagger n}) \cdot (\Phi_{g,z_1}^n(t) - \Phi_{g,z_0}^n(t)) \right.$$

$$+ \frac{\Delta y \Delta z}{\Delta x} \cdot (\Phi_{g,1}^{\dagger n} - \Phi_{g,3}^{\dagger n}) \cdot (\Phi_{g,1}^n(t) - \Phi_{g,3}^n(t)) \quad (2.8.23)$$

$$\left. + \frac{\Delta x \Delta z}{\Delta y} \cdot (\Phi_{g,2}^{\dagger n} - \Phi_{g,4}^{\dagger n}) \cdot (\Phi_{g,2}^n(t) - \Phi_{g,4}^n(t)) \right\}$$

The surface-averaged fluxes can be calculated from the partial currents at the node surface according to relations (2.2.24) by

$$\Phi_{g,i}^{\dagger n} = 2(J_{g,i}^{+\dagger n} + J_{g,i}^{-\dagger n})$$

$$\Phi_{g,j}^n(t) = 2(J_{g,j}^{+n}(t) + J_{g,j}^{-n}(t)) \quad (2.8.24)$$

2.8.3 Calculation of the Different Reactivity Contributions

For the calculation of certain reactivity effects, respective changes in the two group diffusion parameters have to be separated into single effects. The dependence of the parameters has the general form

$$\Sigma_g^n(t) = \Sigma_g^n(T_F^n, T_M^n, \rho_M^n, c_B^n, z_{CR}^n) \quad (2.8.25)$$

with the nodal values of fuel temperature T_F^n , moderator temperature T_M^n , moderator density ρ_M^n , boron concentration c_B^n and control rod position z_{CR}^n .

The dependence of the two group diffusion parameters on these quantities is related to the given data library. Therefore the dependence cannot be described generally in the form

$$\delta\Sigma_g^n(t) = \delta\Sigma_g^n(\delta T_F^n) + \delta\Sigma_g^n(\delta T_M^n) + \delta\Sigma_g^n(\delta\rho_M^n) + \delta\Sigma_g^n(\delta c_B^n) + \delta\Sigma_g^n(\delta z_{CR}^n)$$

The changes of the group diffusion parameters are split in

$$\begin{aligned} \delta\Sigma_g^n(t) &= \Sigma_g^n(T_F^n, T_M^n, \rho_M^n, c_B^n, z_{CR}^n) - \Sigma_g^n(T_{F_0}^n, T_{M_0}^n, \rho_{M_0}^n, c_{B_0}^n, z_{CR_0}^n) = \\ &\Sigma_g^n(T_F^n, T_M^n, \rho_M^n, c_B^n, z_{CR}^n) - \Sigma_g^n(T_{F_0}^n, T_M^n, \rho_M^n, c_B^n, z_{CR}^n) + \\ &\Sigma_g^n(T_{F_0}^n, T_M^n, \rho_M^n, c_B^n, z_{CR}^n) - \Sigma_g^n(T_{F_0}^n, T_{M_0}^n, \rho_M^n, c_B^n, z_{CR}^n) + \\ &\Sigma_g^n(T_{F_0}^n, T_{M_0}^n, \rho_M^n, c_B^n, z_{CR}^n) - \Sigma_g^n(T_{F_0}^n, T_{M_0}^n, \rho_{M_0}^n, c_B^n, z_{CR}^n) + \\ &\Sigma_g^n(T_{F_0}^n, T_{M_0}^n, \rho_{M_0}^n, c_B^n, z_{CR}^n) - \Sigma_g^n(T_{F_0}^n, T_{M_0}^n, \rho_{M_0}^n, c_{B_0}^n, z_{CR}^n) + \\ &\Sigma_g^n(T_{F_0}^n, T_{M_0}^n, \rho_{M_0}^n, c_{B_0}^n, z_{CR}^n) - \Sigma_g^n(T_{F_0}^n, T_{M_0}^n, \rho_{M_0}^n, c_{B_0}^n, z_{CR_0}^n) \end{aligned} \quad (2.8.26)$$

The five parts at the right hand side of (2.8.26) represent the changes of the group diffusion parameters versus T_F^n , T_M^n , ρ_M^n , c_B^n and z_{CR}^n , compared to the initial critical reactor state. These parts are used in equations (2.8.17) and (2.8.18) for the calculation of different reactivity effects.

2.8.4 Calculation of Reactivity by Inverse Point Kinetics

Based on the last equation of (2.8.2) and (2.8.3) the averaged decay constants $\bar{\lambda}_j$ can be calculated by

$$\frac{1}{\bar{\lambda}_j} = \frac{\sum_n \int dV \Phi_1^n(\mathbf{r}) \cdot \frac{1}{v_n} \sum_{g'=1}^2 \beta_{g'}^n v \Sigma_{f,g'}^n(0) \Phi_{g'}^n(\mathbf{r}, 0)}{\sum_n \int dV \Phi_1^n(\mathbf{r}) \sum_{g'=1}^2 \beta_{g'}^n v \Sigma_{f,g'}^n(0) \Phi_{g'}^n(\mathbf{r}, 0)} \quad (2.8.27)$$

where adjoint fluxes are used as weighting functions. The integration over the nodes is replaced by using the node-averaged values for flux and adjoint flux. The averaged values for $\beta_{eff,j} = \beta_{eff,j}(0)$ and $l = l(0)$, calculated from equations (2.8.8) by using node-averaged fluxes, are assumed to be time-independent. Introducing a constant α by

$$\alpha = \frac{\beta_{eff}}{l} \quad (2.8.28)$$

and describing the reactivity $\rho(t)$ in units of β_{eff}

$$\rho(t) \rightarrow \frac{\rho(t)}{\beta_{eff}} \quad (2.8.29)$$

the point kinetic equations take the form

$$\frac{d}{dt}N(t) = \alpha \cdot (\rho(t) - 1)N(t) + \sum_{j=1}^M \bar{\lambda}_j \bar{C}_j(t) + \bar{S} \quad (2.8.30)$$

$$\frac{d}{dt}\bar{C}_j(t) = \frac{\beta_{eff}}{l}N(t) - \bar{\lambda}_j \bar{C}_j(t)$$

The time-dependent flux averaged over the core

$$F(t) = \frac{\sum_n V_n \cdot \sum_{g=1}^2 \Phi_g^n(t)}{\sum_n V_n} \quad (2.8.31)$$

is used for the flux amplitude $N(t)$. In a steady state, the averaged delayed neutron precursors \bar{C}_j are obtained from

$$\bar{C}_j(0) = \frac{1}{\bar{\lambda}_j} \cdot \frac{\beta_{eff,j}}{l} F(0) \quad (2.8.32)$$

If a constant source is present in the steady-state and the reactor is subcritical with $k_{eff} < 1$, the strength \bar{S} of the source can be calculated from the subcriticality by

$$\bar{S} = \alpha \frac{1 - k_{eff}}{k_{eff} \cdot \beta_{eff}} F(0) \quad (2.8.33)$$

with $F(0)$ obtained from the fluxes calculated of the steady state with given source.

The reactivity is determined by the solution of the inverse point kinetic equations (2.8.30) for $\rho(t)$ under the assumption of an exponential behaviour of the averaged fluxes (2.8.31) over the considered neutron kinetic time step Δt with the exponent $\bar{\omega}$ given by

$$\bar{\omega}(t) = \frac{1}{\Delta t} \ln\left(\frac{F(t)}{F(t - \Delta t)}\right) \quad (2.8.34)$$

The integration of the precursors leads to

$$\bar{\lambda}_j \bar{C}_j(t) = \bar{\lambda}_j \bar{C}_j(t - \Delta t) e^{-\bar{\lambda}_j \cdot \Delta t} + \frac{\beta_{eff,j}}{\beta_{eff}} \cdot \alpha \cdot \frac{\bar{\lambda}_j}{\bar{\lambda}_j + \bar{\omega}(t)} \cdot (F(t) - F(t - \Delta t)) \cdot e^{-\bar{\lambda}_j \cdot \Delta t} \quad (2.8.35)$$

The reactivity is given by

$$\rho(t) = 1 + \frac{\bar{\omega}(t)}{\alpha} - \frac{1}{\alpha F(t)} \cdot \left(\sum_{j=1}^M \bar{\lambda}_j \bar{C}_j(t) + \bar{S} \right) \quad (2.8.36)$$

The approximations applied in this derivation naturally will cause differences between the dynamic reactivity (2.8.17) and the point kinetic expression (2.8.36).

References Chapter 2

- [Bel70] G. I. Bell and S. Glasstone, „Nuclear Reactor Theory“, Van Nostrand Reinhold Company, New York (1970).
- [Fis81] H.-D. Fischer, H. Finnemann, „The nodal integration method-A diverse solver for neutron diffusion problems“, *Atomkernenergie-Kerntechnik* **39**, 229 - 236 (1981).
- [Cha95a] Chao, Y. A. and N. Tsoulfanidis; „Conformal Mapping and hexagonal Nodal Methods - I. Mathematical Foundation“, *Nucl, Sci Eng.* **121**, 202 (1995).
- [Fin90] Finnemann, H., Böer R., Böhm R., Müller R.; „Evaluation of Safety Parameters in Nodal Space-Time Nuclear reactor Analysis“, Specialists Meeting on Advanced Methods for Power Reactors, Cadarache, France, September, 10-14 (1990).
- [Gru89] Grundmann U.; Rohde, U.; „DYN3D/M2 - a Code for Calculation of Reactivity Transients in Cores with Hexagonal Geometry“. IAEA Technical Committee Meeting on Reactivity Initiated Accidents, Wien 1989 Report ZfK - 690, Rossendorf (1989).
- [Gru95] Grundmann, U. „The Code DYN3DR for Steady-State and Transient Analyses of Light Water Reactor Cores with Cartesian Geometry“, Report FZR-114, Rossendorf (1995).
- [Gru96b] Grundmann, U.; Rohde, U.; „DYN3D - A 3-dimensional Core Model for Steady State and Transient Analysis in Thermal Reactors“, Proceedings of the International Conference on the Physics of Reactors „PHYSOR 96“, Mito (Japan), J70 - J79, 16-20 Sept. (1996).

- [Gru99a] Grundmann U., Hollstein F., “A Two-Dimensional Intranodal Flux Expansion Method for Hexagonal Geometry”, *Nucl, Sci Eng.* **133**, 201 (1999).
- [Gru99b] Grundmann, U., „HEXNEM - A Nodal Method for the Solution of the Neutron Diffusion Equation in Hexagonal Geometry“, Proceedings of the M&C'99- Conference on Mathematics and Computations in Nuclear Applications, pp. 1086-1095, Madrid, September, 27 - 30 (1999).
- [Gru99c] Grundmann, U., „3D Nodal Expansion Method HEXNEM for the Solution of Neutron Diffusion Equation in Hexagonal Geometry“, Jahrestagung Kerntechnik'99, Karlsruhe, 18.- 20. Mai (1999).
- [Hád97] Hadek, J. and Grundmann, U., „Neutron Flux Reconstruction in a Hexagonal Cassette - Theory and Implementation into the Code DYN3D/H1.1“, *Nucleon*, No. 3, Nuclear Research Institute Rez (Czech Republic) (1997).
- [Rad64] Radkowsky, A., „Naval Reactor Physics Handbook“, Vol. 1, United States Atomic Energy Commission (1964).
- [Raj89] RAJIC, H. L. and OUGOUAG, A. M., „ILLICO: A Nodal Neutron Diffusion Method for Modern Computer Architectures“, *Nucl. Sci. Engng.*, **103**, 392 (1989).
- [Smi86] Smith, K. S., “Assembly Homogenization Techniques for Light Water Reactor Analysis”, *Progress in Nuclear Energy*, **17**, No. 3, pp 303-335 (1986).
- [Wag89] Wagner, M. R.; „Three-Dimensional Nodal Diffusion and Transport Methods for Hexagonal Geometry“, *Nucl. Sci. Engng* **103**, p. 377-391 (1989).

3 Treatment of Two-Group Neutronic Data

3.1 General Handling of Neutronic Data in DYN3D

For the solution of the neutron diffusion equations, the reactor core is divided into prism volume elements which are called nodes (cf. section 2.1). The base areas of these prisms are determined by the geometry of the (quadratic or hexagonal) fuel elements. The axial division of the core into layers defines the prism heights. For the neutronic calculation, a set of homogenized nuclear data is needed for each prism (node).

Homogenized two-group neutronic data, i. e. flux-weighted, node-averaged neutron diffusion coefficients, cross sections, assembly discontinuity factors (ADF), as well as data concerning reactor poisons and delayed neutrons are generated by cell codes and compiled in data libraries that can be used as DYN3D input. These libraries must contain sets of two-group neutronic data for the applied fuel-element types, characterized by U-235 enrichment and MOX or burnable absorber presence/absence. Data for the reactor-core reflectors that have been homogenized due to the respective fuel-element geometry, are also needed. Furthermore, the library has to comprise homogenized data for the presence of control rods in the core.

In DYN3D, the neutronic data have to be provided for the given fuel-element composition, nodal burnup b (see chapter 8), and the actual reactor operation conditions, characterized by the node-averaged values of

- fuel temperature: T_F ,
- moderator temperature: T_M ,
- moderator boron concentration: c_B ,
- moderator density: ρ_M ,

which are calculated by DYN3D itself (cf. chapter 5). Control rod presence or absence has also to be taken into account (see chapter 4).

The records in a library may contain either series of neutronic data, computed for combinations of step-wise varied values $b_l, \rho_{M,l}, T_{M,l}, T_{F,l}, c_{B,l}$ („data points“), and/or parametrized data that have been derived from data-point series. Using such a data basis, DYN3D calculates the actual nuclear data for all nodes.

3.2 Data Libraries for a KWU Konvoi Reactor

The data library, generated by TÜV Bavaria [Mit02] using the cell code CASMO [Cas95], contains seven sets of homogenized two-group neutronic data for four types of Siemens KWU fuel assemblies and three types of corresponding reflectors.

All data sets are built of a series of records each containing neutronic data, such as neutron diffusion coefficients, two-group cross sections, and data concerning reactor poisons and

delayed neutrons.

The first NBASE records of each fuel data set consist of basic data that have been generated for the nominal reactor operation conditions, in the absence of control rods, at NBASE burnup steps from zero burnup to maximum burnup. In the given library, the maximum burnup is $b_{\max} = 80 \text{ MWd/kgU}$. The number NBASE is counted by DYN3D itself. A fuel data set may contain any number NBASE of basic data records. However, the records have to be stored in the order of increasing burnup.

The nominal reactor operation conditions relevant for the data generation by the cell code were:

- fuel temperature: $T_{F,0} = 817.0 \text{ K}$,
- moderator temperature: $T_{M,0} = 584.8 \text{ K}$,
- moderator boron concentration: $c_{B,0} = 500 \text{ ppm}$,
- moderator density: $\rho_{M,0} = 0.70138 \text{ g/cm}^3$.

The following records, beginning at No. NBASE+1 contain data which have been produced by so-called „branch-off“ calculations, carried out under the condition that one of the four operation parameters was varied while the remaining three were kept at their nominal values. The ranges of parameter variation were:

- fuel temperature: (473 - 1700) K,
- moderator temperature: (503 - 615) K,
- moderator boron concentration: (0 - 2400) ppm,
- moderator density: (0.400 - 0.702) g/cm³.

All branch-off calculations have been carried out only for a reduced number NBRAN of burnup steps between zero and maximum burnup. Thus the NBRAN burnup values are a subset of the NBASE burnup values of the basic calculations ($\text{NBRAN} \leq \text{NBASE}$).

NBRAN is counted by DYN3D immediately after counting NBASE, i. e. for the first variation of an operation parameter. In case of the library for the KWU Konvoi PWR, the first variation is made for the boron concentration c_B , varied from the nominal value of 500 ppm down to 0 ppm, for NBRAN = 14 burnup states. Next, c_B is varied to 1000 and 2400 ppm. In the following, records with variations of the remaining operation parameters and the presence of control rods are provided. More branch-off records may be added to the data sets, if necessary. However, the number NBRAN as well as the NBRAN burnup values must be the same for all branch-off variations.

The reflector data sets have the same structure, but contain much less records, as there is no dependence on burnup and control rod presence. The records themselves are shorter, because nuclear fission does not happen within the reflector, so that neither reactor poisons nor delayed-neutron precursors are relevant in this region.

The data records described above contain neutronic data for combinations of step-wise varied values of burnup b and operation parameters ρ_M, T_M, T_F, c_B („data points“). In DYN3D however, the neutronic data are needed for any actual values of b, ρ_M, T_M, T_F, c_B that may occur in

the reactor-core nodes. For this reason, an interpolation or parametrization of the data is necessary.

An actual cross section, diffusion coefficient, or other neutronic parameter is represented in the form

$$\Sigma(b, \rho_M, T_M, T_F, c_B) = \Sigma_{base}(b) + \Delta\Sigma_{\rho_M}(b) + \Delta\Sigma_{T_M}(b) + \Delta\Sigma_{\sqrt{T_F}}(b) + \Delta\Sigma_{\rho_M \cdot c_B}(b) \quad (3.2.1)$$

$\Sigma_{base}(b)$ is the basic cross section at the nominal operation parameters and the actual burnup b . The following four terms represent the corrections respective to the actual thermal-hydraulic conditions. In case of control rod presence, another term has to be added:

$$\Sigma_{(CR)}(b, \rho_M, T_M, T_F, c_B) = \Sigma(b, \rho_M, T_M, T_F, c_B) + \Delta\Sigma_{CR}(b, \rho_M) \quad (3.2.2)$$

DYN3D calculates the base cross sections $\Sigma_{base}(b)$ for the actual burnup b from the first NBASE records of a data set by linear interpolation. The actual burnup must not exceed the maximum burnup provided in the data library, i. e. in case of burnup $b > b_{max}$ the DYN3D run will be stopped.

For the calculation of the additional terms in eqs. (3.2.1) and (3.2.2), a spline interpolation procedure is applied to the respective data available in the library. In the following, this procedure will be explained for the example of the moderator temperature term $\Delta\Sigma_{T_M}(b)$.

In a first step, DYN3D detects all given records related to a T_M -variation, where the remaining parameters are at their nominal values $\rho_{M,0}, T_{F,0}, c_{B,0}$, or show only small deviations from the nominal values (less than 0.01%). Among the NBRAN records of each variation, DYN3D finds the two records that belong to the two burnup values b_b and b_a , next to the actual nodal burnup, i. e. below (b_b) and above (b_a) the given burnup b . For all variations of T_M , the differences between the varied cross sections and the respective base cross section (at $\rho_{M,0}, T_{M,0}, T_{F,0}, c_{B,0}$) are calculated at the burnup value b_b . The differences $\Delta\Sigma_{T_{M,1}}(b_b)$, $\Delta\Sigma_{T_{M,2}}(b_b), \dots, \Delta\Sigma_{T_{M,n}}(b_b)$ are taken as data points for a spline interpolation [Mül00], the number of the resulting spline coefficients depending on the number of given data points. The same procedure is applied for the data records at the burnup b_a . Then the spline coefficients needed for the actual burnup b ($b_b < b < b_a$) are computed by linear interpolation.

Sets of spline coefficients are calculated in this way for the cross sections in each node, characterized by a special burnup value, and for each reactor operation parameter, including the control rod presence or absence. In case of fuel temperature, this spline interpolation is carried out for differences $\sqrt{T_F} - \sqrt{T_{F,0}}$ instead of $T_F - T_{F,0}$ (second last term in eq. (3.2.1)), because Doppler effect is essentially proportional to the average velocity v of nuclei interacting with neutrons ($v \sim \sqrt{kT_F}$). For this reason, better interpolation accuracy, due to better linearity, is

reached by applying the square roots. By the same token, $\rho_M \cdot c_B$ is used instead of c_B , as the relevant cross sections depend on the number of boron nuclei per node being proportional to the product $\rho_M \cdot c_B$.

The approximation by spline interpolation is sufficient. However if the actual operation parameters are rather far from the range covered by the given data points, some caution is necessary. For this reason, DYN3D always gives a warning in case of actual parameters being outside the range of the interpolation data points. In such cases, it may be safer to add to the library more data records covering a wider parameter range.

The nodal base cross sections $\Sigma_{base}(b)$ as well as the sets of spline coefficients for all five feedback terms in eqs. (1) and (2) are calculated only once at the start of a DYN3D calculation, because burnup practically remains constant during a transient. The spline coefficients are stored and later used to determine the neutronic data for the actual operation parameters, which may change dramatically in the course of a transient.

3.3 Parametrized Data Libraries for VVER Reactors

When applying a MAGRU library generated by KAB Berlin with the help of the cell code NESSEL [Agt88], the neutronic data needed in DYN3D are represented in the form

$$\Sigma(b, \rho_M, T_F, c_B) = \Sigma_{base} \cdot K_{\rho_M}(b) \cdot K_{T_F}(b) \cdot K_{c_B}(b) . \quad (3.3.1)$$

$\Sigma_{base}(b)$ are the basic cross sections at the nominal operation parameters $\rho_{M,0}, T_{M,0}, T_{F,0}, c_{B,0}$. They are interpolated for the actual burnup b from data points $\Sigma_{base}(b_l)$ given in the MAGRU library. The following terms represent the corrections respective to the actual thermal-hydraulic parameters such as

- moderator density:

$$K_{\rho_M}(b) = 1 + \alpha_{\rho_M}(b) \cdot (\rho_M - \rho_{M,0}) + \beta_{\rho_M}(b) \cdot (\rho_M - \rho_{M,0})^2, \quad (3.3.2)$$

$$\alpha_{\rho_M}(b) = a_{0,\rho_M} + a_{1,\rho_M} \cdot b + a_{2,\rho_M} \cdot b^2,$$

$$\beta_{\rho_M}(b) = d_{0,\rho_M} + d_{1,\rho_M} \cdot b + d_{2,\rho_M} \cdot b^2,$$

- fuel temperature:

$$K_{T_F}(b) = 1 + \alpha_{T_F}(b) \cdot (\sqrt{T_F} - \sqrt{T_M}), \quad (3.3.3)$$

$$\alpha_{T_F}(b) = a_{0,T_F} + a_{1,T_F} \cdot b + a_{2,T_F} \cdot b^2,$$

- boron concentration:

$$K_{c_B}(b) = 1 + \alpha_{c_B}(b) \cdot (c_B \rho_M - c_{B,0} \rho_{M,0}) + \beta_{c_B}(b) \cdot (c_B \rho_M - c_{B,0} \rho_{M,0})^2, \quad (3.3.4)$$

$$\alpha_{c_B}(b) = a_{0,c_B} + a_{1,c_B} \cdot b + a_{2,c_B} \cdot b^2,$$

$$\beta_{c_B}(b) = d_{0,c_B} + d_{1,c_B} \cdot b + d_{2,c_B} \cdot b^2.$$

The coefficients a_0, a_1, a_2 and d_0, d_1, d_2 have been computed by KAB on the basis of NESSEL branch-off calculations.

Similar data libraries have been generated for the VVER-440 and VVER-1000 by Energo-project Prague using the Russian code KASSETA [Tin93].

3.4 Multi-Dimensional-Table Libraries

In the data libraries described in the two sections above, linear interpolation is applied along the burnup steps, the micro-burnup calculation having been carried out at nominal reactor operation conditions. The operation parameters, such as moderator density and temperature, fuel temperature, and moderator boron concentration (ρ_M, T_M, T_F, c_B) have been varied independently from each other in branch-off calculations at certain burnup states. Independent variation means that three of the parameters are kept at their rated values while the remaining one is varied. The resulting data records have been used as a basis for nuclear-data parametrisation. This approach is widely applied in nuclear reactor technology. However, there are minor effects of neutron spectrum (changing due to parameter variation) that may perturb the supposed independence of operation-parameter influence on macroscopic cross sections. The problem may be tackled by producing multi-dimensional tables of data records, in which all possible combinations of parameter variation are considered. The actual nodal data can then be calculated by multi-dimensional interpolation. The accuracy of this method increases with the density of „data points“ produced by the cell-code calculations. Huge tables however will lead to immense computing times. So it makes sense to choose the data-point density in a way that matches the accuracy of both cell code (including its input data basis) and diffusion code (DYN3D).

A multi-dimensional-table library has been generated for VVER-440 fuel assemblies with the help of the code HELIOS [Hel00]. This library has been coupled to DYN3D by using linear multi-dimensional interpolation. However, there are no data neither for the complicated VVER-440 control assemblies, nor for the reflector region, so that the library cannot be used for reactor calculations so far.

3.5 Approximation-and-Interpolation Libraries

Another type of data library has been proposed in [Pet02, Pet03]. In this approach, homogenized two-group neutronic data are provided for DYN3D applying a combination of approximation by polynomials and interpolation in „two-dimensional“ tables.

Data are present for a number of reference burnup points b_i , depending on the actual assembly type. For each burnup point b_i , the following approximation is used to calculate a neutronic parameter Σ_i :

$$\Sigma_i = \Sigma_{i,0} + A_i^b X_b + B_i^b X_b^2 + A_i^p X_p + A_i^f X_f + B_i^f X_f^2 + C_i^f X_f^3, \quad (3.5.1)$$

where

$$\begin{aligned} X_b &= c_B - c_{B,0}, \\ X_p &= c_{Xe}, \\ X_f &= \sqrt{T_F} - \sqrt{T_{F,0}}, \end{aligned}$$

c_B and $c_{B,0}$ are the actual and reference volume concentrations (densities) of boron, c_{Xe} is the ^{135}Xe number density, and T_F and $T_{F,0}$ are the actual and reference fuel temperatures in Kelvin. The reference neutronic parameters $\Sigma_{i,0}$ and the corresponding approximation parameters in eq. (3.5.1) are provided in the library for the burnup points b_i (at a number of reference points of moderator temperature and density, discussed below). In order to calculate the value of a neutronic parameter Σ at the actual burnup b the following procedure is applied in DYN3D. First, the number i of the burnup subinterval, where b is located, is identified. Using eq. (3.5.1), the values Σ_{i-1} and Σ_i at the burnup-subinterval boundaries b_{i-1} and b_i are calculated. Then, the following interpolation is applied:

$$\Sigma = (1 - c)\Sigma_{i-1} + c\Sigma_i + [Q_{1i} + Q_{2i}(c + 1)]c(c - 1) \quad (3.5.2)$$

where

$$c = \frac{b - b_{i-1}}{b_i - b_{i-1}},$$

Q_{1i} and Q_{2i} are additional approximation coefficients to take into account the non-linear behaviour of Σ with respect to burnup (cubical interpolation).

The whole procedure described above is carried out for certain combinations of moderator temperature and density $T_{M,k}, \rho_{M,l}$ (reference points), near to the actual temperature and density T_M, ρ_M . Two-dimensional interpolation in the (T_M, ρ_M) -plane is applied to approximate the actual neutronic parameters $\Sigma(T_M, \rho_M)$. The respective interpolation coefficients were calculated, e.g. at 24 reference points, 4 over the temperature by 6 over the density, covering wide ranges, with respect to extreme values possibly reached during transients. The number and range of the reference points can be varied. Cubical interpolation is used over both moderator density and temperature.

Beside the standard homogenized two-group diffusion data for the fuel assemblies, assembly discontinuity factors (ADFs) are provided for the assembly sides and corners. Moreover, reference discontinuity factors (RDFs) are provided for the non-multiplying nodes, such as reflector regions and the special control assemblies of the VVER-440, because the conventional procedure for the calculation of diffusion parameters for these nodes would lead to crude errors in the nodal diffusion calculations. These reactor regions have a complicated heterogeneous structure, but in the nodal calculations they are treated as homogeneous. Furthermore, the diffusion approximation is not valid around the boundaries between non-multiplying nodes and fuel nodes, because the angular neutron-flux distribution is strongly anisotropic there. The effect of the RDFs is that the homogeneous diffusion solution becomes equivalent to the reference heterogeneous transport solution; hence they are called reference discontinuity factors. Both ADFs and RDFs are parametrized in the same way as described above, RDFs not depending on fuel properties.

For the axial (bottom and top) reflectors, RDFs have been calculated in one-dimensional geometry, i.e. in axial direction, as described in [Pet03]. They are hidden in the axial-reflector neutronic parameters. In case of radial reflectors and VVER-440 control assemblies, RDFs have been derived in two-dimensional geometry, as described in [Mit03]. The approach applying RDFs is to be preferred against the alternative of using albedos, because albedos are more sensitive to the properties of the fuel (enrichment, temperature) contained in the boundary nodes, to which they are applied. Furthermore, DYN3D does not allow using albedos at „inner boundaries“, such as represented by VVER-440 control assemblies.

Thus the DYN3D option reducing the homogenization and diffusion-theory errors, as described in section 2.2.5, can be fully applied with the present library. Moreover, the pin powers from the single-assembly lattice calculations are provided, in order to be combined with inner-nodal flux reconstruction (cf. section 2.7). The resulting DYN3D pin-power recovery can be applied in a realistic hot channel treatment, outlined in section 5.4. The accuracy of this approach has been validated against measurements in the Moscow V-1000 zero-power facility [Mit05].

Delayed-neutron data for the fuel, as described in [Pet02], are also given in parametrized form. These data are kept at their initial values during the transient, however, as the respective equations in chapter 2.4 are derived under the condition that the delayed-neutron data are independent of time.

Due to the above-described features and the wide parameter range for moderator temperature and density, as well as fuel temperature, this type of neutronic-data library proved to be much more adequate for VVER than the type presented in section 3.3. Using less accurate neutronic data would mean a wasting of the precision reached by DYN3D methods. The accuracy of DYN3D calculations using the type of data described in the present section has been demonstrated in validation and verification calculations for VVER [Mit03, Mit05]. Any library used in future as input for DYN3D calculations should have about the same data content as the one described here, and show similar or improved features to guarantee sufficient accuracy.

References Chapter 3

- [Agt88] Agthe, G., Schulz, G., „Beschreibung einer Bibliothek neutronenphysikalischer Weniggruppensdaten zur Berechnung des Betriebsverhaltens von WWER-440“, Report VEB Kombinat KAB, Berlin, 1988.
- [Cas95] CASMO-4, „A Fuel Assembly Burnup Program, Methodology“, Report Studsvik/ SOA-95/2, Studsvik, September 1995.
- [Hel00] HELIOS System 1.6 (Documentation), Studsvik Scandpower AS, May 2000.
- [Mit02] Mittag, S., Grundmann, U., Koch, R., Semmrich, J., „Erzeugung und Nutzung von Bibliotheken von Zwei-Gruppen-Diffusionsparametern zur Berechnung eines KWU-Konvoi-Reaktors mit dem Reaktordynamik-Programm DYN3D“, FZR-346, Rossendorf, April 2002, ISSN 1437-322X.
- [Mit03] Mittag, S., Petkov, P. T., Grundmann, U., „Discontinuity factors for non-multiplying material in two-dimensional hexagonal reactor geometry“, *Annals of Nuclear Energy* **30**/13, 1347-1364 (2003).
- [Mit05] Mittag, S., Grundmann, U., Weiß, F.-P., Petkov, P. T., Kaloinen, E., Keresztúri, A., Panka, I., Kuchin, A., Ionov, V., Powney, D., „Neutron-kinetic code validation against measurements in the Moscow V-1000 zero-power facility“, *Nuclear Engineering and Design* **235**, 485-506 (2005).
- [Mül00] Müller, E., Rechenzentrum des FZ Rossendorf, Private Communication, December 2000.
- [Pet02] Petkov, P. T., Christoskov, I. D., Kamenov, K., Antov, A., „Generation of a Library of Two-Group Diffusion and Kinetics Parameters for DYN3D“, Proc. of 12th Symposium of AER, Sunny Beach (Bulgaria), 22-28 September 2002.
- [Pet03] Petkov, P. T., Mittag, S., Christoskov, I. D., Kamenov, K., Antov, A., Bakalov, I., Wehner, H., „A new DYN3D library for the WWER-1000 reactors“, Proc. of 13th Symposium of AER, Dresden (Germany), 22-26 September 2003.
- [Tin93] Tinka, I., „VVER Diffusion Data Libraries Prepared by the KASSETA Code“, Proc. of 3rd Symposium of AER, Piestany (Slovak Republic), 27 September - 1 October 1993.

4 Control Rod Description

The presence of control rods in the core is modeled by the automatic assignment of the corresponding nuclear data to the respective prism volume elements, called nodes (see section 3.1). The code user has only to provide the radial and axial positions of the control rod groups in the DYN3D input. For a transient calculation, the velocity of the axial control rod movement may additionally be provided. In case the control rods consist of several axial sections, the lengths and material types (nuclear data) related to these sections must be given.

4.1 Homogeneous Control Rods

If a cluster of control rods, built of one type of absorber material, is fully inserted into a node, DYN3D simply assigns to this node the data set for the actual assembly type containing both fuel and control rods. In most cases, the lower control-rod edge does not fit to any axial-layer boundary chosen for the DYN3D calculation, so that in some nodes the clusters are only partly inserted. Node-averaged (homogenized) nuclear data are calculated by geometrical weighting:

$$\Sigma_{geom} = \frac{\Sigma_{CR} \cdot V_{CR} + \Sigma_{noCR} \cdot V_{noCR}}{V_{CR} + V_{noCR}}, \quad V_{CR} + V_{noCR} = V_{node}, \quad (4.1.1)$$

where V_{CR} and V_{noCR} are the volume portions of the node with and without control rods, respectively. Σ_{CR} and Σ_{noCR} represent the corresponding nuclear data. This approach, however, may lead to the so-called cusping effect that is caused by an overestimation of the absorption, due to geometrically homogenized data in the partially rodded node.

To avoid or at least reduce the cusping effect, a different method of nodal homogenization, a flux weighting, can optionally be used in DYN3D:

$$\Sigma_{flux} = \frac{\Sigma_{CR} \cdot \Phi_{CR} \cdot V_{CR} + \Sigma_{noCR} \cdot \Phi_{noCR} \cdot V_{noCR}}{\Phi_{CR} \cdot V_{CR} + \Phi_{noCR} \cdot V_{noCR}}, \quad (4.1.2)$$

Φ_{CR} and Φ_{noCR} are the relative nodal fluxes (weighting factors) for the totally rodded and rod-free nodes, respectively. The thermal or fast flux is applied, depending on the type of cross section under consideration. The weighting factors are taken from a file produced by a previous calculation, in which the lower control rod end coincided with an axial node boundary.

4.2 Control Rods Consisting of Two or More Axial Segments

If the control rods contain different axial segments, DYN3D calculates their volume portions in all rodded nodes, using the given insertion depths. The homogenized nuclear data are again calculated by geometrical weighting:

$$\Sigma_{geom} = \frac{\Sigma_1 \cdot V_1 + \Sigma_2 \cdot V_2 + \dots + \Sigma_n \cdot V_n}{V_1 + V_2 + \dots + V_n}, \quad V_1 + V_2 + \dots + V_n = V_{node}, \quad (4.2.1)$$

Certainly, the applied nuclear-data library has to contain data sets for the respective types of inserted control-rod material. One of the material types 1, 2,... n in equation (4.2.1) may be that of the un-rodged node.

So far there is no DYN3D option for a flux-weighted treatment of two or more axial control-rod segments in a node. For most of these rod types however, there is no strong necessity to apply flux-weighting. In KWU Konvoi reactors for example, there are steel tips below the absorber segment of the control rods. These steel parts of 42 cm length bring about a rather mild discontinuity in the cross sections at the lower control-rod edges. The discontinuity is much less abrupt as it would be in case of steel-tip absence, so that the cusping effect is significantly mitigated.

4.3 Control Assemblies in Russian VVER-440

In VVER-440, no usual control-rod clusters are inserted, but special control assemblies are used instead. They have the same shape and dimensions as the fuel assemblies. A real fuel assembly, called fuel follower, is connected to the lower edge of the absorber assembly by a coupling part of some 30 cm length. The uppermost 10 cm of the fuel-follower's fuel rods are provided with steel pellets instead of fuel. This „control assembly“ will be moved as a whole. In its uppermost position, the fuel follower stands between the usual fuel assemblies and differs from them only by the 10-cm steel-pellet layer. When the control assembly is fully inserted, the fuel follower is driven below the reactor core, and the lower edge of the coupling part is exactly at the lower edge of the active core.

The different axial parts of the control assembly are treated the same way as described in the previous section. However, there is a major difference originating from the fuel follower motion: the axial burnup distribution is also moved. Given node-averaged burnup values are usually related to totally driven-in fuel followers, which means totally driven-out absorber segments. So when a fuel follower is moved downward, the original burnup distribution is shifted. Now, the burnup values that are needed for the fixed nodes (defined for the actual DYN3D calculation) are determined by geometrical weighting, mostly from two shifted-node values. In case of non-equidistant axial core division, three or even more shifted-node burnup values may be involved. The information, needed for the assignment and weighting, is derived from the control-assembly insertion depth. A similar algorithm is used in burnup calculations by DYN3D, where the calculated values of a step-wise burnup increase have to be weighted and assigned to the right fuel follower nodes (cf. chapter 8).

Naturally, the distributions of xenon and samarium are shifted in the same way as the burnup distribution in the fuel follower in VVER-440. However, the influence of reactor-poison shifting is supposed to be of minor effect. Nevertheless, the effect should be considered in a later version of DYN3D.

5 Core Thermo-Hydraulics Model

5.1 Basic Assumptions and Equations

The model for the description of core thermo-hydraulics within DYN3D under steady-state and transient conditions is based on following principles:

- A The core is represented by one-dimensional parallel coolant channels consisting of a fuel rod and the proportional coolant flow. Each coolant channel is connected to one or more fuel assemblies describing the average conditions. The channels are isolated, i.e. no cross flow between the channels is taken into account. The channels are coupled only over common boundary conditions (see Section 5.4). Furthermore, additional hot channels can be considered for analyzing the effect of local power peaks, coolant temperature, flow rate or fuel rod parameters uncertainties (see Section 5.5).
- B One- or two-phase flow can be considered. The description of two-phase flow is based on four differential balance equations for mass, momentum and energy of the mixture and mass balance of the vapour phase. The two-phase model is closed by the following additional assumptions:
 - One of the phases (vapour or liquid) is in saturation conditions. Its thermo-dynamic state is defined by the equation of state at saturation line.
 - The relation of phase velocities is described by a quasi-stationary phase slip model, that means, an algebraic equation for the phase slip ratio is applied.
- C The thermo-hydraulic model is closed by constitutive relations for the slip ratio, one- and two-phase frictional pressure losses, evaporation and condensation rates, heat transfer correlations and thermo-physical properties of the phases.
- D A fuel rod model considering one-dimensional heat transfer in fuel, cladding and within the gas gap between them is included. It is coupled to the flow model via heat flux at the cladding surface into the fluid (see section 5.3).
- E A model of boron acid tracking within the coolant channels is included by solving boron acid transport equation for each channel.
- F The boundary conditions to be provided for core thermo-hydraulics are:
 - pressure at core outlet,
 - coolant temperature at the core inlet for each channel,
 - boron acid concentration at the core inlet for each channel,
 - pressure drop over the core (equal for all channels) or total coolant mass flow rate through the core.

The boundary conditions can arbitrarily change in time. They can be given explicitly in the form of time tables or provide from coupling with the thermo-hydraulic system code ATHLET (see Section 6).

The distribution of coolant temperature and boron acid concentration at the core inlet can be obtained from given primary circuit cold leg parameters by use of an integrated coolant mixing model for downcomer and lower plenum of the reactor (see Section 5.5).

The following set of equations for the coolant is considered:

- momentum balance of the phase mixture

$$\begin{aligned} \frac{\partial}{\partial t}[\varphi\rho_v u_v + (1-\varphi)\rho_l u_l] + \frac{\partial}{\partial z}[\varphi\rho_v u_v^2 + (1-\varphi)\rho_l u_l^2] + \frac{\partial p_{fric}}{\partial z} + \\ g[\varphi\rho_v + (1-\varphi)\rho_l] + \frac{\partial p}{\partial z} = 0 \end{aligned} \quad (5.1.1)$$

- energy balance of the phase mixture:

$$\frac{\partial}{\partial t}[\varphi\rho_v h_v + (1-\varphi)\rho_l h_l] + \frac{\partial}{\partial z}[\varphi\rho_v u_v h_v + (1-\varphi)\rho_l u_l h_l] = Q \quad (5.1.2)$$

- mass balance of the phase mixture:

$$\frac{\partial}{\partial t}[\varphi\rho_v + (1-\varphi)\rho_l] + \frac{\partial}{\partial z}[\varphi\rho_v u_v + (1-\varphi)\rho_l u_l] = 0 \quad (5.1.3)$$

- mass balance of the vapour phase:

$$\frac{\partial}{\partial t}\varphi\rho_v + \frac{\partial}{\partial z}\varphi\rho_v u_v = \mu \quad (5.1.4)$$

The following notations are used:

φ	-	vapour volumetric fraction,
h	-	specific enthalpy,
u	-	velocity,
ρ	-	density,
p	-	pressure,
μ	-	evaporation / condensation rate,

subscript l for liquid phase, subscript v for vapour phase.

Source terms in the equations are the frictional pressure drop $(\partial p_{fric})/(\partial z)$, the heat volumetric source rate Q in the fluid and the evaporation/condensation rate μ . The heat volumetric source in the fluid is composed by the heat transferred from the fuel rod to coolant with heat flux density q'' at the heated surface and the heat directly released in the coolant by γ -heating:

$$Q = \frac{1}{A}(f_\gamma q' + \pi D q'') \quad (5.1.5)$$

where f_γ is the proportion of heat directly released in the coolant, q' is the linear power rate in the fuel rod, A is the flow cross section and D the fuel rod diameter. The heat transfer from fuel rod to coolant is defined by the heat transfer coefficient α temperature difference between cladding outside temperature T_{cl} and fluid temperature T_f (the fluid being liquid or vapour):

$$q'' = \alpha(T_{cl} - T_f) \quad (5.1.6)$$

The system of fluid flow equations (5.1 - 5.4) is closed by the equations of state for the liquid and the vapour phase:

$$\begin{aligned}\rho_v &= f_v(h_v, p) & \rho_l &= f_l(h_l, p) \\ T_v &= F_v(h_v, p) & T_l &= F_l(h_l, p)\end{aligned}$$

and constitutive relations for the source terms and the ratio of phase velocities or slip ratio (see section 5.2).

Additionally, the **mass balance equation for the boron acid**:

$$\frac{\partial}{\partial t}(1 - \phi)\rho_l c_b + \frac{\partial}{\partial z}u_l(1 - \phi)\rho_l c_b = 0 \quad (5.1.7)$$

and the **one-dimensional heat conduction equation** for the fuel rod are solved:

$$\rho c \frac{\partial T}{\partial t} = \frac{1}{r} \frac{\partial}{\partial r} \left(\lambda r \frac{\partial T}{\partial r} \right) + q''' \quad (5.1.8)$$

q''' is the heat volumetric source in the fuel or cladding, c_b is the boron (or boron acid) concentration.

5.1.1 Basic Equations in Conservative Form

Introducing following two-phase mixture parameters:

- mixture enthalpy h

$$h = xh_v + (1 - x)h_l$$

- mass velocity G

$$G = \phi\rho_v u_v + (1 - \phi)\rho_l u_l$$

- mixture density

$$\rho = \phi\rho_v + (1 - \phi)\rho_l$$

-vapour mass transport density

$$\tilde{\rho} = \frac{\partial \phi}{\partial x} [x\rho_l + (1 - x)\rho_v]$$

- inverse density for momentum transport

$$v_m = \frac{x^2}{\phi\rho_v} + \frac{(1 - x)^2}{(1 - \phi)\rho_l}$$

and taking into account the relation between fluid quality x (vapour mass fraction or relative enthalpy) and vapour volumetric fraction (or void fraction) φ :

$$\varphi = \frac{1}{1 + \frac{(1-x)\rho_v}{x\rho_l} S} \quad (5.1.9)$$

where S is the phase slip ratio, the fluid flow equations (5.1.1 - 5.1.4) can be transformed into the conservative form:

- **momentum balance**

$$\frac{\partial G}{\partial t} + \frac{\partial}{\partial z}(G^2 v_m) + \frac{\partial p_{fric}}{\partial z} + \rho g + \frac{\partial p}{\partial z} = 0 \quad (5.1.10)$$

- **energy balance**

$$\rho \frac{\partial h}{\partial t} + G \frac{\partial h}{\partial z} = q''' + \frac{\partial \chi}{\partial t} \quad (5.1.11)$$

with
$$\chi = (h_v - h_l)[(1 - \varphi)x\rho_l - \varphi(1 - x)\rho_v] \quad (5.1.11a)$$

- **mass balance**

$$\frac{\partial \rho}{\partial t} + \frac{\partial G}{\partial z} = 0 \quad (5.1.12)$$

- **vapour mass balance**

$$\tilde{\rho} \frac{\partial \varphi}{\partial t} + \frac{\partial x}{\partial \varphi} G \frac{\partial \varphi}{\partial z} = \mu + \frac{\partial x}{\partial \varphi} \left(\frac{\partial x}{\partial \varphi} \tilde{\rho} \frac{\partial p}{\partial t} + G \frac{\partial p}{\partial z} \right) \quad (5.1.13)$$

In this representation, the two-phase flow equations correspond formally to the one-phase balance equations with except of additional source terms and different effective velocities for mass, momentum and energy transport. Numerical methods available for conservative hyperbolic equations can be applied. The balance equations for mass, momentum and energy of the two-phase mixture transform automatically into the corresponding one-phase flow equations, if the void fraction or vapour mass fraction are 1 or 0.

The constitutive equations, which are used to calculate the friction pressure drop $(\partial p_{fric})/(\partial z)$ in equation (5.1.10), the heat transfer coefficient in equation (5.1.6) and the boiling/condensation rate in equation (5.1.13) are described in the next section.

5.2 Constitutive Relations in the Thermo-Hydraulics Model

The set of governing equations for the modelling of one- and two phase adiabatic coolant flow described in Section 5.1 is closed by so called constitutive equations for:

- frictional and local pressure losses $\frac{\partial p_{fric}}{\partial z}$,
- heat transfer regime mapping including heat transfer correlations in different regimes and criteria for change of heat transfer regimes,
- evaporation and condensation rate (boiling model) and consistent phase slip correlation,
- mathematical formulations of the equations of state of water and steam including transport properties (thermo-physical properties package).

5.2.1 Hydraulics

Pressure losses due to friction along the coolant channel and single pressure losses at the inlet orifice, at distance lattices and the channel outlet can be taken into account according to following formulae:

$$\Delta p_{fric} = \zeta \frac{G \cdot |G|}{2\rho_l} \Phi \quad (5.2.1)$$

where ζ is the friction coefficient, G the mass velocity, ρ_l the liquid density and Φ the two-phase friction multiplier.

The friction coefficient for distributed friction along the channel is estimated according to the FILONENKO correlation with a bundle correction obtained from [Kir84]:

$$\zeta = \lambda \Delta z / D_{hyd}, \quad \lambda = F(l) \lambda_0, \quad \lambda_0 = [1.82 \lg(\text{Re}/8)]^{-2}$$

D_{hyd} is the equivalent hydraulic diameter of the bundle, Re is the Reynolds number, $F(l)$ is the bundle correction for the trigonal or square bundle. The two-phase multiplier for distributed friction is determined from the OSMACHKIN correlation [Osm71]:

$$\Phi = \Phi_{hom} [1 + x (\eta'/\eta'' - 1)] \Psi(x), \quad \Phi_{hom} = 1 + (\rho'/\rho'' - 1)$$

is the homogeneous two-phase multiplier, η is the dynamic viscosity, x is the vapour mass fraction and $\Psi(x)$ is an empirical function taking into account the increased friction in the case of enhanced surface roughness due to bubble formation:

$$\Psi = [1 + x(\eta'/\eta'' - 1)]^{-0.2x} \left[1 + 0.57x^{0.125} (1-x)^2 \left(\frac{1}{0.2 \cdot Fr \cdot \rho''/\rho'} - 5, 2x \right) \right] \quad (5.2.2)$$

where Fr is the Froude number $Fr = \frac{G^2}{\rho' g D_{hyd}}$.

For single phase pressure losses, the friction coefficients ζ have to be given as input data. Two-phase friction multiplier is taken into account to the homogeneous model.

5.2.2 Heat Transfer

The wall-to-coolant heat transfer model in FLOCAL is based on the heat transfer curve given in figure 5.2.1.

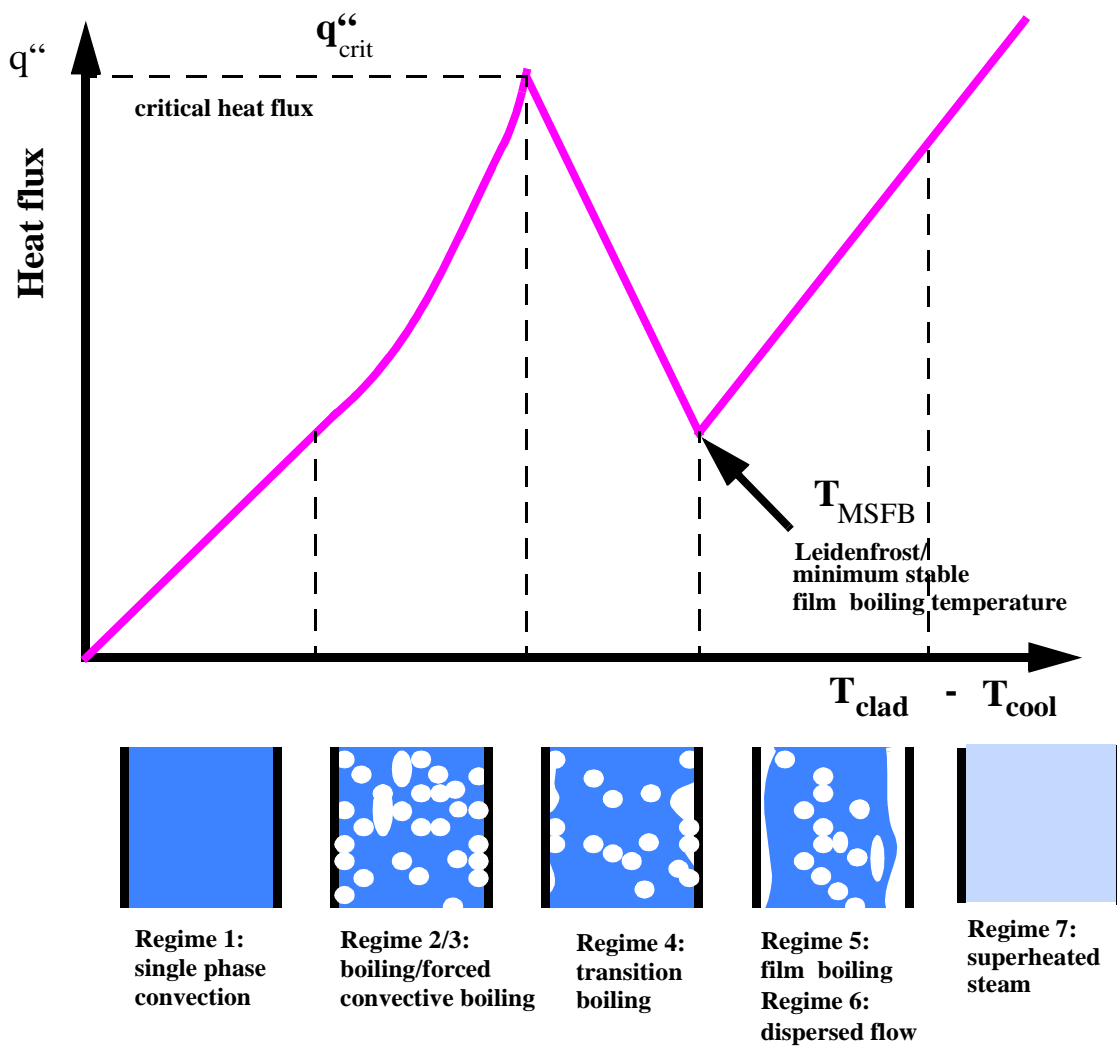


Fig. 5.2.1: Heat transfer regime mapping

The correlations for the heat transfer coefficient (HTC) α for one-phase liquid (laminar/turbulent natural or forced convection, regime 1) and developed boiling heat transfer (regime 2) are chosen from [Pol82].

Convective heat transfer is described by the Nusselt number Nu

$$\alpha_{conv} = \frac{\lambda_l}{L} \cdot Nu \quad (5.2.3)$$

L is the characteristic dimension of the coolant channel. The dominating heat transfer regime (natural or forced convection) is derived from the principle, that the regime is chosen, for which the HTC is maximal:

$$Nu = \max(Nu_{nat}, Nu_{forc})$$

Both natural and forced convection can be laminar or turbulent. For the selection of laminar or turbulent regime, the same principle is applied:

$$Nu = \max(Nu_{lam}, Nu_{turb})$$

Following correlations for the Nusselt number are chosen for the forced convection regime:

$$Nu_{lam} = 4 \quad Nu_{turb} = C_{turb} \cdot Re^{0.8} \cdot Pr^{0.4} \quad (5.2.4)$$

The coefficient C_{turb} depends on the fuel rod lattice geometry (square or triangular). The characteristic dimension of the channel in the case of forced convection is the equivalent heated

diameter of the fuel rod bundle:

$$D_{heat} = \frac{4A_{flow}}{P_{heat}} \quad (5.2.5)$$

where A_{flow} is the free flow cross section of the bundle and P_{heat} is the heated perimeter.

For natural convection, the Nusselt number depends on the Rayleigh number:

$$Nu_{nat} = C_{nat} \cdot Ra^m \quad (5.2.6)$$

and the characteristic dimension is the height of the channel. The constants C_{nat} and m in equation (5.2.6) are

$$C_{nat} = 0.59, \quad m = 1/4 \quad (5.2.6a)$$

for laminar flow and

$$C_{nat} = 0.1 \quad m = 1/3 \quad (5.2.6b)$$

for turbulent flow. It should be noted, that the turbulent forced convection heat transfer regime is dominating under nominal pump operation and developed natural circulation conditions in the reactor core. To select the appropriate heat transfer regime in the one-phase convection region (laminar or turbulent, forced or natural convection), the maximum of the Prandtl number calculated according to correlations (5.2.4) and (5.2.6) is taken.

For heat transfer regime 2 (developed boiling), the RASSOKHIN correlation from [Pol82] is used:

$$q'' = C_{boil} \cdot (T_{cl} - T_{sat})^3 \quad (5.2.7a)$$

The boiling heat transfer is sufficiently non-linear. The coefficient C_{boil} depends from the pressure:

$$C_{boil} = 0,55 \cdot p^{1/4} \quad \text{if } 0,1 \leq p \leq 8,0 \text{MPa}$$

and

$$C_{boil} = 0,0581 \cdot p^{4/3} \quad \text{if } 8 \leq p \leq 20 \text{MPa}$$

Therefore,
$$\alpha_{boil} = C_{boil} \cdot (T_{cl} - T_{sat})^2 \quad (5.2.7b)$$

Heat transfer regime 2 can dominate also in the case, that the bulk of fluid is still subcooled. The heat transfer regime is selected between convection and boiling which gives the lower temperature of the heated wall.

In the case of high mass flow rates and low pressure, convective effects can influence the boiling heat transfer. If these effects become significant, the boiling heat transfer coefficient is corrected by using the convective heat transfer coefficient in accordance with the method of BORISHANSKJI (from [Pol82])

$$\alpha = \alpha_{boil} \cdot \sqrt{1 + 7 \cdot 10^{-9} \cdot \alpha_{boil}^2 / (\alpha_{boil}^2 + \alpha_{conv}^2)} \cdot C_{corr}^{2/3} \quad (5.2.8a)$$

with $C_{corr} = G \cdot [1 + \dot{x} \cdot (\rho' / \rho'' - 1)] \frac{r}{q''}$. r is here the evaporation heat.

The correction is applied if the criterion

$$C_{corr} \cdot \left(\frac{\alpha_{boil}^2}{\alpha_{boil}^2 + \alpha_{conv}^2} \right)^{2/3} > 50000 \quad (5.2.8b)$$

is fulfilled. α_{boil} and α_{conv} are the boiling HTC and the convection HTC from equations (5.2.3) and (5.2.7b), respectively. If the convective correction to boiling heat transfer is relevant, the heat transfer regime key is switched to 3.

If with increasing intensity of boiling there is formed a closed vapour film at the heated surface, the heat transfer significantly decreases (first kind of heat transfer crisis or DNB). This situation is typical for high pressure, high heat flux conditions. It is called the departure from nucleate boiling (DNB). The occurrence of DNB is achieved if the heat flux reaches the critical one. The flow regime switches from bulk or convective boiling (regime 2 or 3) to film boiling (regime 5), if the heat flux q'' is higher than the critical heat flux q''_{crit} . The critical heat flux q''_{crit} is calculated by one of the correlations OKB-2 [Bez76], [Ast82], IAE-4 [Osm78] or BIASI [Bia67]. At lower pressures and lower heat flux densities, the so called dryout is the dominant heat transfer crisis mechanism, where the bulk of the liquid evaporates and a dispersed flow containing water droplets in steam is observed (regime 6). For the detection of this second kind of heat transfer crisis critical dryout quality \dot{x}_{crit} is considered being an empirical function of pressure and mass velocity. If one of these criteria is fulfilled, the heat transfer is switched from pre-crisis boiling to post-crisis film boiling or dispersed flow. Under steady-state conditions the heat flux is fixed. In that case the change from pre-crisis to post-crisis heat transfer leads to a jump of the heated surface temperature from one vertical position of the heated channel to the next. In transients, of course no jump of temperature in time is possible. If one of the heat transfer crisis criterions is reached, a transition boiling region is crossed (regime 4), where the heat flux is reduced with increasing temperature, until the minimum sta-

ble film boiling temperature T_{MSFB} is reached. Because the heat transfer becomes worse with increasing temperature, no stable conditions can be reached in the transition boiling region.

In the following, the critical heat transfer criteria are described. It is important to note, that critical heat flux correlations can be used in different manner. Usually, q''_{crit} is correlated against local vapour mass fraction x (or quality), mass flow density G , pressure p and other parameters: $q''_{crit} = f(x, G, p, D, \dots)$.

These correlations are implicit with respect to q'' , because the local quality in the coolant channel at axial position z and thus q''_{crit} depend from the heat flux in the following way:

$$x(z) = \frac{h(z) - h_{sat}}{r} = \frac{q''(z) P_{heat}}{G \cdot A_{flow}} F(z) - x(0) \quad \text{with} \quad F(z) = \int_0^z \frac{q''(z')}{q''(z)} dz' \quad (5.2.9)$$

where $F(z)$ is an integral form-factor of the heat flux, h - the coolant enthalpy, $x(0)$ - the quality at the channel inlet, P_{heat} and A_{flow} see equation (5.2.5). If this expression is put into the critical heat flux correlation, it becomes an explicit, so called „true critical heat flux“ or critical power correlation. In our model, the IAE-4 and BIASI correlations are transformed into this form.

The original form of the IAE-4 correlation is

$$q''_{crit} = f(G, D_{hyd}, p) \cdot \frac{\frac{We}{We + 25} - \frac{\dot{x}(z)}{3,5} \cdot We^{1/5}}{619,5 \cdot \Psi} \quad (5.2.10)$$

$f(G, D_{hyd}, p)$ is an empirical function of mass flow density G , hydraulic diameter D_{hyd} and pressure p . We is the Weber number $We = \frac{G^2 \cdot D_{hyd}}{\rho' \sigma}$ and Ψ is a so-called form factor defined by:

$$\Psi = \int_0^z \frac{q''(z')}{q''(z)} \cdot e^{-\lambda(z-z')} \cdot \lambda dz' \quad (5.2.11)$$

λ is a relaxation length of the influence of heat flux changes, $\lambda = 75.6 D_{hyd}$.

By using the relation (5.2.9), equation (5.2.10) can be transformed to following form:

$$q''_{crit}(z) = \frac{\frac{We}{We + 25} + \frac{We^{1/5}}{3,5} x(0)}{\frac{619,6}{f(G, D_{hyd}, p)} \Psi(z) + \frac{4We^{1/5}}{3,5GrD} F(z)} \quad (5.2.12)$$

In equation (5.2.12), the right hand side is no more implicitly dependent from the heat flux. The equation determines the so-called true critical heat flux or, if divided by the actual heat flux at position z , the so-called critical power ratio.

In [Osm78], a methodological approach is proposed to take into account a dynamical correction of the critical heat flux. Usually, critical heat flux correlations are derived from experiments at steady-state conditions and do not comprise the effect of transient changes of the parameters. To consider a dynamical correction, the form-factors F and Ψ are proposed to be calculated in the following way:

$$F = \int_0^z \frac{q''(z', t - \frac{z-z'}{w})}{q''(z)} dz' \quad (5.2.13a)$$

$$\Psi = \int_0^z \frac{q''(z', t - \frac{z-z'}{w})}{q''(z)} \cdot e^{-\lambda(z-z')} \cdot \lambda dz' \quad (5.2.13b)$$

Thus, the history of heat flux in space and time, how it is seen by a fluid particle moved with the flow, is taken into account. Since the numerical realization of the above integrals is rather complicated (the heat flux history must be stored for an a priori not known number of time steps), the following assumption is used for simplification: the time-dependent behaviour of the heat flux is assumed to be exponentially, so that a time constant can be derived from the last two time steps.

The BIASI correlation can be transformed in an equivalent manner like the IAE-4 correlation yielding:

$$q''_{crit, 1} = F_1(G, D_{hyd}) \cdot \frac{\frac{f(p)}{G^{1/6}} + x(0)}{1 + F_1 \cdot a \cdot F(z)} \quad (5.2.14a)$$

$$q''_{crit, 2} = F_2(G, D_{hyd}) \cdot h(p) \cdot \frac{1 + x(0)}{1 + F_2 \cdot a \cdot F(z)} \quad (5.2.14b)$$

$$q''_{crit} = \max\{q''_{crit, 1}, q''_{crit, 2}\} \quad (5.2.14c)$$

where $f(p)$ and $h(p)$ are empirical functions of the pressure, F_1 and F_2 are empirical functions of the mass flow rate and the hydraulic diameter [Bia67], $F(z)$ is the integral form-factor according to equation (5.2.13a) and

$$a = \frac{4 \cdot L}{G \cdot r \cdot D_{heat}}$$

The OKB–correlation:

$$q''_{crit} = 795 \cdot \Phi \cdot (1 - \dot{x})^{0,105p - 0,5} \cdot G^{0,184 - 0,311\dot{x}} \cdot (1 - 0,0185p) \quad (5.2.15)$$

is considered with a form–factor Φ proposed in [Ast82] for taking into account non–uniform heat flux shape, but can also be used without this form–factor. By our experience, the form–factor causes instabilities in the heat transfer calculation in the transition boiling region, when the axial shape of the heat flux has been changed significantly due to the occurrence of heat transfer crisis. The OKB-2 correlation cannot be transformed to the explicit form.

For low mass flow densities ($G \ll 200 \text{ kg/m}^2\text{s}$) the Kutateladse correlation for q''_{crit} with a non-equilibrium correction is used [Pol82]:

$$q''_{crit} = 0,16 F_{sub} r \sqrt{\rho''} \sqrt{g \sigma (\rho' - \rho'')} \quad (5.2.16)$$

with $F_{sub} = 1 - 0,1 \left(\frac{\rho'}{\rho''} \right)^{0,76} x_0$ if $x_0 < 0$

and $F_{sub} = 1$ if $x_0 > 0$.

x_0 is the equilibrium quality, F_{sub} is a correction due to liquid subcooling. The validity range of this correlation is typical for nearly stagnant fluid conditions. The transition between regions of high and low flow rates is done by linear interpolation.

For the detection of dryout, the second kind of heat transfer crisis being typical for lower pressures and lower heat flux densities, a criterion of Doroshchuk-Nigmatulin [Huh75] is considered, where the critical dryout quality \dot{x}_{crit} is an empirical function of pressure and mass velocity:

$$\dot{x}_{crit} = \sqrt{0,0031 \cdot \frac{\sigma \rho'}{G v (\rho' - \rho'')}} \quad \text{for } p \leq 5 \text{ MPa} \quad (5.2.17a)$$

and

$$\dot{x}_{crit} = 12,6 \cdot p^{0,15} \cdot G^{-0,45} \quad \text{for } p > 5 \text{ MPa} \quad (5.2.17b)$$

In the transient boiling region (regime 4), no heat transfer coefficient is determined, but the transition boiling heat flux is estimated. This heat flux is used in the heat transfer equation, until the calculated temperature reaches the minimum stable film boiling point. The transition boiling heat flux is estimated by the Kirchner and Griffith interpolation formulae [Ris85]:

$$q''_{tran} = q''_{crit} \left(\frac{T_W}{T_{W,crit}} \right)^\gamma \quad \gamma = \ln \left(\frac{q''_{crit}}{q''_{MSFB}} \right) / \left(\ln \left(\frac{T_W}{T_{W,MSFB}} \right) \right) \quad (5.2.18)$$

T_W is the corresponding wall (cladding outside) temperature. The Leidenfrost or minimum stable film boiling point T_{MSFB} is determined by an empirical correlation describing experimental results from the literature [Got86]:

$$T_{MSFB} = T_{sat} + 100 + 8(T_{sat} - T_{liq}) \quad (5.2.19)$$

In the stable post-crisis region (regime 5 or 6) for inverted annular or dispersed flow the modified Bromley (from [Pol82]) or Groeneveld - Delorme [Gro76] correlations are used:

$$\alpha_{pc} = \max \{ \alpha_{GD} ; \alpha_{BR} \} \quad (5.2.20)$$

$$\alpha_{BR} = \lambda_g / L \max \{ 0,62 \cdot Ra^*{}^{1/4} ; 0,15 \cdot Ra^*{}^{1/3} \} \quad (5.2.21a)$$

λ_g is the vapour thermal conductivity, Ra^* is a modified Rayleigh-number:

$$Ra^* = gL^3(\rho' - \rho'') \frac{(r + 0,4 \cdot c_{p,g} \Delta T_{w,sat})}{\lambda_g \nu_g \Delta T_{w,sat}} \quad (5.2.21b)$$

with the Taylor wavelength L . $\Delta T_{w,sat}$ is the difference between wall and saturation temperature, the liquid and vapour properties symbols are explained in the list of symbols. The Groeneveld - Delorme correlation is of convective type like equation (5.2.4):

$$\alpha_{GD} = 0,008348 \cdot \frac{\lambda_{film}}{D_{heat}} \cdot Re_{film}^{0,8774} \cdot Pr_{film}^{0,6112} \quad (5.2.22)$$

where λ_{film} is the thermal conductivity of the vapour phase in the film close to the heated wall, Re_{film} an effective vapour film Reynolds number, Pr_{film} the Prandtl number of the vapour at film temperature. The film temperature is approximated as the average value of heated wall and bulk vapour temperature. The model comprises an estimation of possible vapour superheating in the bulk of the dispersed flow. A rather complicated empirical function is given for the estimation of steam superheating depending on Reynolds number, equilibrium quality and steam properties. The temperature of the superheated steam is used as the reference temperature for the heat transfer calculation.

In the case of subcooled liquid, the following additional non-equilibrium correction is applied to the heat transfer coefficients in the post crisis region:

$$\alpha_{pc}|_{T=T_l} = \alpha_{pc}|_{T=T_{sat}} \cdot (2 \cdot T_{sat}/T_l - 1)^{3/2} \quad (5.2.23)$$

This correlation is a modified form of the formulae recommended in [Fri85].

Additionally, the heat transfer from wall to coolant by radiation is added with some weight factor:

$$\alpha_{pc} = \alpha_{pc} + 0.75\alpha_{rad} \quad (5.2.24)$$

After full evaporation of coolant, the heat transfer to superheated steam is estimated by a forced convection correlation (forced steam convection, regime 7).

5.2.3 Boiling Model

The thermal-hydraulic module FLOCAL in DYN3D is based on a four equation model for two-phase flow comprising conservation equations for mass, momentum and energy of the mixture and the mass balance of the vapour phase. The source term in the vapour mass balance equation consists of evaporation and condensation rates due to heat transfer and pressure changes. The adiabatic evaporation rate due to pressure changes (second part of the source term in equation 5.13) is obtained from equilibrium conditions, the derivative of the vapour mass fraction from pressure is taken along the saturation curve. The vapour mass source term μ is divided into evaporation and condensation rates:

$$\mu = \mu_{evap} - \mu_{cond}$$

Evaporation and condensation rates due to heat transfer from the heated wall to the fluid and between the phases are calculated according to the MOLOCHNIKOV boiling model [Mol82]:

$$\mu_{evap} = \frac{\theta Q}{r} \quad (5.2.25)$$

$$\text{with } \theta = \tanh\left(3,5 \frac{h_l - h_{OB}}{\Delta h_{OB}}\right) \quad \text{if } h_l > h_{OB}$$

and

$$\theta = 0 \quad \text{if } h_l \leq h_{OB}$$

Q is the volumetric density of heat transferred to the fluid, r is the evaporation heat, h_l is the liquid enthalpy, h_{sat} is the saturation enthalpy of the liquid, h_{OB} is the liquid enthalpy at the point of boiling onset. The point of boiling onset is obtained from the condition, that the cladding surface temperature reaches the saturation temperature.

The condensation rate of vapour in subcooled liquid is estimated from the correlation [Mol82]:

$$\mu_{cond} = C_{cond} \cdot F(G) \cdot \frac{h_l - h_{sat}}{r} \cdot \varphi \cdot \{1 + 5 \exp(-20\varphi)\} \quad (5.2.26)$$

$C_{cond} = 17 \text{ m}^{-1}$ (empirical constant), φ is the volumetric void fraction, $F(G)$ is an empirical function of the mass flux density G .

The phase slip ratio S occurring in equation (5.1.9) is calculated within the MOLOCHNIKOV model by following correlation:

$$S = 1 + \frac{(0,6 + 1,5\beta^2)}{Fr^{1/4}} \cdot \left(1 - \frac{p}{p_{crit}}\right) \cdot \sqrt{1 - \exp(-20\beta)} \quad (5.2.27)$$

where β is the vapour volumetric flow ratio, Fr is the Froude number, p_{crit} is the critical pressure.

5.2.4 Thermo-Physical Properties of Water and Steam

The following thermo-physical properties of water and steam are used in the DYN3D thermo-hydraulic model:

On the saturation line:

- saturation temperature as function of pressure and pressure as function of temperature on saturation line,
- enthalpy, density and transport properties of the phases as functions of pressure,
- surface tension as function of pressure.

In the subcooled liquid and superheated steam regions:

- temperature and density of the phases as functions of pressure and enthalpy,
- enthalpy as function of pressure and temperature,
- transport properties as functions of pressure and temperature.

Two different analytical presentations of the water and steam properties can be used

- a software package based on the IFC67 [Gri90] and IAPWS-IF97 [Wag00] approaches using the formulations of [Wag90] for properties on saturation line,
- a simplified presentation based mostly on formulas developed by KOKOREV and BOIKO (from [Kir84]).

The software package [Art97] based on IFC67 and IAPWS-IF97 approaches provides a full range presentation of the water and steam thermo-physical properties including near-critical and post-critical regions. The package provides the properties in the pressure range from 0.61 kPa to 100 MPa and temperature range from 273.16 K to 1073.15 K with accuracy corresponding to the international IFC67 and IAPWS-IF97 framework tables. It is recommended especially in the case of benchmark calculations. The KOKOREV and BOIKO package provides the functions in the pressure region from 5.0 MPa until 18.85 MPa and temperature interval from 0 °C until 700 °C. It is fast running, but the accuracy of the water and steam properties is lower than for the IFC67/IAPWS-IF97 package. Some functions from the VDI63 presentation [Sch63] (thermal conductivity of water) and the MEYER-PITROFF formulation [Mey69] (density and thermal conductivity of steam) are used.

5.3 Core Thermohydraulic Boundary Conditions

The following parameters have to be provided as boundary conditions for the thermal hydraulics of the core:

- coolant temperature at the inlet of each coolant channel,
- boron acid concentration at the inlet of each coolant channel,
- pressure at the core outlet,
- coolant mass flow rate for each coolant channel or for the whole core or pressure drop over the core.

These boundary conditions have to be explicitly provided as functions of time, if DYN3D is used as stand alone code. If DYN3D is coupled with a thermohydraulic system code for modelling the whole plant behaviour, the boundary conditions will be provided by the system code and have not to be specified as input data.

The coolant temperature and boron acid concentration distributions at the core inlet are obtained from the parameters in the cold legs of the primary circuit loops based on different assumptions on coolant mixing in the downcomer and the lower plenum of the reactor. These assumptions are:

- homogeneous mixing,
- mixing model for VVER-440 type reactors,
- absence of any mixing in the downcomer and the lower plenum.

The temperature and the boron concentration in each loop (at the outlet of the cold leg) must be given as functions of time in the form of input data tables.

In the homogeneous mixing model, the average coolant temperature and boron concentration at the core inlet are obtained by mass flow weighted averaging of the parameters in the loops:

$$x_{core} = \frac{1}{\dot{m}_{core}} \sum_i \dot{m}_i \cdot x_i \quad (5.3.1)$$

where x is the averaged parameter (temperature or boron concentration), \dot{m} is the mass flow rate and i is the index of the loop. That means, a homogeneous parameter distribution at the core inlet is used. This option is available for all reactor types.

Concerning VVER-440 type reactors, a special mixing model is implemented into DYN3D, which allows the determination of the temperature and boron concentration distribution at the core inlet based on a physical model, which is described in the next section. This model is based on the potential flow approximation for the downcomer and the lower plenum. An individual temperature and boron concentration value is obtained for each coolant channel in the core. The model can be used only for VVER-440 type reactors and full core calculations without radial reflector.

Assuming the absence of any mixing in the downcomer and the core, each primary circuit loop is connected to a certain sector of the reactor core. A perturbation of the temperature or the boron concentration in each loop is taken into account only for the coolant channels belonging to the sector which corresponds to this loop. A map of coolant channels must be implemented into the code, which describes this correspondence. This map depends on the core geometry and the position of the primary circuit cold legs relative to the core and, consequently, is different for each reactor type. Recently, these maps are implemented only for VVER-440 and VVER-1000 type reactors. Thus, the option of no mixing can be used only for these reactor types. However, such a map could easily be implemented into a DATA operator of one subroutine of the code. In this way, the no mixing option can be made available for each reactor type.

For each of the mixing options, the time delay due to coolant transport time from the cold leg outlet to the core inlet can be taken into account. Only an average transport time can be considered, which is estimated as the ratio between coolant mass inventory in the downcomer and the lower plenum to the core mass flow rate. The corresponding coolant inventory must be given as input.

Concerning the hydraulic boundary conditions, following options are possible:

- given pressure drop over the core,
- given total mass flow rate through the core,
- given individual mass flow rate at the inlet of each coolant channel.

In the case of given pressure drop over the core, the mass flow rate for each individual channel is calculated in an iterative way, so that the condition of equal pressure drop over all channels is fulfilled. The mass flow rate for each channel is calculated from the given pressure drop solving the momentum balance equation (see section 5.6). If the total mass flow rate through the core is given, an additional iteration procedure is necessary to fulfill the conditions:

- the sum of the mass flow rates of all channels is equal to the given total mass flow rate,
- the pressure drop over all channels is the same.

This iteration procedure is organized in the following way:

- A rough estimation for the pressure drop $\Delta p^{(j)}$ is provided in the iteration cycle j . Using this pressure drop value, the mass flow rate of each individual channel is calculated.
- If the sum of all channel mass flow rates $\dot{m}_{tot,j}$ is not equal to the given total mass flow rate $\dot{m}_{tot,0}$, the pressure drop estimation is corrected in the way:

$$\Delta p^{(j+1)} = \Delta p^{(j)} \cdot \left(\left(\frac{\dot{m}_{tot,0}}{\dot{m}_{tot,j}} \right)^2 \cdot \theta + 1 - \theta \right) \quad (5.3.2)$$

θ is a relaxation parameter, which is set by default to 0.8. It can not be changed by input, but only in the FORTRAN text. The iteration cycle is repeated until the sum of the channel mass flow rates approaches the given total mass flow rate with a given maximum deviation. During a transient, where the mass flow rate can change along the channels, the given total mass flow rate is understood as the core inlet total mass flow as default option. By data input the option can be chosen, that the total mass flow rate is interpreted as the axially averaged mass flow.

Additional to the physical boundary conditions “pressure drop over the core” or “total mass flow rate”, the mass flow rate can be given individually for each channel. In the transient case, this is understood as the mass flow rate value at the channel inlet. However, specifying arbitrary mass flow rates for the channels, the physical boundary condition of equal pressure drop over all channels is not fulfilled.

The pressure at the core outlet is used as the boundary condition for obtaining the axial pressure distribution in the core. The pressure distribution is calculated simultaneously with the mass flow rate distribution by solving the momentum balance equation. The individual pressure distribution for each coolant channel is used in the calculation of the thermodynamic parameters. The pressure at the core outlet has to be given as a time table in the input.

Besides of deriving the core inlet boundary conditions from physical models (coolant mixing model, condition of equal pressure drop over all channels), arbitrary individual time tables for for the mass flow rate, the coolant inlet temperature and the boron concentration can be given for each coolant channel. This is especially important for methodical investigations or for cases, where the implemented models are not valid or not sufficient.

5.4 Hot Channel Treatment

Besides of the coolant channels connected to fuel elements of the reactor core, hot channels can be considered for analyzing the effect of local power peaks, coolant temperature, flow rate or fuel rod parameters variations. These hot channels are connected each to a certain core channel. An arbitrary number of hot channels can be considered, different hot channels can be connected to one core channel. A hot channel is calculated with the same pressure drop as the core channels, the same axial power distribution is applied as for the related core channel. Following parameters of the hot channel can be varied in comparison with the related core channel:

- channel power,
- coolant inlet temperature,

- flow resistance coefficient at the channel inlet,
- fuel rod geometry and properties.

The channel power is multiplied by a hot channel factor given as input data which describes the power peaking inside the fuel element (neutron flux tilt due to the surrounding fuel elements, pinwise power distribution) and uncertainty factors. The power peaking inside the fuel element can be estimated from inner nodal flux reconstruction and/or fine mesh/cell calculations with transport codes. The implementation of a method for the on-line calculation of the hot channel power distribution from inner nodal flux reconstruction in DYN3D during the transient analysis and pre-calculated pin-wise power distribution is under development.

Concerning the inlet temperature, a difference to the related core channel can be given. Thus, the inlet temperature of the hot channel follows the time behaviour of the related core channel inlet temperature with a constant difference. For estimating the hot channel behaviour with reduced mass flow, the flow resistance coefficient of the hot channel can be changed in comparison with the related core channel.

Additionally, different fuel rod types can be defined for the hot channels. A fuel rod type is given by the geometry and thermo-physical properties of fuel and cladding as well as the gas gap properties (see Section 6.6). In this way, the influence of uncertainties in the fuel rod data on results of the transient calculation can be considered.

Using the hot channels, DNB analysis for the hottest fuel rods can be performed on-line with the transient calculation. However, the hottest fuel element must be known in advance. It must be outlined, that the DNBR calculation in DYN3D is performed not only for the hot channels, but for all core channels.

5.5 VVER-440 Coolant Mixing Model

The distribution of the coolant temperature and/or boron acid distribution at the core inlet is especially important for the neutron kinetics in the case of asymmetrical perturbations of these parameters. It has been shown, that the reactivity insertion by overcooling due to leaks in the steam system or boron dilution strongly depends on the degree of mixing of the coolant on the way from the cold legs to the core inlet. Thus, a realistic estimation of the coolant mixing is of great importance. This can be done by Computational Fluid Dynamics (CFD) codes, but these computations are very time consuming and can still not be integrated into reactor dynamics codes. Therefore, simplified approaches have been developed to estimate the coolant mixing.

In [Pra83a,b], [Ack85, 87] and [Drä85], an analytical mixing model for VVER-440 types reactors has been developed allowing the estimation of temperature and/or boron concentration distribution at the core inlet in the case of quasi steady state flow conditions.

The model is based on the fact, that the flow in the downcomer of VVER-440 type reactors can be well described in the potential flow approximation. This is due to special constructive features of this reactor - the existence of six primary circuit loops with relative low flow rates and the absence of a diffuser type increase of the flow cross section along the downcomer. While in most reactor types the high flow velocities in the loops and the diffuser effect in the

downcomer lead to large vortexes and re-circulation areas in the downcomer, the downcomer flow in VVER-440 downcomers is mostly parallel, but in general, not free of any vortexes.

The flow area inside the reactor pressure vessel is divided into the downcomer, the lower plenum, the control rod chamber (only for VVER-440 type reactors where the control elements have fuel followers), the core and the upper plenum. A schematic view of the flow areas with co-ordinates used in the mixing model is shown in figure 5.5.1.

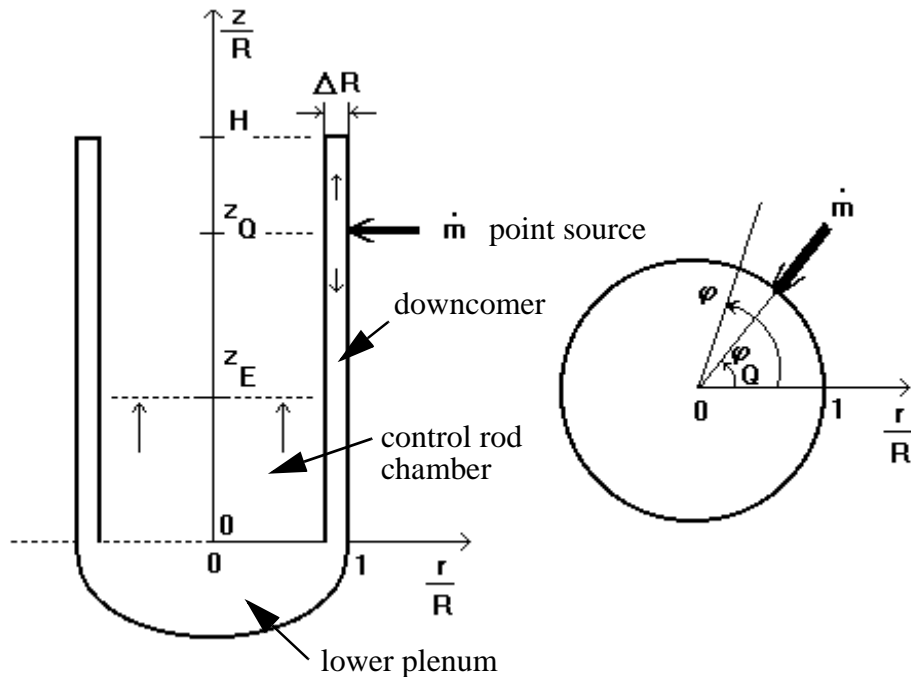


Fig. 5. 5.1: Principal view of the flow area in a VVER-440 type reactors showing the co-ordinates used in the mixing model

The highly turbulent flow in the downcomer is assumed to be incompressible and free of vortexes. In the control rod chamber, the flow is additionally assumed to be parallel to the z axis. Further, the absence of constructive internals is assumed in this region. The lower plenum is considered as a flow area without energy and mass exchange in the flow. The mixing in the downcomer and the control rod chamber is described by turbulent Peclet numbers. These assumptions have been shown to be sufficient for the conditions in VVER-440 type reactors under certain conditions.

Taking into account the small downcomer gap width in comparison to the radius of the reactor pressure vessel ($\Delta R/R \ll 1$), the downcomer flow is considered two-dimensional in the coordinates z and φ . A cold leg connection is described as a point source with the source strength \dot{m} and the co-ordinates (z_Q, φ_Q) .

The steady state, space dependent dimensionless temperature or concentration distribution $\Theta(\vec{r})$, which is called in the following the scalar distribution, is described by a diffusion - convection equation for incompressible fluids. In the 2D geometry of the downcomer this equation gets the form:

$$\frac{Pe_{DC}}{R\bar{v}_z} \left(v_\varphi(\varphi, z) \cdot \frac{1}{R} \frac{\partial}{\partial \varphi} + v_z(\varphi, z) \cdot \frac{\partial}{\partial z} \right) \Theta_{DC}(\varphi, z) = \left(\frac{1}{R^2} \cdot \frac{\partial^2}{\partial \varphi^2} + \frac{\partial^2}{\partial z^2} \right) \Theta_{DC}(\varphi, z) \quad (5.5.1)$$

where v_φ and v_z are the components of the fluid velocity vector, Pe_{DC} is the Peclet number in the downcomer and R is the radius of the downcomer.

In the downcomer, following boundary conditions have to be fulfilled;

$$\Theta(z_Q, \varphi_Q) = \Theta_Q \quad (5.5.2a)$$

$$\bar{e}_z \bar{v}(H, \varphi) = 0 \quad \bar{e}_\varphi \bar{v}(z, \varphi_Q \pm \pi) = 0 \quad (5.5.2b)$$

$$\bar{v}(-\infty, \varphi) = -\frac{\dot{m}}{2\pi R \Delta R \rho_Q} \bar{e}_z \quad (5.5.2c)$$

The boundary conditions (5.5.2) correspond to the flow in a semi-infinite rectangular flat region of the width $2\pi R$ with a point source at the axial symmetry axis. Condition (5.5.2a) defines the value of Θ at the point source location z_Q, φ_Q . The relations (5.5.2b) and (5.5.2c) describe the following boundary conditions:

- no flow out of the downcomer at the upper end,
- no flow across the symmetry axis,
- parallel flow along the z - axis at minus infinity with flow rate according to the source strength.

ρ_Q is the fluid density at the point source, \bar{e}_z and \bar{e}_φ are the unity vectors of the (φ, z) -coordinate system.

In dimensionless form, the equation (5.5.1) is written as:

$$Pe_{DC} \left(v_\varphi^*(\varphi, z^*) \cdot \frac{\partial}{\partial \varphi} + v_z^*(\varphi, z^*) \cdot \frac{\partial}{\partial z^*} \right) \Theta_{DC}(\varphi, z^*) = \left(\frac{\partial^2}{\partial \varphi^2} + \frac{\partial^2}{\partial z^{*2}} \right) \Theta_{DC}(\varphi, z^*) \quad (5.5.1a)$$

The dimensionless velocities and co-ordinates are defined as:

$$v_\varphi^* = \frac{v_\varphi}{v_{z,m}} \quad v_z^* = \frac{v_z}{v_{z,m}} \quad z^* = \frac{z}{R}$$

where $v_{z,m}$ is the average velocity in axial direction.

For the solution of equation (5.5.1a) for scalar transport and diffusion, the velocity field in the downcomer must be known. It is obtained assuming the potential flow approximation. Using this approximation, the velocity field can be eliminated by the help of the potential functions Φ and Ψ . The potential functions fulfill the Cauchy - Riemann condition and, therefore, the Laplace equation:

$$\frac{\partial \Phi}{\partial \varphi} = \frac{\partial \Psi}{\partial z^*} \qquad \frac{\partial \Phi}{\partial z^*} = -\frac{\partial \Psi}{\partial \varphi} \qquad (5.5.3a)$$

$$\nabla^2 \Phi = 0 \qquad \nabla^2 \Psi = 0 \qquad (5.5.3b)$$

The velocity field is in potential flow theory obtained as the gradient of the potential function Φ . Therefore,

$$v_\varphi^*(\varphi, z^*) = \frac{\partial \Phi}{\partial \varphi} \qquad v_z^*(\varphi, z^*) = \frac{\partial \Phi}{\partial z^*} \qquad (5.5.3c)$$

Using (5.5.3a) and (5.5.3c), equation (5.5.1a) can be transformed into:

$$Pe_{DC} \frac{\partial}{\partial \Phi} \Theta_{DC}(\Phi, \Psi) = \left(\frac{\partial^2}{\partial \Phi^2} + \frac{\partial^2}{\partial \Psi^2} \right) \Theta_{DC}(\Phi, \Psi) \qquad (5.5.4)$$

Therefore, the velocity is eliminated from equation (5.5.1a).

The transformation from equation (5.5.1a) to (5.5.4) is equivalent to the following co-ordinate transformation:

$$\begin{bmatrix} Rd\varphi \\ dz \end{bmatrix} = \frac{1}{v_\varphi^2 + v_z^2} \cdot \begin{bmatrix} v_\varphi & -v_z \\ v_z & v_\varphi \end{bmatrix} \begin{bmatrix} d\Phi \\ d\Psi \end{bmatrix}$$

In terms of Φ and Ψ , Θ has to fulfill the periodicity condition with respect to Ψ

$$\Theta_{DC}(\Psi) = \Theta_{DC}(\Psi + 2n\pi) \qquad (5.5.5a)$$

and the inlet boundary condition:

$$\Theta_{DC}(\Phi_0, \Psi) = \Theta_0(\Psi) \qquad (5.5.5b)$$

Condition (5.5.5b) defines the value of the scalar Θ at the line of constant potential $\Phi = \Phi_0$.

For the solution of equation (5.5.4), the following expansion is used:

$$\Theta_{DC}(\Phi, \Psi) = \sum_{n=-\infty}^{n=\infty} A_n \exp(in\Psi) \exp\left(-\frac{Pe_{DC}}{2} \left(\sqrt{1 + \frac{4n^2}{Pe_{DC}^2}} - 1 \right) (\Phi - \Phi_0) \right) \qquad (5.5.6)$$

The integration constants are obtained taking into account symmetry and boundary conditions. The expansion coefficients A_n are obtained using the orthogonality condition for the harmonic functions:

$$A_n = \frac{1}{2\pi} \int_{-\pi}^{\pi} d\Psi \Theta_0(\Psi) \exp(in\Psi) \qquad (5.5.6a)$$

For obtaining $\Theta_0(\Psi)$ it is assumed that we have a parallel flow at the end of the downcomer. Thus, $\Theta_0(\Psi)$ is defined by the position and the width of the flow sectors at the end of the

downcomer, which are connected with each cold leg (point source). In this sectors, $\Theta_0(\Psi)$ is equal to the normalized value of the mixing scalar in the corresponding loop. If e.g. in one of the six primary circuit loops of a VVER-440 there is a perturbation of the normalized mixing scalar (dimensionless boron concentration or temperature), $\Theta_0(\Psi)$ is 1.0 a 60 degree sector with respect to Ψ and 0 in the other sectors. The position and the width of these sectors are obtained from the condition, that the width b_i of each sector i is proportional to the mass flow rate \dot{m}_i of the corresponding loop:

$$b_i = 2\pi R \frac{\dot{m}_i}{\dot{M}} \quad (5.5.7a)$$

and the angle shift $\Delta\gamma_i$ of the centerline of each sector relative to the azimuthal position of the corresponding loop γ_i is given by the relations

$$\Delta\gamma_i = (\gamma_{ij} - \beta_{ij}) + \Delta\gamma_j \quad (5.5.7b)$$

where γ_{ij} is the angle between loops i and j and β_{ij} is the angle between the centerlines of the sectors connected to the loops i and j :

$$\beta_{ij} = \left(\frac{1}{2} \cdot \frac{\dot{m}_i + \dot{m}_j}{\dot{M}} \right) 2\pi \quad (5.5.7c)$$

The angle shift for each loop is obtained by solving the equation system (5.5.7b). A schematic sketch of flow sectors and connected loops (cold leg inlets) is shown in figure 5.5.2.

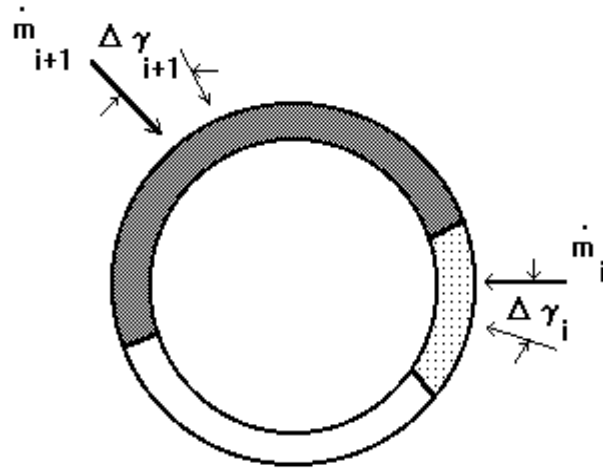


Fig. 5.5.2 Schematic sketch of two neighbouring flow sectors

Taking into account the assumption of homogeneous parallel flow, in the control rod chamber region only the diffusion equation for Θ has to be solved. The velocity of the fluid does not occur in this equation:

$$\frac{Pe_{CRC}}{R} \frac{\partial}{\partial z} \Theta_{CRC}(r, \varphi, z) = \left(\frac{1}{r} \frac{\partial}{\partial r} r \frac{\partial}{\partial r} + \frac{1}{r^2} \frac{\partial^2}{\partial \varphi^2} + \frac{\partial^2}{\partial z^2} \right) \Theta_{CRC}(r, \varphi, z) \quad (5.5.8)$$

Following boundary conditions have to be fulfilled for the control rod chamber region:

$$\Theta(r, \varphi, 0) = \Theta_0(\varphi) \quad (5.5.9a) \quad \frac{\partial}{\partial r}\Theta(r, \varphi, z)|_{r=R-\Delta R} = 0 \quad (5.5.9b)$$

$$\Theta(r, \varphi, -\infty) = \frac{1}{\pi(R-\Delta R)^2} \int_{-\pi}^{\pi} d\varphi \int_0^{R-\Delta R} dr r \Theta_0(r, \varphi) = \Theta_m \quad (5.5.9c)$$

These conditions correspond to the diffusion in a semi-infinite, isolated cylinder, where a distribution $\Theta = \Theta_0(\varphi)$ at the axial position $z=0$ is given and where homogenization of the J-distribution at $-\infty$ is assumed (Θ_m in 5.5.9c is the average value of the mixing scalar, which can be obtained from the inlet boundary conditions). This distribution corresponds to the distribution at the end of the downcomer:

$$\Theta_0(\varphi) = \Theta_{DC}(\varphi, z)|_{z=0} \quad (5.5.10)$$

The isolation condition is given by equation (5.5.9b). Relation (5.5.10) is used to connect the solutions in the downcomer and in the control rod chamber. No energy and mass exchange is assumed in the lower plenum situated between the downcomer and the control rod chamber. For the solution of equation (5.5.8), following expansion is used:

$$\Theta_{CRC} = \sum_{n=-\infty}^{n=\infty} \exp(in\varphi) g_n(r, z) \quad (5.5.11a)$$

$$g_n(r, z) = \sum_{m=0}^{m=\infty} a_{nm} J_n\left(\alpha_{nm} \frac{r}{R}\right) \exp\left(-\frac{z}{R} \frac{Pe_{CRC}}{2} \left(\sqrt{1 + \frac{4\alpha_{nm}^2}{Pe_{CRC}^2}} - 1\right)\right) \quad (5.5.11b)$$

The application of the isolation condition (5.5.9b) leads to $\frac{d}{dr}J_n(\alpha) = 0$. Therefore, α_{nm} is the m-th extremum of the Bessel function $J_n(x)$. The width ΔR of the downcomer is here set to zero. Equation (5.5.11b) satisfies the conditions of rotational symmetry in relation to the z-axis, the isolation condition at $r = R$ and the condition of homogenization of the Θ -distribution at $z = \infty$, if the constant α_{00} is set to Θ_m (see 5.5.9c). The other expansion coefficients a_{nm} are obtained from the boundary condition at $z = 0$ using the orthogonality relations of the Bessel functions:

$$\int_0^1 dr r J_n\left(\alpha_{nk} \frac{r}{R}\right) J_n\left(\alpha_{nl} \frac{r}{R}\right) = \frac{1}{2} J_n^2(\alpha_{nk}) \left(1 - \frac{n^2}{\alpha_{nk}^2}\right) \delta_{kl} \quad (5.5.12)$$

$$a_{nm} = \frac{1}{2\pi} \frac{2}{J_n^2(\alpha_{nm}) \left(1 - \frac{n^2}{\alpha_{nm}^2}\right)} \int_{-\pi}^{\pi} d\varphi \int_0^1 dr r \Theta_0(r, \varphi) J_n\left(\alpha_{nm} \frac{r}{R}\right) \exp(in\varphi) \quad (5.5.13)$$

Thus, a closed analytical solution for the dimensionless temperature or boron acid concentration at the reactor core inlet described by the function $\Theta_{\text{CRC}}(r, \phi, z)$ at $z = z_E$ can be derived under the assumptions discussed above. The two model parameters Pe_{DC} and Pe_{CRC} have to be obtained by adopting the solutions to experimental results or CFD solutions.

Validation activities are reported about in [Drä87]. Calculated temperature distributions at the core inlet are compared with measurement data from VVER-440 type reactors in Paks and Loviisa. Further, the model has been validated on experimental results measured at a 1:5 scaled, air operated geometrical flow model of VVER-440 type reactors. Both versions V-213 (with elliptical sieve construction in the lower plenum) and V-230 (without elliptical sieve construction) of VVER-440 reactors have been investigated. The influence of the elliptical sieve construction is described by adopting the turbulent Peclet numbers. A good agreement between calculated and measured temperature distributions at the core inlet was achieved. These results were confirmed by recent CFD calculations [Kli99]. The dimensionless distribution of a scalar (temperature or boron concentration) at the end of the downcomer and at the core inlet obtained in calculations by help of the code CFX-4 was compared with results from the analytical model and the air operated test facility measurements. A good agreement can be stated, the mixing is slightly under-estimated in the CFD calculation.

Therefore, it can be concluded that the analytical model of DYN3D described in this chapter can be used for VVER-440 type reactors under quasi steady-state conditions with all loops in operation. These conditions are given in the case of normal reactor operation or e.g. during a main steam line break accident scenario, where the temperature changes slowly in comparison with the transport time of the coolant from the cold leg outlet until the core inlet, and coolant is flowing in all loops. However, the model must not be used for other reactor types, where the assumption of potential flow in the downcomer is poor, and where is no control rod chamber. In the frame of a recently ongoing research project on the experimental and theoretical investigation of coolant mixing in PWRs improved mixing models will be developed, validated and implemented into DYN3D.

5.6 Numerical Methods and Iterative Procedures in Thermohydraulics

In the following, a brief description of the numerical methods for solving the basic equations of the thermohydraulic model is given.

5.6.1 Numerical Solution of the Energy and Vapour Mass Balance Equations

The equations for energy balance (5.1.11) and mass balance of the vapour phase (5.1.13) are given in the conservative form:

$$\frac{\partial y}{\partial t} + u \frac{\partial y}{\partial z} = q \quad (5.6.1)$$

That's why the method of characteristics (MOC) with linear interpolation between the mesh points can be used. This method can be interpreted as the tracking of a fictive fluid particle along its way within a mesh grid in space and time (see figure 5.6.1)

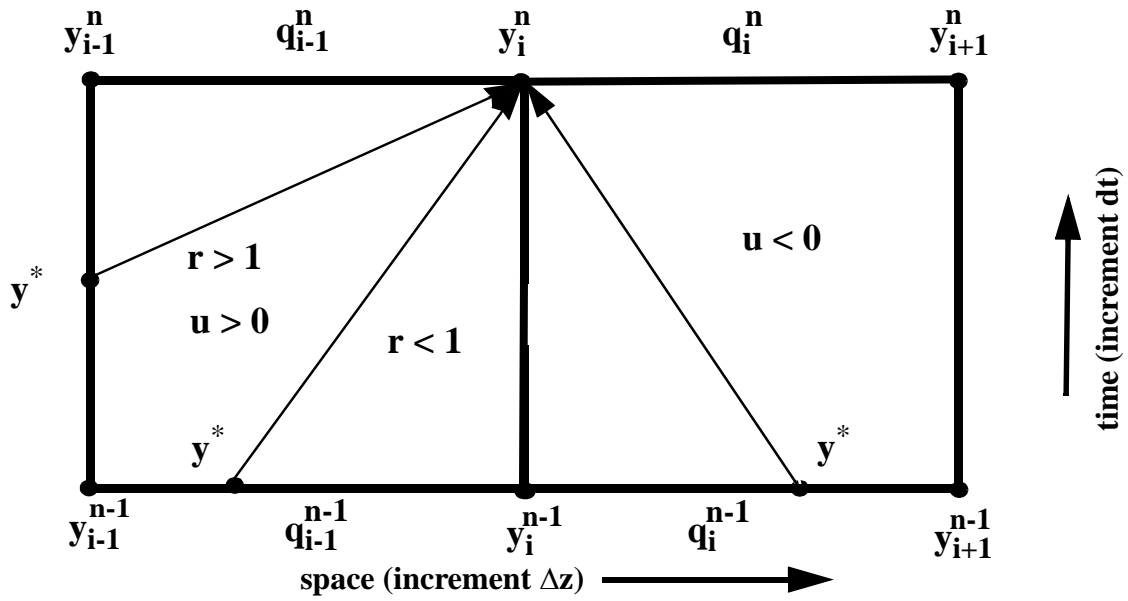


Fig. 5.6.1 Discretisation scheme for the method of characteristics (MOC)

The time steps are described by the superscript n , while the steps in spatial mesh are indicated by the subscript i . A fictive fluid particle is moving during one time step Δt from the starting point $*$ of the characteristic line to the point (n, i) .

The equation (5.6.1) is integrated along its characteristic $u = dz/dt$ from the point $(*)$ to the point (n, i) of the characteristic line::

$$y_i^n = y^* + \int_{t^*}^{t + \Delta t} q_i(t') dt'$$

In the normal case of positive flow velocity (coolant flow from the bottom to the top of the core) following scheme illustrated at the left part of figure 5.6.1 is used: If the Courant parameter r is less than 1, the particle moves less than one step in then spatial mesh (along the z -axis). The starting point of the characteristic line is interpolated between mesh points $(n-1, i-1)$ and $(n-1, i)$ at the previous time step level. If the Courant parameter is larger than 1, the particle moves during one time step more than one step in the spatial mesh. The starting point of the characteristic line in this case is interpolated between the mesh points $(n-1, i-1)$ and $(n, i-1)$ at the previous spatial step level. The slope of the characteristic line is defined by the velocity u in equation (5.6.1). The Courant parameter r is defined as:

$$r = |u_{i-1/2}^{n-1/2}| \cdot \frac{\Delta t}{\Delta z} \tag{5.6.2}$$

If a linear interpolation for the starting point (*) is used and the integral is approximated by the product of the time interval and the average value of the source, we obtain the following finite difference approximation for equation (5.6.1):

$$y_i^n = (1-r) \cdot y_i^{n-1} + r \cdot y_{i-1}^{n-1} + \frac{\Delta t}{2} \cdot (q_{i-1}^{n-1} + q_{i-1}^n) \quad \text{if } r \leq 1 \quad (5.6.3a)$$

$$y_i^n = \frac{r-1}{r} y_{i-1}^n + \frac{1}{r} y_{i-1}^{n-1} + \frac{\Delta t}{2r} \left(\frac{2r-1}{r} q_{i-1}^n + \frac{1}{r} q_{i-1}^{n-1} \right) \quad \text{if } r > 1 \quad (5.6.3b)$$

The source term q is interpolated between old and new time step (in the case $r < 1$) or between new time step and time level corresponding to point (*).

This simple first order scheme is unconditionally stable. The numerical diffusion is zero, if the condition $r = 1$ is fulfilled. However, due to other requirements to the time and spatial step sizes and changing velocity u this condition cannot be fulfilled in general, but choosing the discretisation mesh sizes, the criterion should be approached as well as possible.

In the case of negative flow rate (coolant velocity), the integration along characteristic line is performed according to the right part of figure 5.6.1 Negative velocities can occur locally and temporarily due to the mass conservation equation 5.1.12 in the case of large changes of fluid density in time. DYN3D is not able to handle reversal of flow direction in the core in general. If $u < 0$, following scheme is used:

$$y_i^n = (1-r) \cdot y_i^{n-1} + r \cdot y_{i+1}^{n-1} + \frac{\Delta t}{2} \cdot (q_i^{n-1} + q_i^n) \quad \text{if } r \leq 1 \quad (5.6.3c)$$

In the case of flow reversal, only the explicit scheme according to equation (5.6.3c) is used, because otherwise the scheme must be solved with changing directions of subsequent solution of the difference equations along the channel (downstream and upstream). Because the explicit scheme is stable only for $r < 1$, in that case time sub-steps will be introduced by subdividing the basic time step for thermohydraulics into sub-steps for solving the energy equation until the condition $r < 1$ will be fulfilled.

5.6.2 Numerical Solution of the Mass and Momentum Balance Equations

The momentum balance equation (5.1.10) is linearized for numerical solution. The quadratic terms in the mass flow density G are approximated in the following way:

$$G|_k^2 = 2G|_k \cdot G|_{k-1} - G|_{k-1}^2 \quad (5.6.4)$$

where k is the iteration index. The friction term $\frac{\partial p_{fric}}{\partial z}$ in the momentum balance equation is

written in the form $\frac{RG^2}{\Delta z}$ with $R = \frac{1}{\rho_l} \left(\frac{\lambda}{D} \Delta z + \zeta \right)$ according to (5.2.1).

For the coupled solution of the momentum and the mass balance equations (5.1.10) and (5.1.12), following difference scheme proposed by MIRONOV [Mir82] is applied:

$$\frac{\rho_{i-1/2}^n - \rho_{i-1/2}^{n-1}}{\Delta t} + \frac{G_i^n|_k - G_{i-1}^n|_k}{\Delta z_{i-1}} = 0 \quad (5.6.5a)$$

$$\begin{aligned} & \frac{G_{i-1/2}^{n(k)} - G_{i-1/2}^{n-1}}{\Delta t} + \frac{p_i^n - p_{i-1}^n}{\Delta z_{i-1}} + \\ & \frac{2G_i^{n(k)} \cdot G_i^{n(k-1)} - (G_i^{n(k-1)})^2}{\Delta z_{i-1}} v_{m,i}^n - \\ & \frac{2G_{i-1}^{n(k)} \cdot G_{i-1}^{n(k-1)} - (G_{i-1}^{n(k-1)})^2}{\Delta z_{i-1}} v_{m,i-1}^n + \\ & \frac{2G_i^{n(k)} \cdot |G_i^{n(k-1)}| - G_i^{n(k-1)} \cdot |G_i^{n(k-1)}|}{\Delta z_{i-1}} \cdot R_i^n + \\ & \frac{2G_{i-1}^{n(k)} \cdot |G_{i-1}^{n(k-1)}| - G_{i-1}^{n(k-1)} \cdot |G_{i-1}^{n(k-1)}|}{\Delta z_{i-1}} \cdot R_{i-1}^n + g\rho_{i-1/2}^n = 0 \end{aligned} \quad (5.6.5b)$$

The superscript n indicates the time step, the subscript i - the spatial mesh and the index k the iteration number. The values at mesh centers (i-1/2) are obtained by linear interpolation of the mesh edged values. The absolute values of G in the friction terms are necessary for flow reversal treatment.

With respect to the unknown variables, the system (5.6.5) can be written in the following form:

$$p_i^n = p_{i-1}^n - a_{1,i} G_i^{n(k)} + a_{2,i} G_{i-1}^{n(k)} + b_{1,i} \quad (5.6.6a)$$

$$G_i^{n(k)} = G_{i-1}^{n(k)} - b_{2,i} \quad (5.6.6b)$$

where the coefficients a1, a2, b1 and b2 contain only known parameters (from the previous time step or iteration cycle).

For large variations of the coolant densities (for instance, due to sudden or strong boiling), and/or very small integration time steps, the coefficient $b_{2,i}$ can become very large, and equation (5.6.6b) might yield strong under- or over-estimation of the mass flux $G_i^{n(k)}$ and lead to unstable flow rate/pressure iteration. To overcome this problem a simple relaxation algorithm has been implemented. The time derivative of the local density variations is multiplied by a relaxation factor Θ_{GI} that can range from zero to unity. In this case, equation (5.6.6b) reads:

$$G_i^{n(k)} = G_{i-1}^{n(k)} - \Theta_{GI} \cdot b_{2,i}$$

At the beginning of the mass flow/pressure iteration, Θ_{GI} is set to zero (no mass-fluxes spatial gradient). Successively, it is linearly increased until after a certain number of iterations the value unity is reached. Note, that equation (5.6.6b) is used to evaluate the spatial gradient (in the axial direction) of the mass flux, therefore no relaxation is needed when axial gradients of the mass flux are not to be expected or are small. The relaxation algorithm can be controlled by input parameters.

The system of algebraic equations (5.6.6) is re-arranged using the so-called RICATTI transformation:

$$p = G \cdot r + s$$

Putting this transformation in equation (5.6.6) and setting equal the coefficients of terms with the same order of G yields the following equations for the new variables r and s:

$$r_{i-1} = r_i + a_{1,i} - a_{2,i} \quad (5.6.7a)$$

$$s_{i-1} = s_i - b_{1,i} - b_{2,i} \cdot (r_i + a_{1,i}) \quad (5.6.7b)$$

Considering the boundary conditions for the pressure at the inlet and the outlet of the core, we obtain the boundary values for solving the system (5.6.7):

$$s_N = p_{out} \quad r_N = 0 \quad \text{at the core outlet (i = N) and} \quad G_{in} = \frac{p_{in} - s_0}{r_0} \quad \text{at the core inlet (i = 0).}$$

Using these boundary conditions, in the first sweep of solution of the system (5.6.7) the coefficients r and s can be obtained starting with i = N (downwards sweep), in the second sweep the pressure and mass flow density values p and G can be obtained starting from i = 0 (upwards sweep) with known r_0 and s_0 from the downwards sweep. In this way, a simultaneous determination of pressure and mass flow density distribution for parallel channels with given pressure drop (i.e., pressure boundary conditions at the core inlet and outlet) is performed.

5.6.3 Solution of the Boron Transport Equation

For the solution of the balance equation (5.1.7) for boron or boron acid concentration, two algorithms are available which can be used alternatively. One way is to solve the equation written in the characteristic form (5.6.1) by method of characteristics. However, suppression of numerical diffusion is of special importance for the description of boron transport. It has been shown, that numerical diffusion can lead to artificial smoothing of a boron perturbation front, what can cause a significant underestimation of the reactivity insertion and therefore of the consequences of a boron dilution transient [Gru94], [Roh97]. That's why the MOC has been modified and combined with a higher order scheme (Lax-Wendroff) to minimize numerical diffusion.

Another way is to apply a so-called particle-in-cell (PIC) method [Roh97]. By the help of this method, numerical diffusion can be completely excluded. The accuracy of the method depends on the number of fictive fluid particles to be defined. Enhancing the number of particles can lead to high demand of computer memory. That's why this method can be used as an option.

In the MOC approach, the boron transport equation is considered in a simplified form:

$$\frac{\partial}{\partial t} \rho c_b + \frac{\partial}{\partial z} \rho u c_b = 0 \quad (5.6.8)$$

That means, the boron transport is considered to be performed within homogeneous fluid flow instead of liquid flow according to equation (5.1.7). In the case of one-phase liquid flow there is no difference, but in the case of two-phase flow the boron acid is considered to be solved homogeneously in the two-phase mixture instead of being solved only in the liquid. The latest assumption is better from physical point of view, because the solubility of boron acid in vapour is very small.

By the help of the mass balance equation (5.1.12), equation (5.6.8) can be transformed to the characteristic form (5.6.1) with zero source term:

$$\frac{\partial c_b}{\partial t} + u \frac{\partial c_b}{\partial z} = 0 \quad (5.6.9)$$

For the solution of that equation of type (5.6.1) following procedure is applied. If $r < 1$, the Lax-Wendroff scheme [Ric67] is used:

$$y_i^n = a_i^n \cdot y_{i+1}^{n-1} + b_i^n \cdot y_i^{n-1} + c_i^n \cdot y_{i-1}^{n-1} \quad (5.6.10a)$$

$$a_i^n = \frac{1}{4} \left[\left(\frac{\Delta t}{\Delta z} \right)^2 \cdot u_i^{n-1} \cdot (u_{i+1}^{n-1} + u_i^{n-1}) - \frac{\Delta t}{\Delta z} \cdot (u_i^{n-1} + u_i^n) \right] \quad (5.6.10b)$$

$$b_i^n = 1 - \frac{1}{4} \cdot \left(\frac{\Delta t}{\Delta z} \right)^2 \cdot u_i^{n-1} \cdot (u_{i+1}^{n-1} + 2u_i^{n-1} + u_{i-1}^{n-1}) \quad (5.6.10c)$$

$$c_i^n = \frac{1}{4} \left[\left(\frac{\Delta t}{\Delta z} \right)^2 \cdot u_i^{n-1} \cdot (u_i^{n-1} + u_{i-1}^{n-1}) + \frac{\Delta t}{\Delta z} \cdot (u_i^{n-1} + u_i^n) \right] \quad (5.6.10d)$$

The scheme is of second order of accuracy and is stable in the case $r < 1$. It produces reduced numerical diffusion in comparison with the first order MOC. In the case $r > 1$, following algorithm is used.

1) Integration of equation (5.6.9) over one spatial mesh along the characteristic:

$$y_i^n = y_{i-1}^* \quad \text{with } y_{i-1}^* \text{ at time } t_{i-1}^* = t_i^n - \frac{\Delta z_i}{u_{i-1/2}^n}$$

2) For the successive mesh point it follows:

$$y_{i-1}^* = y_{i-2}^* \quad \text{with } y_{i-2}^* \text{ at time } t_{i-2}^* = t_{i-1}^* - \frac{\Delta z_{i-1}}{u_{i-3/2}^{n-1}} \quad \text{etc.}$$

3) At the beginning of the characteristic and in correspondence with $r < 1$ the Lax-Wendroff scheme is used. The procedure is illustrated in figure 5.6.2 (for the case of tracking the characteristics over four nodes).

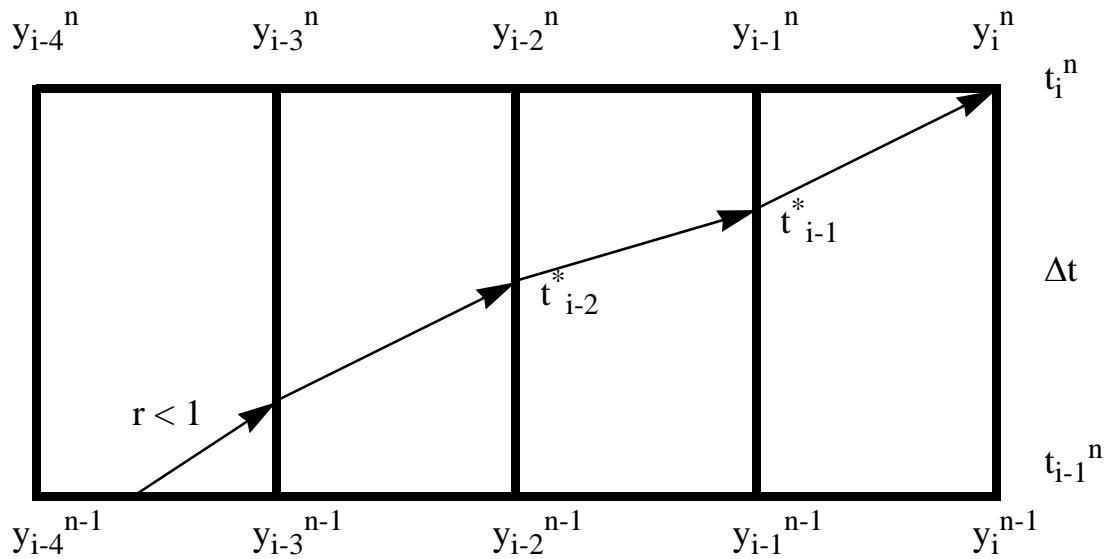


Fig. 5.6.2 Schematic illustration of the MOC/Lax-Wendroff tracking scheme

The second method used for the description of boron transport is an one-dimensional particle model. There is no direct fluidmechanical feedback from local concentrations of boron acid on the fields of velocities. This fact enables a calculation of the transport of boron acid on base of the previously calculated velocities. In the boron concentration conservation equation (5.1.7):

$$\frac{\partial}{\partial t}(1 - \varphi)\rho_l c_b + \frac{\partial}{\partial z}u_l(1 - \varphi)\rho_l c_b = 0$$

c_b is the mass of boron (or boron acid) related to the mass of liquid water. However, in reactor physics the concentration of boron \tilde{c}_b is defined as the boron mass related to the whole mass of the fluid (liquid and vapour). That means, we have the relation:

$$c_b = \tilde{c}_b \left(1 + \frac{\varphi \rho_v}{(1 - \varphi)\rho_l'} \right)$$

The balance equation (5.1.7) can be formulated for the mass of boron m_b within a defined volume as:

$$\frac{\partial}{\partial t}m_b + \frac{\partial}{\partial z}u_l m_b = 0 \quad (5.6.11)$$

That means, the transportation of boron acid is done by the velocity of the water, however the local dependence of the velocity has to be considered.

The particle model was developed especially for the transport of boron in a channel with constant area without consideration of any crossflows. The channel is subdivided in a number of axial layers (nodes). The height of the single layers may be different. The mass of boron within a given volume is determined by the number of particles. Each particle presents a certain mass of boron. This mass per particle is determined at the begin of the calculation by an assignment of a particle number to a reference value of the boron concentration within the average node

volume. The higher the number of particles the lower the statistical error implied by this method. However the effort of calculation (calculation time and memory) also increases with the number of particles.

Every particle is assigned to an actual location. The transport of boron is done by a movement of the single particles with the velocity of the water u_1 . Sources may occur only at the inlet of the channel. Particles that leave the channel at the upper end are removed from the calculational cycle.

The particle model realizes two essential steps within one time step:

1. Shift of the particles including consideration of sources and
2. Counting of particles within the single nodes and calculation of the concentration of boron acid.

The velocities of water are available at the node boundaries. Because there is no direct fluid-mechanical feedback from local concentrations of boron acid on the fields of velocities, the calculation of the transport of boron can be performed based on the previously calculated velocities. For the particle transport, a continuous axial velocity distribution is taken as a basis. For this purpose a linear transition of the velocities between the values at the node boundaries was assumed within the nodes (see figure 5.6.3).

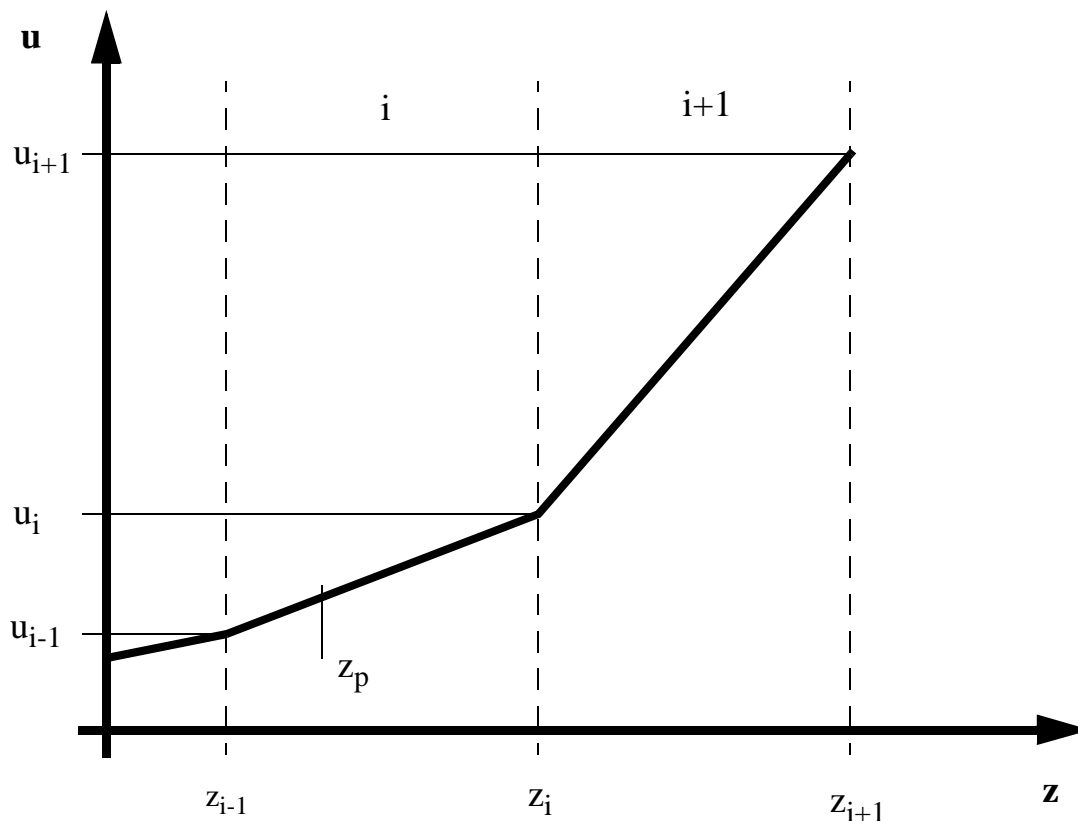


Fig. 5.6.3 Continuous axial velocity distribution

Within the node i the velocity is calculated according to:

$$u(z) = u_{i-1} + \frac{u_i - u_{i-1}}{z_i - z_{i-1}}(z - z_{i-1}) = m_i z + n_i$$

with

$$m_i = \frac{u_i - u_{i-1}}{z_i - z_{i-1}} \quad n_i = u_{i-1} - \frac{u_i - u_{i-1}}{z_i - z_{i-1}} z_{i-1}$$

That means that for the particle shift within the node the following differential equation is valid:

$$\frac{dz}{dt} - m_i z = n_i \quad z(0) = z_p \quad (5.6.12)$$

z_p is the initial position of the particle. If the particle does not leave the node within the time step, the new position is calculated as solution of the differential equation (5.6.12):

$$z(\Delta t) = \left(z_p + \frac{n_i}{m_i} \right) e^{m_i \Delta t} - \frac{n_i}{m_i} \quad (5.6.13)$$

If the particle reaches the node boundary within the time step, that means if $z(\Delta t)$ is greater than z_i or less than z_{i-1} , the time Δt_i for the movement to this node boundary is calculated:

$$\Delta t_i = \frac{1}{m_i} \ln \left(\frac{z_i + \frac{n_i}{m_i}}{z_p + \frac{n_i}{m_i}} \right)$$

This time is subtracted from the time step Δt , the particle position is set to the position of the corresponding node boundary and the calculation is continued with m and n values for the next node. This is repeated until the final position of the particle is found. So a particle may also move over several nodes within one time step.

The number of source particles N is calculated from the total mass of boron entering the channel at the inlet within the time step. The mass of boron can be considered only in discrete steps according to the mass carried by one particle. So in general remains a mass which enters the channel, but is not considered by the transport model. This mass is considered at the next time step. This guarantees an exact fulfilment of the conservation of mass. The initial position of the source particles is always the inlet of the channel. The new position of the source particles is calculated according to equation (5.6.13), but with an individually modified Δt for each particle:

$$\Delta t_{mod}^j = \frac{j}{N} \Delta t$$

j is a counter for the source particle, which will be moved ($1 \leq j \leq N$). That means the particles are added within the time step with steps constant in time and moved according to the remaining time to the end of the time step.

After the shift of all particles the number of particles within each node is counted and the concentration of boron acid is calculated.

5.6.4 Iterative Procedures

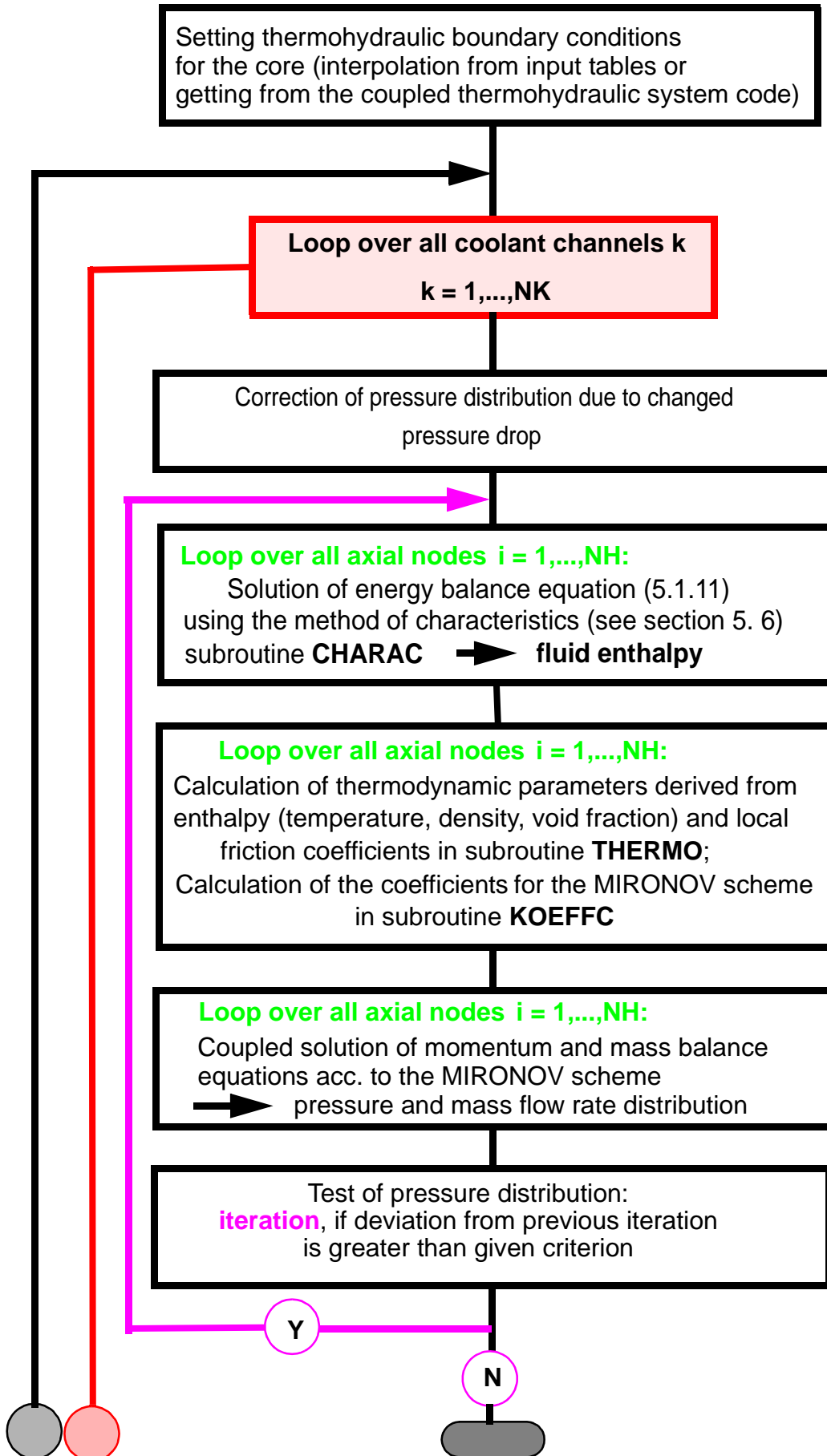
The solution of the energy and vapour mass balance equations, on the one hand, and the mass and momentum balance equations, on the other hand, is iteratively coupled. In the iteration sweep $k-1$, using an estimation of mass flow densities (e.g. values from the previous time step or previous iteration), the energy and vapour mass balance equations for a coolant channel are solved. Actual values of the enthalpies, densities and friction coefficients are obtained. Using these values, the mass and momentum balance equations are solved again in an iterative way, varying the mass flow rates of the individual coolant channels to obtain the given pressure drop over the core (being equal for all channels). The new pressure and mass flow density distributions are then used, after updated steam and water properties, in the next iteration sweep for solving again the energy and vapour mass balances. Then follows the iteration sweep k , until convergence of pressure and mass flow density distributions is obtained.

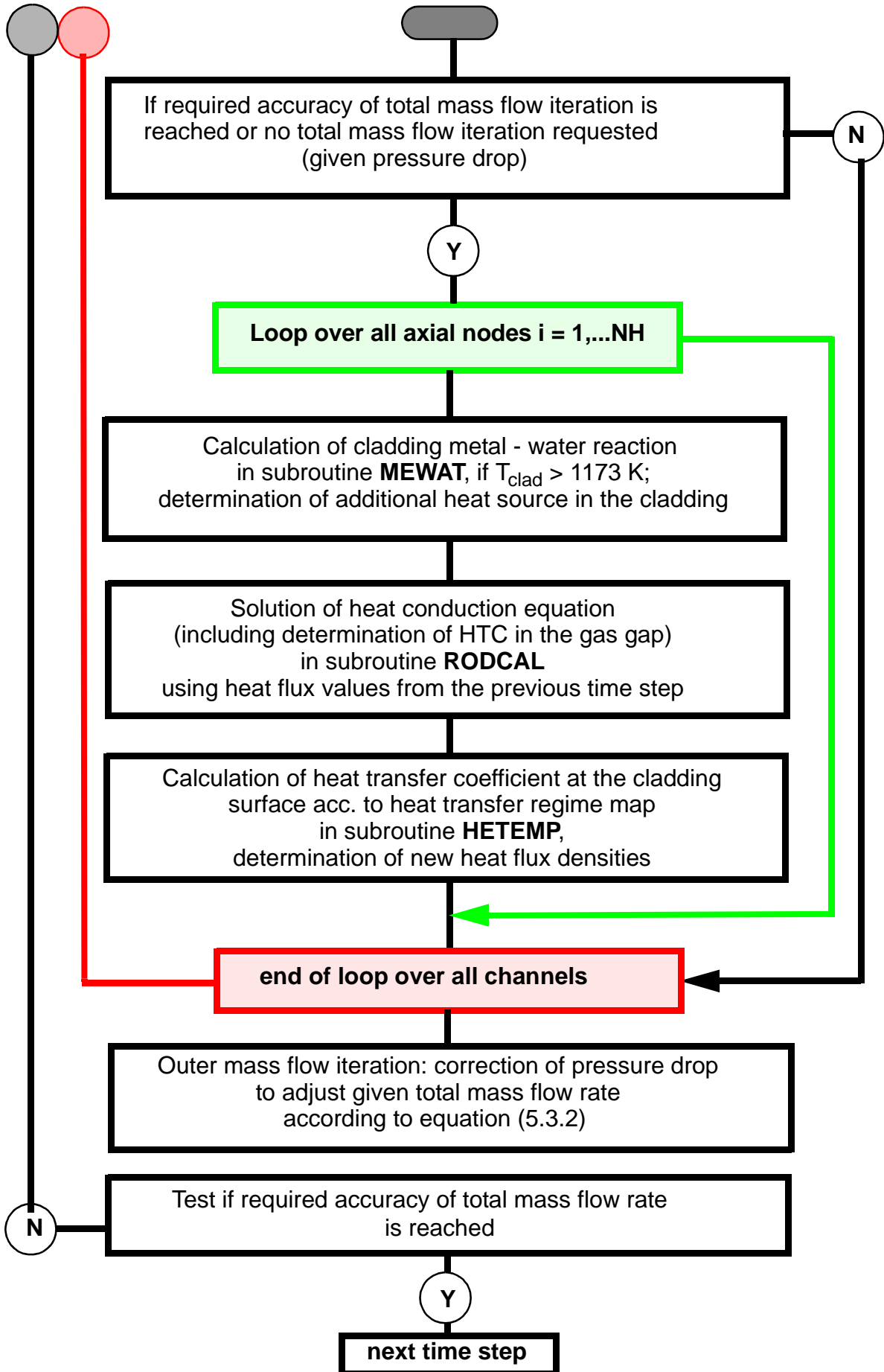
In the case of given total mass flow rate through the core, an additional iteration level is necessary. First, an estimation of the pressure drop over all channels was used to obtain the mass flow distribution. Then, the total mass flow through the core is calculated. If this value does not agree with the given total mass flow rate value, the pressure drop is modified and the calculation is repeated for all coolant channels (see section 5.3).

For each iteration sweep of solving the thermohydraulic equations, the heat flux density values from the previous time step are used. After finishing the solution of the thermohydraulic equations, the fuel to coolant heat transfer package is called. Using the actual coolant temperature, void fraction and mass flow rate values, the heat transfer coefficients are updated. After that, the fuel rod model is considered and the heat conduction equation for the fuel rod is solved. Updated values for the cladding to coolant heat flux rates are obtained. An under-relaxation of the heat flux with the previous values is applied, where the under-relaxation coefficients can be given in the input.

The above described iteration procedure is performed for each thermohydraulic time step. An automatic control of the time step is carried out considering the rate of change of relevant thermohydraulic parameters (fuel temperature, coolant density and heat flux density at the cladding wall) in time. The maximum relative change of these parameters during a time step is calculated. If these maximum changes exceed some threshold values given in the input, the time step size for the next time step is reduced by a factor two. If the maximum changes are smaller than a half of the given limit, the time step size is increased by a factor two. The automatic time step control can be switched off and a fixed time step size can be used within a given time interval. That may be useful in some special situations.

A schematic sketch of the thermohydraulic - fuel rod model iteration procedure performed during one time step is shown in the following flow sheet.





References Chapter 5

- [Ack85] Ackermann, G.; Dräger, P.; Siklossy, P.: Theoretische und experimentelle Ermittlung der Temperaturverteilung am Eintritt in die Spaltzone des WWER-440; *Kernenergie* **28** (1985) 7, S. 293-297
- [Ack87] Ackermann, G.; Dräger, P.: Makroskopische Kühlmittelvermischung in Druckwasserreaktoren; *Kernenergie* **30** (1987) 11/12, S. 454-458
- [Art97] Artym, R. I.: Computerprogramme für die thermodynamischen Zustandsgrößen und Transporteigenschaften von Wasser und Wasserdampf, *internal report F00811/4*, Moscow, 1997
- [Ast82] Astakhov, V. I., Yu. A. Bezrukov and S. A. Logvinov: *International Seminar „Teplofizika - 82“*, Karlovy Vary (Czechoslovakia), May 1982, Proc. Vol. 4, p. 168
- [Bez76] Bezrukov, Yu. A. et al.: *Teploehnergetika* 1976, Nr. 2, p. 80
- [Bia67] Biasi, L. et al.: *Energia Nucleare* **14**, Nr. 9, September 1967
- [Drä87] Dräger, P.: Makroskopische Kühlmittelvermischung in Druckwasserreaktoren, *PhD Thesis*, Ingenieurhochschule Zittau, 1987
- [Fri85] Frick, E.: Fluid-und Thermodynamik der instationären Zweiphasenströmung bei der Notkühlung von Kernreaktoren, *Report EIR-588*; Würenlingen, 1985
- [Got86] Gotovskij, M. A. e al.: The influence of fluid subcooling on the minimum temperature difference in film boiling (in Russian), in Compendium: *Teploobmen v ehnergooboruvanii AEhS*, p. 156-165, Nauka, Moscow, 1986
- [Gri90] Grigull, U.: *Properties of water and steam in SI-units*, Springer Verlag, Berlin - Heidelberg - New York, 1990
- [Gro76] Groeneveld, D. C.; G. G. J. Delorme: *Nuclear Engineering and Design* **36**, 17
- [Gru94] Grundmann, U., U.Rohde: Investigations on a Boron Dilution Accident for VVER-440 type Reactor by the Help of the Code DYN3D, *ANS Topical Meeting on advances in Reactor Physics*, Knoxville, April 11-15, 1994, Proc. Vol. 3, p. 464
- [Huh75] Huhn, J.; J. Wolf: *Zweiphasenströmung gasförmig - flüssig*; VEB Fachbuchverlag, Leipzig, 1975
- [Kir84] Kirillov, P.L. et al.: *Spravochnik po teplogidravlicheskim raschjotam*, Ehnergoizdat, Moscow, 1971
- [Kli99] Kliem, S., Höhne, T., Weiß, F.-P.: Main steam line break analysis of a VVER-440 reactor using the coupled thermohydraulics system / 3D-neutronkinetics code DYN3D/ATHLET in combination with the CFD code CFX-4, *9th International Topical Meeting on Nuclear Reactor Thermal Hydraulic Meeting on Nuclear Reactor*

- Thermal Hydraulics (NURETH-9)*, San Fransisco, California, Oct. 3-8, 1999, ISBN 0-89448-650-0
- [Mey69] Meyer-Pittroff, R., H. Vesper, U. Grigull.: Einige Umkehrfunktionen und Näherungsgleichungen zur 1967 IFC Formulation for Industrial Use für Wasser und Wasserdampf, *Brennstoff - Waerme - Kraft* **21** (1969) 239
- [Mir82] Mironov, Y. V.: Analyis of instationary thermo-hydraulic problems for water-steam flows (in Russian), *International Seminar „Teplofizika - 82“*, Karlovy Vary (Czechoslovakia), May 1982, Proc. Vol. 2 pp. 111-128
- [Mol82] Molochnikov, Yu. S.: *Teploehnergetika* 1982, Nr.7, p. 47
- [Osm71] Osmachkin, V. S.; V. D. Borisov: *Report IAE-1957*, Kurchatov Institute, Moscow, 1971
- [Osm78] Osmachkin, V. S.: *International Seminar „Teplofizika - 78“*, Budapest, March 1978, Proc. Vol. 1, p.27
- [Pol82] Poljanin, L. N.; M. Ch. Ibragimov, G. P. Sabeljev: *Teploobmen v jadernikh reaktorakh*, Ehnergoizdat, Moscow, 1982
- [Pra83a] Prasser, H.-M.: Ermittlung der Massenstromverteilung an der unteren Lochplatte von WWER-Reaktoren durch eine dreidimensionale Potentialfeldnäherung; *Kernenergie* **26** (1983) 4, pp. 159-162
- [Pra83b] Prasser, H.-M.: Ein Beitrag zur Ermittlung der Kühlmittelmassenstromverteilung in Druckwasserreaktoren vom Typ WWER mit eingebautem elliptischem Siebboden; *Kernenergie* **26** (1983) 11, pp. 443-448
- [Ric67] Richtmyer, R. D., K. W. Morton: *Difference Methods for Initial-Value Problems*, Interscience Publishers, New York - London - Sydney, 1967
- [Ris85] *Heat Transfer Correlations in Nuclear Reactor Safety Analysis*, Report Riso-M-2504, 1985
- [Roh97] Rohde, U., D. Lucas: Solution of the 4th Dynamic Benchmark by Use of the Code DYN3D with a Particle-in-Cell Method for the description of Boron Transport, *7th Symposium of Atomic Energy Research*, Hörnitz (Germany), September 23 - 26, 1997, Proc. p. 387
- [Sch63] Schmidt, E. : *VDI Wasserdampftafeln*, Springer Verlag, Berlin, 1963
- [Wag90] Wagner, W. and A. Pruss: International equations for the saturation properties of ordinary water substance. Revised according to the international temperature scale of 1990. *Addendum to J. Phys. Chem. Ref. Data* **16** (1987) 893 / *J. Phys. Chem. Ref. Data* **22** (1993) 783

- [Wag00] Wagner, W., J.R.Cooper, J.Kijima et al.: The IAPWS Industrial Formulation 1997 for the Thermodynamic Properties of Water and Steam, *J. of Engineering for Gas Turbines and Power* **122** (2000) 150-18

6 Fuel Rod Model

6.1 Fuel and Cladding Temperature Estimation

For the estimation of fuel and cladding temperatures the heat conduction equation in one-dimensional radial geometry is solved:

$$\rho c \frac{\partial T}{\partial t} = \frac{1}{r} \frac{\partial}{\partial r} \left(\lambda r \frac{\partial T}{\partial r} \right) + q''' \quad (6.1)$$

q''' is the thermal power generation density due to fission in fuel and due to γ -heating or metal-water-reaction in the cladding. The parameters of the equation (1) can be temperature-dependent. The boundary conditions for equation (6.1) are:

$$\frac{\partial T}{\partial r} = 0 \quad \text{at the fuel inner radius } r = R_{f,i} \quad (6.2a)$$

$$-\lambda \frac{\partial T}{\partial r} = \alpha_{gap} (T_{f,o} - T_{c,i}) \quad \text{at the fuel outer radius } r = R_{f,o} \quad (6.2b)$$

$$-\lambda \frac{\partial T}{\partial r} = \alpha_c (T_{c,o} - T_{cool}) \quad \text{at the cladding outer radius } r = R_{c,o} \quad (6.2c)$$

The determination of heat transfer coefficients α_{gap} at the gas gap between fuel and cladding and α_c from cladding to coolant is a main problem of fuel rod behaviour modelling.

6.2 Thermo-Physical Properties of Fuel and Cladding

For the description of temperature dependent properties of fuel and cladding, following correlations are used. The correlation for the thermal conductivity of the fuel is taken from [Wol75], while the other thermal and mechanical properties correlations are taken from the MATPRO handbook, version 09 [Mat76].

Thermal conductivity of fuel (λ in kW/mK, T in K)

$$\lambda_{fuel} = \frac{3,8}{T+130} + 3,4 \times 10^{-17} \cdot T^4 \quad (6.3)$$

Thermal conductivity of cladding (λ in kW/mK, T in K)

$$\lambda_{clad} = 0,001(7,51 + 0,0209 \cdot T - 1,45 \times 10^{-5} \cdot T^2 + 7,67 \times 10^{-9} \cdot T^3) \quad (6.4)$$

Heat capacity of fuel (c_p in kJ/kgK, T in K)

$$c_{p,fuel} = C_1 \frac{\Theta^2 \exp \Theta}{(\exp \Theta - 1)^2} + C_2 \cdot T + C_3 \frac{E}{RT^2} \exp\left(\frac{-E}{RT}\right) \quad (6.5)$$

where $\Theta = T/T_0$. The constants have following values:

$$\begin{array}{lll} C_1 = 0.2967 & C_2 = 0,243 \cdot 10^{-5} & C_3 = 8.745 \cdot 10^4 \\ T_0 = 535.3 & E = 1,577 \cdot 10^5 & R = 8.3143 \end{array}$$

Heat capacity of cladding:

if $T < 1092$ K - interpolation from the table

T (in K)	300	400	640	1090
c_p (in kJ/kgK)	0.281	0.302	0.331	0.375

if 1092 K $< T < 1248$ K - interpolation from the table

T (in K)	1093	1113	1133	1153	1173	1193	1213	1233	1248
c_p (in kJ/kgK)	0.502	0.590	0.615	0.719	0.816	0.770	0.619	0.469	0.356

At temperatures higher than 1248 K, a constant specific heat of 0.356 kJ/kgK is assumed. The discontinuity at $T = 1092$ K is due to a phase change in Zirkaloy material at this temperature.

The fuel density is considered to be constant, because in the nodalised form of equation (6.1) there occurs the mass of fuel (density multiplied by volume) which is constant.

6.3 Gas Gap Conductance

The general idea of the gas gap behaviour modelling in DYN3D is that the parameters for the stationary reference state (e.g. geometrical gap width, gas pressure and composition) are given and have to be obtained from detailed fuel rod behaviour codes. One of these codes is the code STOFFEL [Re85]. Data from this code were used for burn-up dependent fuel behaviour estimation in DYN3D. The changes of the gas gap parameters during the transient process due to variation of gap width, gas temperature and pressure, coolant and fuel - cladding contact pressure are estimated by the model.

In the gas gap between fuel and cladding the heat transfer components due to conduction in the gas, radiation and fuel-cladding contact are considered:

$$\alpha_{\text{gap}} = \alpha_{\text{cond}} + \alpha_{\text{rad}} + \alpha_{\text{contact}}$$

The estimation of the different components of the gap conductivity is performed in a similar way as it is implemented in various fuel behaviour analysis codes e.g. GAPCON-THERMAL [Bey75] or SSYST [Bor82]. The heat transfer coefficient due to conduction in the gas is determined by

$$\alpha_{\text{cond}} = \frac{\lambda_{g, \text{mix}}}{\delta_{\text{gap}} + \delta_{\text{roug}} + \delta_{\text{ext}}} \quad (6.6)$$

where $\lambda_{g, \text{mix}}$ is the thermal conductivity of the filling gas mixture. A fixed ratio of xenon and krypton mole fractions is assumed. The helium mole fraction is a function of the actual depletion state and must be obtained from detailed fuel rod behaviour codes. δ_{gap} is the geometrical gap width and is determined by the thermo-mechanical model described in the next section.

δ_{roug} represents the heat transfer resistances at the fuel and cladding surfaces and is related to the surface roughness values of fuel and cladding. δ_{ext} is a gas kinetics extrapolation length. The radiation component α_{rad} is given by the STEFAN–BOLTZMANN law:

$$\alpha_{\text{rad}} = \frac{\varepsilon_f \cdot \sigma_{\text{STB}} \cdot (T_{f,s}^2 + T_{c,s}^2) \cdot (T_{f,s} + T_{c,s})}{1 + \varepsilon_f \cdot [(1/\varepsilon_c - 1) \cdot R_{f,o}/R_{c,i}]}$$

ε_f and ε_c are the thermal emissivity of fuel and cladding (being functions of the surface temperature), σ_{STB} is the Stefan-Boltzmann constant, $T_{f,s}$ the fuel and $T_{c,s}$ the cladding surface temperatures, $R_{f,o}$ the fuel outer and $R_{c,i}$ the cladding inner diameter.

In the case of closed gap, heat transfer due to contact conductance is taken into account (see e.g. [Rei85]):

$$\alpha_{\text{cont}} = \frac{C \lambda_{f,c} \left(\frac{p_{\text{cont}}}{H} \right)^m}{\delta_{sr}^n} \quad (6.7)$$

where C , m and n are constants, δ_{sr} is the square averaged surface roughness,

$$\delta_{sr} = \sqrt{(\delta_f^2 + \delta_c^2)/2}$$

p_{cont} the contact pressure, H the Meyer hardness of the softer material (fuel or cladding), $\lambda_{f,c} = 2\lambda_f\lambda_c/(\lambda_f + \lambda_c)$. The contact pressure is estimated by using the following mechanical model.

6.4 Thermo-Mechanical Model

The aim of the thermo-mechanical model is not the exact description of fuel and cladding mechanical behaviour, but the estimation of gas gap conductance for a realistic temperature calculation. The simple thermo-mechanical model of the fuel rod is based on following assumptions:

- one-dimensional modelling of mechanics in radial direction,
- linear superposition of radial thermal, elastic and plastic deformations without axial coupling,
- elastic deformation of the fuel is taken into account only in the case of fuel–cladding contact, plastic deformations of the fuel are not considered,
- cladding is described in the thin shell approximation.

On the basis of these assumptions the expressions for fuel and cladding radius changes can be written as:

$$\delta R_f = \delta R_{f,th} + \delta R_{f,el} \quad (6.8a)$$

$$\delta R_c = \delta R_{c,th} + \delta R_{c,el} + \delta R_{c,pl} \quad (6.8b)$$

The thermal expansion of fuel $\delta R_{f,th}$ and cladding $\delta R_{c,th}$ is described by linear thermal expansion coefficients γ , which can be functions of temperature:

$$\delta R_{th} = \gamma_{th}(T) \Delta T \quad (6.9)$$

The elastic deformation is proportional to the stress σ divided by the elastic modulus E , which is also a function of temperature:

$$\delta R_{el}/R = \sigma/E(T) \quad (6.10)$$

The mechanical stress in the cladding is considered in the thin shell approximation, while for the fuel a hollow cylinder model is applied:

$$\delta R_{c,el} = \frac{1}{E_c} \frac{(R_{c,i} + R_{c,o})^2}{4(R_{c,o} - R_{c,i})} (p_{cont} + p_{gas} - p_{cool}) \quad (6.11a)$$

$$\delta R_{f,el} = \left(-\frac{R_{f,o}}{E_f} \right) \left(\frac{R_{f,o}^2 + R_{pl}^2}{R_{f,o}^2 - R_{pl}^2} - \nu_f \right) p_{cont} \quad (6.11b)$$

R_{pl} is the outer radius of the fuel plastic zone. Plasticity of fuel is assumed in the temperature region above a limit T_{pl} . The pressure difference at the cladding is determined by gas pressure p_{gas} , contact pressure p_{cont} and coolant pressure p_{cool} , while only the contact pressure is assumed to be relevant for fuel elastic deformation. ν_f is here the Poisson's ratio for fuel describing the ratio between radial and axial deformation.

The gas pressure p_{gas} is obtained ideal gas law for the filling gas and taking into account change of gas temperature as well as change of free volume by change of gas gap width. It must be noted, that for realistic estimation of depleted fuel rods behaviour the change of gas pressure and composition due to fission product release during the transient has to be taken into account, what is not done in the present model.

The plastic deformation of the cladding is considered in accordance with the creeping law:

$$\varepsilon = \frac{\delta R_{c,pl}}{R_c} = \left(\frac{\sigma}{K \dot{\varepsilon}^m} \right)^{1/n} \quad (6.12)$$

where the coefficients K , m and n are material properties. $\dot{\varepsilon}$ is the strain rate, that means, the time-derivative of the strain $\varepsilon = \delta R/R$. Plastic deformation is considered, when the stress exceeds the yield strength σ_{yield} , which is a material property and a function of temperature and strain rate.

The real gap width is: $\delta_{gap} = \delta_0 + \delta R_c - \delta R_f$

δ_0 is the gap width for a reference state and must be given as input (e. g. the normal steady state dependent on burnup).

If we consider only thermal and elastic deformations without contact pressure, the gap width can become less than zero. That means, the gap is closed and a contact pressure will occur. The contact pressure can be obtained from the condition of vanishing the real gap width $\delta_{gap} = 0$ [Bor82]:

$$p_{cont} = -\frac{\delta_0 + \delta R_{c,th} - \delta R_{c,th} + \frac{1}{E_c} \frac{(R_{c,i} + R_{c,o})^2}{4(R_{c,o} - R_{c,i})} (p_{gas} - p_{cool})}{\frac{1}{E_c} \frac{(R_{c,i} + R_{c,o})^2}{4(R_{c,o} - R_{c,i})} + \frac{R_{f,o}}{E_f} \left(\frac{R_{f,o}^2 + R_{pl}^2}{R_{f,o}^2 - R_{pl}^2} - \nu_f \right)} \quad (6.13)$$

Note that the contact pressure is zero if $R_{pl} = R_{f,o}$, that means, fuel outer radius temperature is larger than the plasticity limit (ideal plasticity of the fuel). If the stress obtained with taking into account the contact pressure exceeds the yield strength, plastic deformation of the cladding is considered. The system of equations (6.11) - (6.13) is solved iteratively to obtain the strain including plastic deformation and the contact pressure. Following assumptions are made for plastic creeping of the cladding in different cases:

- A) If the pressure outside the cladding (coolant pressure) is larger than inner pressure (contact pressure plus gas pressure), prompt creeping of the cladding on the fuel is assumed so that the gap vanishes and the cladding stress is zero. Contact pressure is obtained from this condition.
- B) If the pressure difference over the cladding is positive (inner pressure exceeds outer pressure), two different situations are considered:

If the gap is closed and contact pressure is non-zero, prompt creeping will be assumed until the stress is equal to the yield strength.

If there is no fuel - cladding contact and the gas pressure exceeds the coolant pressure, time-dependent creeping will be considered according to equation (6.12).

The last situation is typical for low coolant pressures like in the RIA experiments at the pulsed research reactors or in LOCA cases and leads to cladding ballooning, while the case A) is typical for RIA conditions in power reactors.

At least some words about material properties for the thermo-mechanical model. For most of these properties (elastic modulus E , Meyer hardness H , Poissons' ratio ν , yield strength σ_{yield}) the MATPRO [Mat76] representations are used. This is not correct for analysing VVER type reactors, but the mechanical properties at high temperatures for VVER cladding materials were not available in the literature. The subroutines and functions describing material properties can easily be changed, if better representations become available.

6.5 Fuel Rod Failure Estimation

A deterministic model of fuel rod failure during accidents is not included in DYN3D, but some parameters for diagnostic of possible fuel rod failure are given, that are:

- fuel enthalpy for each axial node of the rod,
- cladding oxide thickness,
- signalization of possible cladding rupture, when the cladding stress is positive

(inner pressure is larger than outer pressure) and exceeds the yield strength. The cladding oxidation due to metal-water reaction (MWR) at high temperatures is described by equation:

$$D \frac{dD}{dt} = \frac{A}{C^2} \exp\left(\frac{-B}{T}\right) \quad (6.14)$$

where D is the oxide layer thickness, T the cladding surface temperature, C the mass density of oxygen in ZrO₂, A and B are constants. The MWR is considered as an additional heat source in the cladding, but the additional heat transfer resistance at the cladding surface and the change of mechanical properties of the cladding caused by the oxide layer are not taken into account (restriction to thin oxide layers).

6.6 Numerical Methods for Fuel Rod Behaviour Calculations

For the numerical solution of the heat conduction equation (6.1), a nodal method is used. Equation (6.1) is transformed to finite difference equation using effective heat transfer coefficients between the radial nodes of the fuel rod. These coefficients are determined from the exact analytical solution of the steady state equation with piecewise constant thermal conductivity and heat source. The fuel is subdivided into a given number radial nodes with equal area, the cladding is not subdivided. Using this method, a high accuracy of the solution is achieved already for a few number of radial nodes. An iteration procedure is used to take into account the temperature dependence of thermo-physical properties of fuel and cladding material and changing heat transfer coefficient in the gas gap. The second order Crank-Nicolson scheme is used for the discretisation in time.

6.7 Input Data for the Fuel Rod Model

In DYN3D, different types of fuel rods can be defined. A fuel rod type is described by the geometry and properties of fuel and cladding and the gas gap properties. Each core channel or hot channel can be related to a given fuel rod type. A fuel rod type is described by the following data:

- geometrical data of the hydraulic channel (free flow area per rod, equivalent hydraulic and heated diameters),
- inner and outer diameter of fuel and cladding,
- density, thermal conductivity and specific heat of fuel and cladding,
- portion of heat release in fuel and cladding,
- distribution of the heat release over the radial nodes,
- gas gap data.

Thermo-physical properties of fuel and cladding as well as the heat transfer coefficient in the gas gap can be considered constant (input data are used) or temperature dependent. In this case, the correlations (6.3) - (6.5) for thermal conductivity and specific heat are used and the gas gap model is activated.

For the estimation of changing heat transfer coefficient in the gas gap, following data are required:

- gap width for a reference state (e.g. cold state) and corresponding radial averaged fuel

- and cladding temperatures for this reference state,
- cold filling gas pressure,
- helium mole fraction in the filling gas,
- surface roughness of fuel and cladding material (needed for contact conductivity estimation).

Further details of the model are given in [Roh88], validation on experiments is reported about in [Roh92] and [Roh01].

References Chapter 6

- [Bey75] Beyer, C. E. et al.: GAPCON-THERMAL-2: A computer code for calculating the thermal behavior of an oxide fuel, *Report BNWL - 1898* (1975)
- [Bor82] Borgwaldt, H. and Gulden, W.: SSYST, a Code-System for Analysing Transient LWR Fuel Rod Behaviour under Off-Normal Conditions, *Report KFK - 3359*, Karlsruhe, 1982
- [Mat76] MATPRO Version 09 - A Handbook of Materials Properties for Use in the Analysis of Light Water Reactor Fuel Rod Behaviour, *Report TREE - NUREG - 1005*, Idaho National Engineering Laboratory, 1976
- [Rei85] Reinfried, D.: Zur mathematischen Modellierung des Bestrahlungsverhaltens von Druckwasserreaktorbrennstäben, *PhD Thesis*, Rossendorf, 1985
- [Roh88] Rohde, U.: Das Programm FLOCAL-DWR zur Berechnung instationärer Zweiphasenströmungen des Kühlmittels in Druckwasserreaktoren, *Internal report RPT - 3/88*, Rossendorf, 1988
- [Roh92] Rohde, U.: „Modeling of Fuel Rod Behaviour and Heat Transfer in the Code FLOCAL for Reactivity Accident Analysis of Reactor Cores“, *1st Baltic Heat Transfer Conference, Göteborg, August 1991*, publ. in: „Recent Advances in Heat Transfer“, Elsevier Publ. Amsterdam, 1992
- [Roh01] Rohde, U.: The modeling of fuel rod behaviour under RIA conditions, *Annals of Nuclear Energy* **28** (2001) 13, pp.1343-1363
- [Wol75] Wolter, W.: Programmbericht INCO, *Internal report KKAB-81-75-0*, Berlin, 1975

7.1 Steady-State Iteration

Considering the steady-state calculation an eigenvalue iteration is performed in the solution of the nodal equation system derived from the neutron diffusion equation. The calculated power densities are used for the solution of the thermal-hydraulic equations and the fuel rod heat conduction equations. Based on the node averaged thermal-hydraulic parameters fuel temperature T_f , coolant density ρ_c , coolant temperature T_c and boron concentration c_B the macroscopic nodal cross sections are calculated by using the cross section library.

The iteration starts with the thermal-hydraulic input parameters, as the averaged core inlet temperature of the coolant. It is used for all nodes despite of the power of the core. The coolant density is estimated from coolant temperature by means of the thermo-physical water properties. The fuel temperature is assumed to agree with the coolant temperature, i.e. the reactor power is neglected. The averaged value of the boron concentration at the core inlet is used for all nodes. With the help of the library of the macroscopic cross sections the nodal cross sections are estimated. The fast neutron fluxes in all nodes are set to one and the thermal fluxes are estimated with the help of nodal cross sections:

$$\bar{\Phi}_1^n = 1000, \bar{\Phi}_2^n = \frac{\sum_s^n \bar{\Phi}_1^n}{\sum_a^n} \quad (7.1)$$

The partial currents at the different sides i are determined by

$$J_{s,i,g}^{\pm,n} = \frac{1}{4} \bar{\Phi}_g^n \quad (7.2)$$

If the HEXNEM2 method is applied, the partial currents at the corner points i are $J_{c,i,g}^{\pm,n}$ estimated in the same way. The initialisation is finished in the input routine.

In the steady-state iteration, the cross sections are used for the calculation of this first estimation of power densities, which are used for the thermal-hydraulic calculations. The new thermal-hydraulic parameters give a new estimation of cross sections which is used for the calculation of the neutron flux distributions. Based on the new flux distributions the new distribution of power density is determined. Before the thermal-hydraulic calculation follows a relaxation Θ_p between old and new power densities is applied to improve the convergency.

Considering the iteration step $(j+1)$ the power densities $P_n^{*(j+1)}$ are given by

$$P_n^{*(j+1)} = \Theta_p P_n^{(j+1)} + (1 - \Theta_p) P_n^{(j)} \quad (7.3)$$

The relaxation factor $\Theta_p \approx 0.5$ is recommended for the most cases. If convergency problems concerning the neutron kinetic - thermal-hydraulic iteration (NK - TH iteration) occurs, the relaxation should be decreased. Depending on the used option of the code the calculation of Xe and Sm concentrations and the decay heat power is included in the iteration process. The criteria for the end of NK - TH iteration is the change of the eigenvalue k_{eff} which is determined in the neutron kinetics iteration and the changes of fuel temperatures and the coolant

densities. The main criteria for the end of the neutron kinetic iteration itself is the change of fission source between two successive iterations. The eigenvalue k_{eff} is determined in the most cases. If the initial state belongs to a critical reactor the eigenvalue k_{eff} should be close to one. Sometimes the critical boron concentration has to be determined. The search for the critical boron concentration is included in the NK - TH iterations. A rough scheme of steady-stat iteration can be seen in Fig. 7.2.

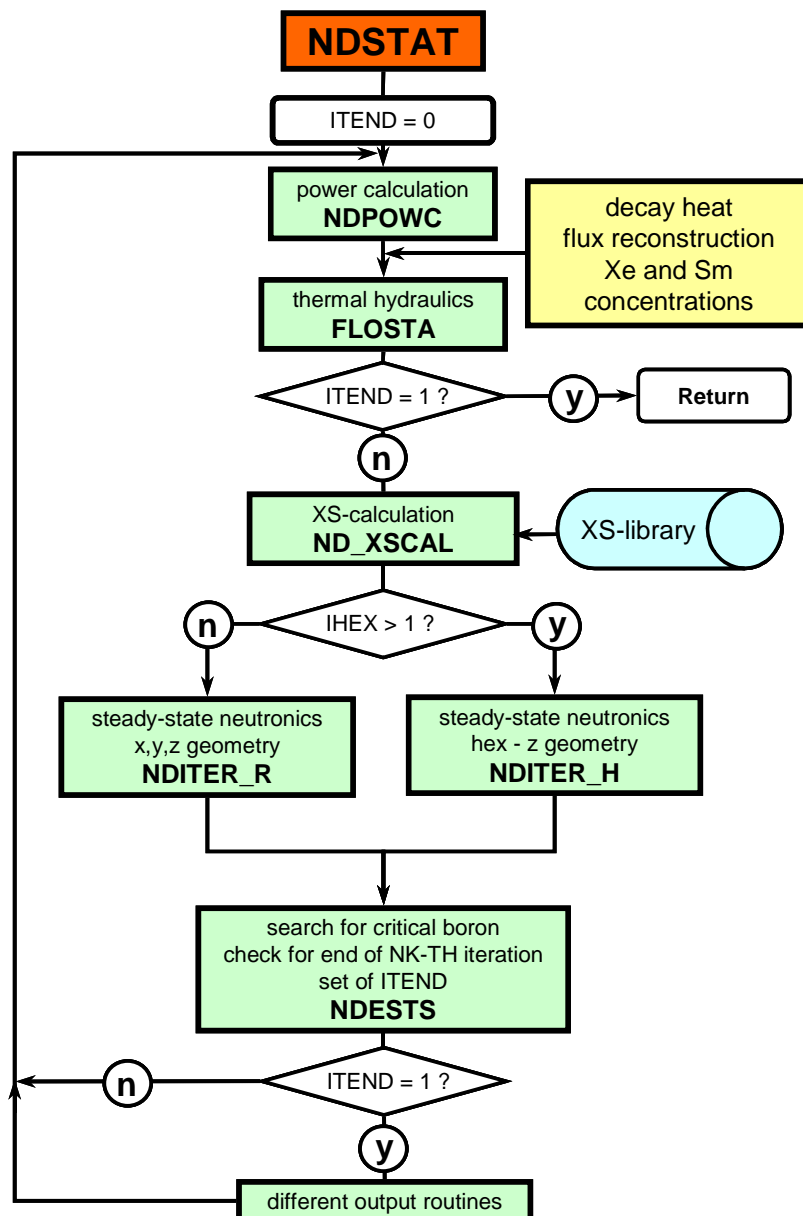


Fig. 7.2 Rough scheme of subroutine NDSTAT for steady-state iteration

7.2 Transient Iteration

The iterations of the transient calculations are similar to the steady state iteration with some specific features. instead of the eigenvalue iteration of the steady-state neutronics we have an

iteration with a given source obtained from the integration of precursor equations. It is clear that the convergency properties are a function of the time step and the changes of the neutron kinetic parameters. If we have for example changes leading to a fast increase of the neutron flux, the convergency of the neutron kinetic iteration requires a small time step, for example in the order of milliseconds. The thermal-hydraulic processes are often slower and a larger time step can be used. Sometimes the thermal-hydraulic time step is determined by the Courant criteria to avoid numerical diffusion in the description of the coolant transport. Therefore separate time steps for neutron kinetics (Δt_{NK}) and thermal-hydraulics (Δt_{TH}) were introduced in DYN3D. The two time steps are automatically controlled. It is required that

$$\Delta t_{NK} \leq \Delta t_{TH}. \quad (7.4)$$

A whole number of neutronic steps is included in one thermal-hydraulic step. The global control of the thermal-hydraulic steps is performed in the subroutine NDTRAN (Fig. 7.3)

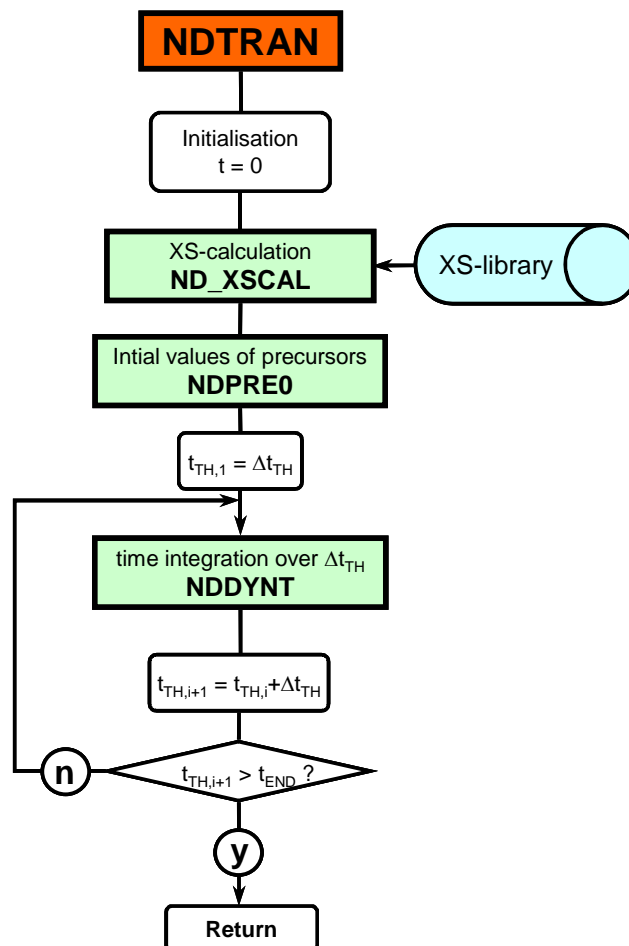


Fig. 7.3 Rough scheme of subroutine NDTRAN for transient calculations

The subroutine NDDYNT performs the integration over the thermal-hydraulic step. The NK - TH iteration scheme can be seen in Fig. 7.4. The neutron kinetic iteration for the time steps Δt_{NK} is performed in the subroutine NDTRIT. The thermal-hydraulic model needs the power densities at begin and end of the thermal-hydraulic step. The average value of the two densi-

ties is used in the numerical equations. As several steps Δt_{NK} are inside the thermal-hydraulic step Δt_{TH} the average value of the power densities about the steps Δt_{NK} is estimated. The average values of power densities at begin and end of thermohydraulic step represent the average over the different neutronic steps instead begin and end values of interval Δt_{TH} .

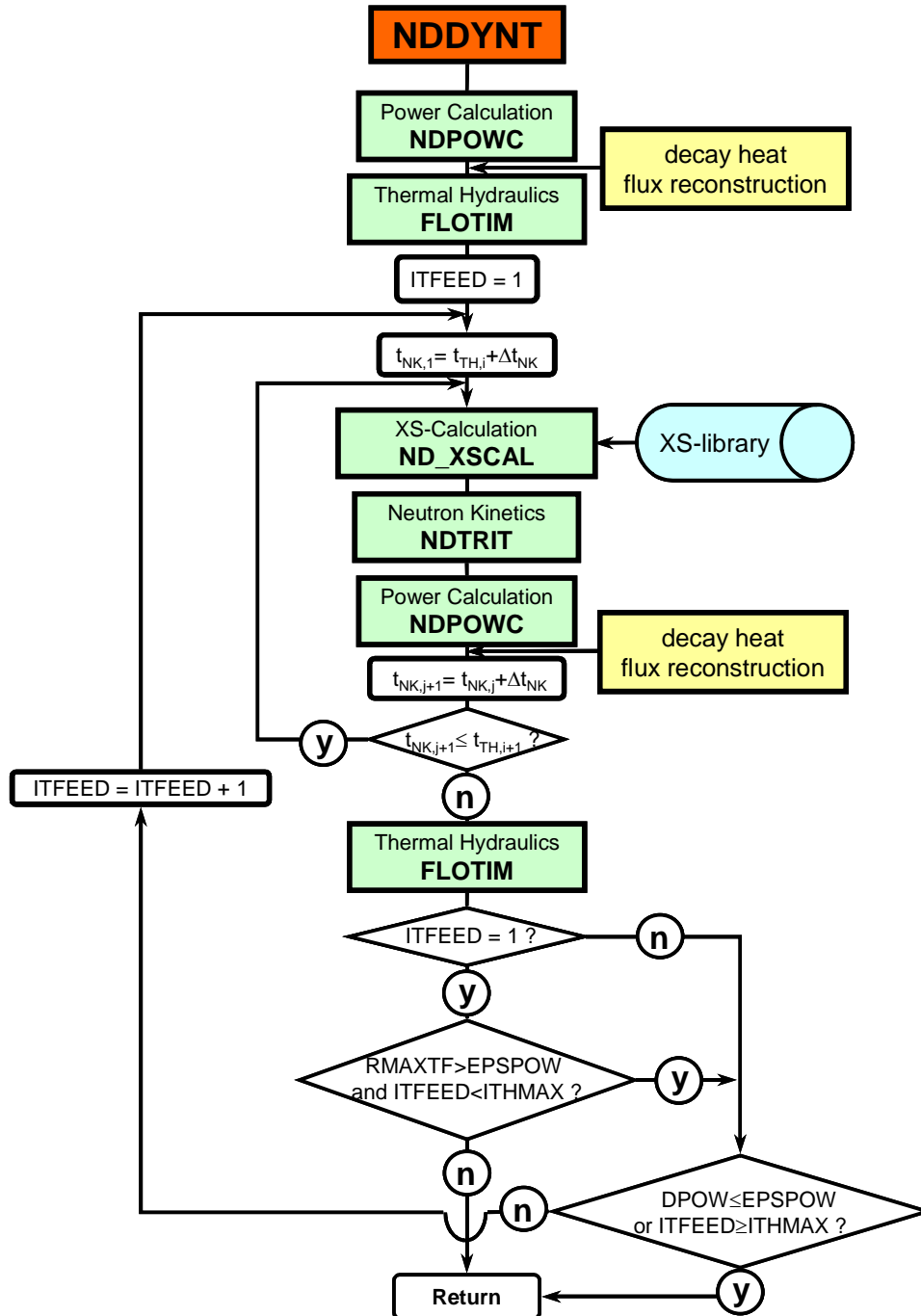


Fig. 7.4 Rough scheme of NK - TH iteration in the time step Δt_{TH}

The length of time steps is estimated in the subroutine NDTRIT. The neutron kinetic steps Δt_{NK} depend on the changes of the neutron distribution during the previous step. The changes of the averaged spatial distribution given by the average exponent of the exponential transfor-

mation, the exponent itself, the changes of the shape of the flux distribution and the number of neutronic iterations are used for the time step control. The time steps are doubled or divided in half depending on the given criteria of the changes. At the end of the step Δt_{TH} the estimated neutron kinetic step is changed to meet the end of the thermal-hydraulic step. The thermohydraulic step is repeated until convergency of the reactor power or the given number of iterations is reached. At the first step the changes of the fuel temperatures against the previous step are used for limiting the iteration. If the power level is low, for example hot zero power, an increase of power during the time step does not influence the fuel temperatures. An iteration is not necessary in this case.

The relaxation applied in the steady-state iteration (equation 7.3) is also applied for the transient iteration.

8 Burnup Calculation

As the energy in a reactor is produced by nuclear fission, the reactor operation leads to a continuous loss, i. e. burning out of fissile material (fuel). During reactor operation, more and more uranium / plutonium nuclei are destroyed by fission yielding fission products. Furthermore, nuclei are converted by other reactions with neutrons. Especially the neutron capture by uranium isotopes produces other actinides, which on their part may vanish by fission or further neutron capture; there is spontaneous decay. The continuous production and destruction of different nuclides during the depletion process is calculated by the cell codes that are applied for the generation of the two-group neutronic-data libraries (cf. chapter 3). Sets of neutronic data are produced for chosen burnup steps in a cell-burnup calculation, the depletion state determining the actual two-group data. The degree of depletion is characterized by the energy produced per fuel mass up to the actual step. Thus the unity of burnup is MWd/kgHM, i. e. megawatt days per kilogramme heavy metal (uranium / plutonium) that was originally present in the fresh fuel.

The neutronic data produced step-wise by the cell-burnup calculation are applied in DYN3D, interpolating these data for the actual burnup values given for each reactor-core volume element (node). Such a three-dimensional burnup distribution of the core can be provided as the result of a macro-burnup calculation, also called reactor-cycle calculation. In order to enable DYN3D users to independently calculate nodal burnup distributions for all possible states occurring during a reactor cycle, a macro-burnup option of the code has been developed.

In the steady-state part of the DYN3D code, the power density is calculated by solving the neutron diffusion equation for a given material distribution within the core. Essentially, the extension of DYN3D to a macro-burnup option is done by putting a burnup loop around the stationary kernel of the code, in which the nodal fluxes and temperatures are calculated. Starting point of the loop is a given material and burnup distribution reflecting the previous reactor-core operational history. For the given state, the code calculates the actual burnup-specific nodal two-group data using a neutronic-data library. Next, the nodal distributions of neutron flux, power density, fuel temperature, coolant density and steady-state concentrations of the reactor poisons xenon and samarium (fission products) are calculated by an iteration which includes temperature feedback. The calculation of the critical boron concentration is also part of the iteration process which finally leads to a stationary core state. The nodal power densities are assumed to be constant for a certain time interval, in which the nodal burnup values increase only little, compared to their increase during a whole reactor cycle. For this burnup time-step interval, DYN3D calculates a burnup growth within each node using the steady-state power densities. Now, a new two-group data distribution belonging to the updated nodal burnup values is derived for the next time step. In this way, the burnup calculation proceeds step by step until the end of cycle, or an otherwise interesting burnup state is reached, which then can be studied by dynamic DYN3D calculations.

During the whole operation period of a reactor, the material distribution within the core is modified, for example by changing the positions of partially burnt-out fuel elements, by putting in new ones, and also by control rod movements. All these manipulations, as well as changes in total power and coolant mass-flow through the core, are modelled by special routines and can easily be controlled by additional input data. Modelling the nodal material and burnup distributions is somewhat complicated in the case of VVER-440 because of the special construction of its control rods. In fact, there are no rods, as usually used in pressurized water

reactors, but absorbing assemblies that have the same hexagonal shape and length as fuel assemblies. They are followed by real fuel assemblies which are attached to the absorbers bottom by a coupling part (cf. section 4.3). „Changing control rod positions“ in case of VVER-440 means moving such long assemblies along the vertical axis. The axial burnup distribution of a fuel follower is moved up or down during „control rod movements“. All these special features are taken into account in the DYN3D burnup option.

In principle codes other than DYN3D can be used to calculate a three-dimensional burnup distribution, needed as input for the analyses of a transient by DYN3D. However, using the same neutronic code and group-data library for both the macro-burnup and transient calculations has some advantage. In case the neutronic calculation tends to over-(under-)estimate the real neutron flux in a core volume element, the macro-depletion calculation will yield an over-(under-)estimated burnup value there. Applying this burnup in a transient code using the same neutronic solver and data will lead to reduction in the over-(under-)estimation in the flux, thus producing more accurate results.

9 Reactor-Poison Dynamics

9.1 Xenon and Iodine

The balance for the iodine ^{135}I and xenon ^{135}Xe concentrations in the node n is described by the differential equations [Lam66]:

$$\frac{dc_I^n(t)}{dt} = \gamma_I^n \sum_{g=1}^2 \Sigma_{f,g}^n \bar{\Phi}_g^n(t) - \lambda_I c_I^n(t) \quad (9.1.1)$$

$$\frac{dc_{Xe}^n(t)}{dt} = \gamma_{Xe}^n \sum_{g=1}^2 \Sigma_{f,g}^n \bar{\Phi}_g^n(t) - \lambda_{Xe} c_{Xe}^n(t) + \lambda_I c_I^n(t) - c_{Xe}^n(t) \sum_{g=1}^2 \sigma_{Xe,g}^n \bar{\Phi}_g^n(t) \quad (9.1.2)$$

As the node-averaged concentrations $c_{Xe}^n(t)$ are time-dependent, the absorption cross sections and thus the fluxes $\bar{\Phi}_g^n$ in equations (2.2.2) and (9.1.1-2) become functions of time as well. The time characteristics of xenon-iodine redistributions is largely determined by the half-lives of these nuclides, i.e. 6.7 hours for xenon-135 and 9.2 hours for iodine-135, respectively. On the one hand, those half-lives are large compared with characteristic times linked with effects arising from delayed neutrons (cf. section 2.4). Fuel burnup, on the other hand is characterized by much larger time intervals (section 8). Therefore, the poison dynamics can be treated separately from both effects. That means all delayed neutrons are included in the fraction of the prompt neutrons in equations (2.2.2), and fuel burnup is kept constant in modelling the xenon-iodine redistributions.

The solution of the equation system (2.2.2), (9.1.1-2) is complicated, due to the coupling between neutron fluxes and xenon balance. The xenon concentration in (9.1.2) influences the absorption cross sections in (2.2.2), thus affecting the neutron balance. The neutron fluxes, in turn, determine the rates of both nuclear fission and neutron absorption by xenon, which effects are responsible for the xenon production and the burnup of xenon, respectively. For this reason, the differential equations (9.1.2) are solved approximately in small time steps Δt , in which the neutron fluxes can be considered constant ([Lau72], [Mit89]).

The solution of the ordinary differential equation (9.1.1), assuming constant fluxes $\bar{\Phi}_g^n(t_k)$ in a time interval Δt , yields for the iodine concentration:

$$c_I^n(t_{k+1}) = c_I^n(t_k + \Delta t) = c_I^n(t_k) \exp(-\lambda_I \Delta t) + \frac{\gamma_I^n}{\lambda_I} \sum_{g=1}^2 \Sigma_{f,g}^n \bar{\Phi}_g^n(t_k) \cdot \{1 - \exp(-\lambda_I \Delta t)\} \quad (9.1.3)$$

The solution of equation (9.1.2) is

$$\begin{aligned}
c_{Xe}^n(t_{k+1}) = c_{Xe}^n(t_k + \Delta t) = & c_{Xe}^n(t_k) \exp(-\lambda_x \Delta t) + \frac{\gamma_{Xe}^n}{\lambda_x} \sum_{g=1}^2 \Sigma_{f,g}^n \bar{\Phi}_g^n(t_k) \cdot \{1 - \exp(-\lambda_x \Delta t)\} + \\
& + \left(\frac{\lambda_I}{\lambda_x - \lambda_I} c_I^n(t_k) \exp(-\lambda_x \Delta t) \right) \cdot \{ \exp([\lambda_x - \lambda_I] \Delta t) - 1 \} + \\
& + \gamma_I^n \left[\sum_{g=1}^2 \Sigma_{f,g}^n \bar{\Phi}_g^n(t_k) \right] \exp(-\lambda_x \Delta t) \cdot \\
& \cdot \left\{ \left(\frac{1}{\lambda_x} \{ \exp(\lambda_x \Delta t) - 1 \} \right) - \left(\frac{1}{\lambda_x - \lambda_I} \{ \exp([\lambda_x - \lambda_I] \Delta t) - 1 \} \right) \right\},
\end{aligned}$$

with

$$\lambda_x = \lambda_{Xe} + \sum_{g=1}^2 \sigma_{Xe,g}^n \bar{\Phi}_g^n(t_k). \quad (9.1.4)$$

The values $\bar{\Phi}_g^n(t_k)$ are the node-averaged fluxes for both groups determined by a steady-state calculation for the time t_k . The new xenon concentration (9.1.4) is used in calculating the macroscopic capture cross sections for the next time step $t_{k+1} = t_k + \Delta t$, according to (2.6.5). The extension of DYN3D to a poison-dynamics option is done by putting a loop around the steady-state kernel of the code, where the nodal fluxes and temperatures are calculated. The same approach has already been applied in the burnup option (chapter 8).

9.2 Promethium and Samarium

The balance for the promethium ^{149}Pm and samarium ^{149}Sm concentrations in the node n is described by similar differential equations as in the previous section:

$$\frac{dc_{Pm}^n(t)}{dt} = \gamma_{Pm}^n \sum_{g=1}^2 \Sigma_{f,g}^n \bar{\Phi}_g^n(t) - \lambda_{Pm} c_{Pm}^n(t) \quad (9.2.1)$$

$$\frac{dc_{Sm}^n(t)}{dt} = \lambda_{Pm} c_{Pm}^n(t) - c_{Sm}^n(t) \sum_{g=1}^2 \sigma_{Sm,g}^n \bar{\Phi}_g^n(t) \quad (9.2.2)$$

By contrast to xenon-135, samarium-149 is not produced directly by fission, and there is no spontaneous radioactive decay of this nuclide; cf. equations (9.1.2) and (9.2.2).

The solution of equation (9.2.1) is in total analogy to the iodine case, thus yielding for the nodal promethium concentrations:

$$c_{Pm}^n(t_{k+1}) = c_{Pm}^n(t_k) \exp(-\lambda_{Pm} \Delta t) + \frac{\gamma_{Pm}^n}{\lambda_{Pm}} \sum_{g=1}^2 \Sigma_{f,g}^n \bar{\Phi}_g^n(t_k) \cdot \{1 - \exp(-\lambda_{Pm} \Delta t)\} \quad (9.2.3)$$

The time-step-wise calculation of the samarium concentrations is carried out according to the solution of equation (9.2.2):

$$\begin{aligned} c_{Sm}^n(t_{k+1}) = & c_{Sm}^n(t_k) \exp(-\lambda_s \Delta t) + \gamma_{Pm}^n \left[\sum_{g=1}^2 \Sigma_{f,g}^n \bar{\Phi}_g^n(t_k) \right] \exp(-\lambda_s \Delta t) \cdot \\ & \cdot \left\{ \left(\frac{1}{\lambda_s} \{ \exp(\lambda_s \Delta t) - 1 \} \right) - \left(\frac{1}{\lambda_s - \lambda_{Pm}} \{ \exp([\lambda_s - \lambda_{Pm}] \Delta t) - 1 \} \right) \right\} - \\ & + \left(\frac{\lambda_I}{\lambda_s - \lambda_{Pm}} c_{Pm}^n(t_k) \exp(-\lambda_s \Delta t) \right) \cdot \{ \exp([\lambda_s - \lambda_{Pm}] \Delta t) - 1 \}, \end{aligned}$$

with

$$\lambda_s = \sum_{g=1}^2 \sigma_{Sm,g}^n \bar{\Phi}_g^n(t_k) \quad . \quad (9.2.4)$$

This solution for the promethium-samarium dynamics has been incorporated into the DYN3D poison-dynamics subroutines that have originally been developed for modelling xenon oscillations (see previous section).

Setting the left-hand sides of equations (9.1.1-2) and (9.2.1-2), (time derivatives) to zero yields the equilibrium concentrations for the reactor poisons ^{135}Xe , ^{149}Sm and their precursors ^{135}I , ^{149}Pm (equations (2.6.1-4) in section 2.6).

References Chapter 9

- [Lam66] Lamarsh, J. R., „Nuclear Reactor Theory“, Addison-Wesley Publishing Company, Inc., Reading, Massachusetts, 1966.
- [Lau72] Lauer, A., „Räumliche Xenon-Schwingungen in Hochtemperaturreaktoren“, Report Jül-850-RG, Jülich 1972.
- [Mit89] Mittag, S., „Axial Xenon Oscillations in WWER-1000 Reactor Cores“, Kernenergie **32**, 461 (1989).

10 Decay Heat Model

10.1 Basic Assumptions

The decay heat power is the thermal power produced by the radioactive decay of fission and activation products of the nuclear fuel. This physical quantity plays an important role in the design and accident analysis of nuclear systems in which the decay heat power has to be taken into consideration as a heat source [Kes95], [Sch95]. The following components have to be considered to evaluate the decay heat power:

- Contribution of the fission products coming from the nuclear fission of the four nuclides ^{235}U , ^{238}U , ^{239}Pu , and ^{241}Pu
- Contribution from the decay of actinides resulting from the neutron capture (the main contribution is due to ^{239}U and ^{239}Np)
- Contribution from the decay of nuclides formed by neutron capture in fission products

Values of the different contributions and the calculation procedures for a constant power operation of a light water reactor fueled with non-recycled nuclear fuel can be found in [DIN90].

A model for calculating the space dependent decay heat power delivered from the operational history as well as during the transient is integrated in DYN3D.

10.2 Decay Heat Power Equations

The decay heat power is defined as the amount of thermal power released by the radioactive decay of fission and activation products. The contribution of the fission products to the decay heat power is calculated from the individual contributions of the four fissile isotopes ^{235}U , ^{238}U , ^{239}Pu and ^{241}Pu . The decay heat power delivered by each of these isotopes is divided into 24 groups having each a characteristic decay constant [DIN90]. The decay heat power is calculated for the different nodes n in order to take into account its space dependence. The different contributions of the fission products to decay heat power can be obtained from a system of balance equations

$$\frac{d}{dt}w_{ij}^n(t) = \alpha_{ij}^d \frac{P_i^n(t)}{Q_i} - \lambda_{ij}^d w_{ij}^n(t) \quad (10.1)$$

with

- $w_{ij}^n(t)$: decay heat power at time t from the decay group j of the fission isotope i in the node n
- α_{ij}^d : fraction of decay heat power originating from decay group j for a fission of the isotope i

- $\frac{P_i^n(t)}{Q_i}$: fission rate of isotope i in the node n (depends on the initial enrichment e_0 and the burnup b)
- λ_{ij}^d : decay constant of fission product of decay group j from fission of isotope i

The system described by (10.1) consists of $i * j * n$ balance equations of the decay groups of fission products. The rate of energy release by fission of the isotope i is the following

$$P_i^n(t) = Q_i \sum_{g=1}^2 \Sigma_{f,g,i}^n(t) \cdot \Phi_g^n(t) \quad (10.2)$$

where

- $\Sigma_{f,g,i}^n(t)$: macroscopic fission cross section of the isotope i for neutrons of energy group g in the node n
- $\Phi_g^n(t)$: neutron flux of energy group g in the node n
- Q_i : energy per fission of a nucleus of isotope i

The integration of the inhomogeneous system of equations (10.1) for a time interval between $t - \Delta t_k$ and t_k provides the part of decay heat of fission products generated during the transient $w_{t,ij}^n(t)$

$$w_{t,ij}^n(t) = w_{t,ij}^n(t - \Delta t_k) e^{-\lambda_{ij}^d \Delta t_k} + \frac{\alpha_{ij}^d}{Q_i} \int_{t - \Delta t_k}^t P_i^n(t') e^{-\lambda_{ij}^d (t - t')} dt' \quad (10.3)$$

The variation of thermal powers $P_i^n(t')$ in the interval Δt_k is linearly approximated

$$P_i^n(t') = P_i^n(t - \Delta t_k) + \frac{P_i^n(t) - P_i^n(t - \Delta t_k)}{\Delta t_k} (t' - t + \Delta t_k) \quad (10.4)$$

Integration in equation (10.3) by using (10.4) yields

$$w_{t,ij}^n(t) = w_{t,ij}^n(t - \Delta t_k) e^{-\lambda_{ij}^d \Delta t_k} + \frac{\alpha_{ij}^d}{Q_i \lambda_{ij}^d} [P_i^n(t - \Delta t_k) I_{ij}^1(\Delta t_k) + (P_i^n(t) - P_i^n(t - \Delta t_k)) I_{ij}^2(\Delta t_k)] \quad (10.5)$$

with the results of integration

$$I_{ij}^1(\Delta t_k) = \left(1 - e^{-\lambda_{ij}^d \Delta t_k}\right) \quad (10.6)$$

$$I_{ij}^2(\Delta t_k) = \left(1 - \frac{I_{ij}^1(\Delta t_k)}{\lambda_{ij}^d \Delta t_k} \right) \quad (10.7)$$

It is worth noting that equation (10.5) is suitable for transient calculations because it takes into account the variation of the power released by fission during the different integration time steps. During the transient, the contribution of this part to the total decay heat is relatively small in comparison to the decay heat from the power history. Some of groups with longer decay constants can be neglected in the transient. Therefore only the first 10 groups with the shortest decay constants are taken into account. It was checked that this approximation is sufficient for time intervals lower than 1000 seconds.

Equation (10.1) can also be applied for the calculation of the decay heat power from the previous operation of the reactor. This contribution is the dominant one in most cases. Considering the example of a power histogram with 4 power levels in Fig. 10.1, the decay heat of fission products $w_{s,ij}^n(t)$ after shut down is the sum over the 4 power intervals k

$$w_{s,ij}^n(t) = \sum_{k=1}^4 \frac{P_{i,k}^n \alpha_{ij}^d}{Q_i \lambda_{ij}^d} \left(1 - e^{-\lambda_{ij}^d \Delta T_k} \right) e^{-\lambda_{ij}^d t_k} \quad (10.8)$$

The decay heat power in node n at time t originating from the fission products of the four isotopes $w_{fp}^n(t)$ is obtained as the sum of contributions by the isotopes i and the decay groups j

$$w_{fp}^n(t) = \sum_i \sum_j (w_{s,ij}^n(t) + w_{t,ij}^n(t)) \quad (10.9)$$

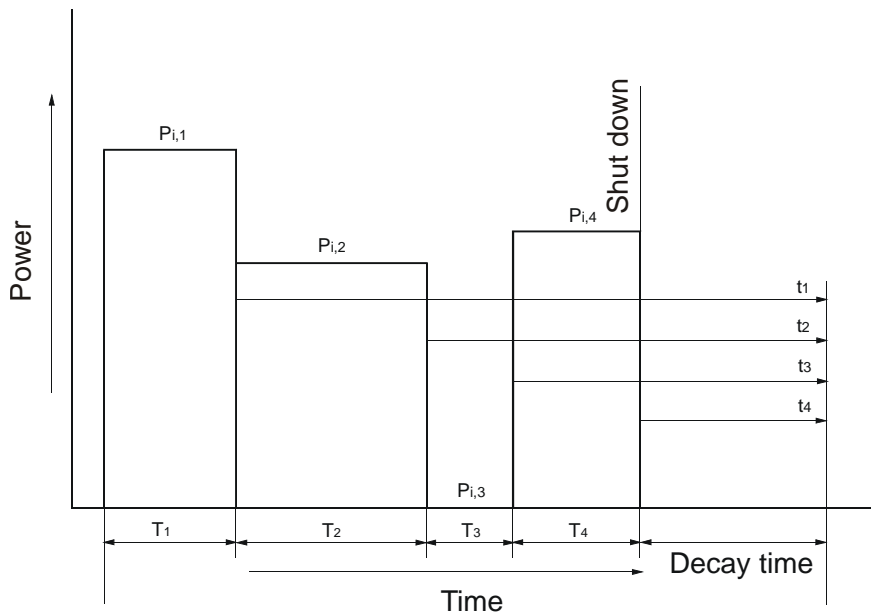


Fig. 10. 1: Example of a power histogram with 4 power levels

The first term of the right hand side gives the decay heat power during a steady-state operation of the reactor [DIN90].

The neutron capture contribution to the decay heat power by actinides (^{239}U , ^{239}Np and others) as well as by fission products from the steady-state power operation was considered as described in [DIN90]. The contributions $w_{239U}^n(t)$ of ^{239}U and $w_{239Np}^n(t)$ of ^{239}Np are given by

$$w_{239U}^n(t) = \sum_{k=1}^4 \frac{P_k^n}{Q} E_U \cdot R (1 - e^{-\lambda_U T_k}) e^{-\lambda_U t_k} \quad (10.10)$$

with

$$\frac{P_k^n}{Q} = \sum_{i=1}^4 \frac{P_{i,k}^n}{Q_i}: \text{ total fission rate in the node } n \text{ during the time interval } T_k$$

$E_U = 0.474 \text{ MeV}$: average decay heat of ^{239}U

$\lambda_U = 4.91 \times 10^{-4} \text{ s}^{-1}$: average decay constant of ^{239}U

R : ratio of neutron capture rate to total fission rate at the end of power operation

An approximation of R can be obtained by

$$R \approx 1, 18 \cdot e^{-0,141 \cdot e_0} - 0, 2 + 0, 0062 \cdot BU$$

e_0 : initial enrichment of ^{235}U

BU : burnup of fuel at time of shut down in $\text{MWd/kg}_{\text{Uranium}}$

$$w_{239Np}^n(t) = \sum_{k=1}^4 \frac{P_k^n}{Q} E_{Np} \cdot R \left[\frac{\lambda_U}{\lambda_U - \lambda_{Np}} (1 - e^{-\lambda_{Np} T_k}) e^{-\lambda_{Np} t_k} - \left(\frac{\lambda_{Np}}{\lambda_U - \lambda_{Np}} (1 - e^{-\lambda_U T_k}) e^{-\lambda_U t_k} \right) \right]$$

with

$E_{Np} = 0.419 \text{ MeV}$: average decay heat of ^{239}Np

$\lambda_{Np} = 3.41 \times 10^{-6} \text{ s}^{-1}$: average decay constant of ^{239}Np

The equations above give conservatively high results. They can be used for initial enrichments between 1.9 and 4.1 %. The contribution of the other actinides $w_{act}^n(t)$ is represented by

$$w_{act}^n(t) = A(t) \sum_i \sum_j w_{s,ij}^n(t) \quad (10.4)$$

The decay heat power released by neutron capture in $^{133}\text{Cs} + n = ^{134}\text{Cs}$ was not taken into account because it significantly contributes for long decay times (in the region of 10^8 sec).

The contribution of capture by other fission products $w_{cap}^n(t)$ is given by

$$w_{cap}^n(t) = H(t) \sum_i \sum_j w_{s,ij}^n(t) \quad (10.5)$$

The functions $A(t)$ and $H(t)$ are given by tables in [DIN90]. They contain conservatively high values for

- initial enrichment (percent by weight) $1.9\% \leq e_0 \leq 4.1\%$
- burnup in MWd/kg_{uranium} $BU \leq 12.5 e_0$
- power density S in kW/kg_{uranium} $S \geq 5 e_0$.

The total decay heat power in node n is given by

$$w^n(t) = w_{fp}^n(t) + w_{239U}^n(t) + w_{239Np}^n(t) + w_{act}^n(t) + w_{cap}^n(t) \quad (10.6)$$

Some of the numerical evaluations related to the decay heat model are described in [Gru97].

References Chapter 10

- [DIN90] DIN Norm 25463, Part 1, "Berechnung der Nachzerfallsleistung der Kernbrennstoffe von Leichtwasserreaktoren" (1990).
- [Kes95] Kessler, G., Kuczera, B., Ehrhardt, J., Henneges, G., Scholtyssek, W., and Wiese, H. W., "Confinement of the Radiological Source Term During Beyond-Design-Basis Events in Future Pressurized Water Reactors", Nuclear Technology 111,305 (1995).
- [Gru97] Grundmann, U., Laggiard E., Mittag S., "Calculation of the Stationary and Transient Space Dependent Decay Heat Power by Means of the DYN3D Code", Internal report, Rossendorf, (1997).
- [Sch95] Scholtyssek, W., "Long-term Containment Thermal-Hydraulic Loads in Pressurized Water Reactor Core-Melt Accidents", Nuclear Technology 111,319 (1995).

11 Coupling with Thermo-Hydraulic System Codes

If DYN3D is used as stand-alone code, the time-dependent boundary conditions for the core calculation like.

- coolant temperature at the core inlet,
- boron acid concentration at the core inlet,
- pressure at the core outlet,
- coolant mass flow rate or pressure drop over the core.

have to be given as input information to the code (see section 5.3).

However, only the coupling of the core model with a thermo-hydraulic system code provides the possibility of taking into account the feedback from the plant behaviour to core dynamics and vice versa. This is important e. g. in the case of a reactivity initiated accident with strongly asymmetric neutron flux distribution in the core caused by perturbation in one of the primary circuit loops. Such types of accidents are steam line break or boron dilution scenarios. Therefore, recently large efforts have been undertaken to couple 3D neutron kinetics codes with thermo-hydraulic system codes [Lab96, Roh99].

DYN3D has been coupled with the system codes ATHLET and RELAP5/MOD3.

11.1 Coupling DYN3D - ATHLET

The code ATHLET [Tes96] has been developed by the Gesellschaft für Anlagen- und Reaktorsicherheit (GRS). It can be applied to the whole spectrum of operational and accident transients, small and intermediate leaks up to large breaks of coolant loops at PWRs and BWRs. The code includes basic modules for the thermo-hydraulics, heat transfer and heat conduction, neutron kinetics (point kinetics and 1D kinetics) and reactor control simulation. Within the General Control and Simulation Module (GCSM) an interface is available, that allows to couple other independent modules to ATHLET without changes of the code architecture. Interface subroutines are integrated in the ATHLET code, by means of that the integration of these models can be performed.

In accomplishing the coupling of ATHLET and DYN3D three basically different ways were considered, internal, parallel and external coupling.

11.1.1 Internal Coupling

The internal coupling [Gru95a-c] has been implemented straightforward by defining modules for the exchange of the coupling parameters and interfaces routines which organise the correct transfer of these parameters to the single models. Using the new FORTRAN90 versions of the two codes the coupled code DYN3D-ATHLET is easy to generate. Running the same code, internal and parallel coupling are controlled only by the input data. Dummy routines of ATHLET for coupling different 3D neutron kinetic models and the main program of DYN3D have to be removed from the codes. In order to obtain the coupled code, the remaining routines together with the specific coupling routines have to be compiled and linked together. If new versions of the codes are released, no changes of the coupling routines are necessary to generate the coupled code.

In this type of coupling, only the neutron kinetic part of DYN3D is used, the fuel temperatures T_f , moderator temperatures T_m , moderator densities ρ_m and boron acid concentrations c_b are calculated by ATHLET and transferred to DYN3D as feedback parameters for calculating the actual macroscopic cross sections in the nodes from a cross section library linked to DYN3D.

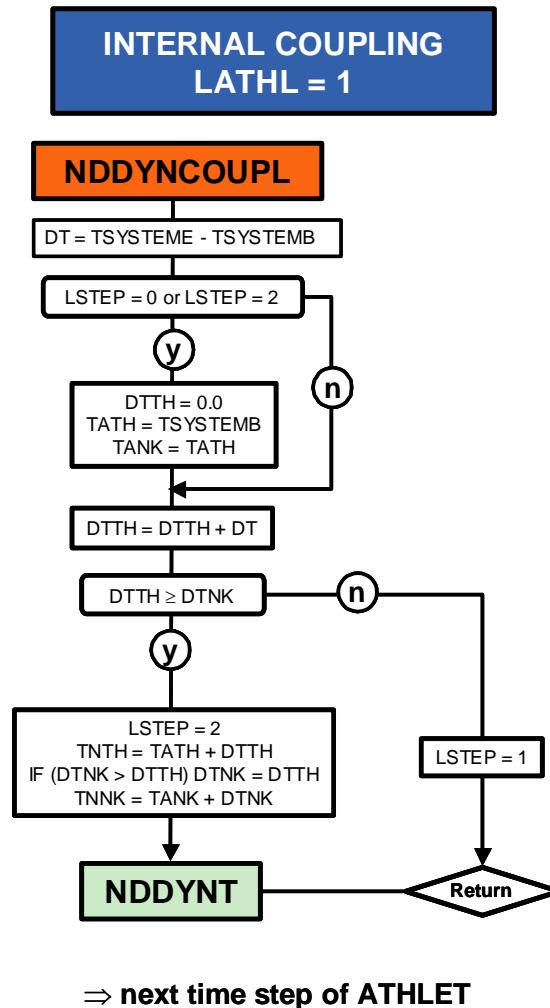


Fig. 11.1: Time step control in DYN3D for internal coupling

The power distribution q is transferred from the neutron kinetics of DYN3D to ATHLET in a similar way as it is done for the 1D neutron kinetics model of ATHLET. The actual mesh sizes used in ATHLET and DYN3D can be different. Therefore, for the parameter transfer an interpolation procedure must be carried out. Further, as DYN3D has the possibility to combine several fuel assemblies to one thermal hydraulic channel, the mapping scheme between the fuel assemblies and the thermal hydraulic channels is organized in DYN3D and described in the DYN3D input data. The ATHLET thermo-fluid objects describing the DYN3D core channels are part of the ATHLET input.

Fig. 11.1 shows the time step control by the subroutine NDDYNCOUPL which is called by the coupling routines. Firstly, the time integration is performed in ATHLET over the ATHLET step DT which is obtained from the time $TSYSTEME$ at the end and $TSYSTEMB$ at begin of the ATHLET step. The neutron kinetics of DYN3D is called after the ATHLET step without any

iteration between ATHLET and DYN3D. Two different time steps are used in stand alone version of DYN3D. The thermal-hydraulics time step can contain several neutron kinetic steps DTNK. The time steps are changed during the transient by changing of system variables. The time steps DTNK are changing within a minimum and a maximum step. In a given time interval, a calculation with a fixed DTTH and a given number of fixed DTNK can be performed in DYN3D. This possibility has to be switched off in the DYN3D input data by using a time interval out of the considered one. The end of a thermo-hydraulic step is also the end of neutron kinetic step in DYN3D. In the internal coupling, the neutron kinetic step only is controlled in DYN3D, because the thermo-hydraulic step DTTH is obtained from ATHLET. If the ATHLET step is smaller than the minimum neutron kinetic step, the next ATHLET step is performed. If the sum of the ATHLET steps exceeds the minimum neutron kinetic step, the neutron kinetic calculations are performed by call of the subroutine NDDYNT.

11.1.2 External Coupling

In the external coupling, the whole core is cut out of the ATHLET plant model [Gru95a-c]. The core is completely modelled by DYN3D. The thermal hydraulics is split into two parts: one part describes the thermal hydraulics of the core, the other part models the coolant system. As a consequence of this local cut it is easy to define the interfaces. They are located at the bottom and at the top of the core. The pressures, mass flow rates, enthalpies and concentrations of boron acid at these interfaces have to be transferred. It is effectively supported by the GCSM of the ATHLET code. The external coupling uses the GCSM-interface. DYN3D is used within the GCSM formalism as an user defined subroutine. The coupling parameters are defined explicitly as so called GCSM-signals. These data are the above mentioned thermal-hydraulic parameters. The pressures at the bottom and the top of the core and the enthalpy at the bottom of the core are calculated by ATHLET. The interface routine transfers them to DYN3D as boundary conditions for the next DYN3D time step. The ATHLET model includes the special junction „FILL“. It enables the user to simulate a fluid injection or draw off within the ATHLET input data set. The mass flow rate, and in the case of flow injection, additionally the enthalpy of the injected fluid, have to be given to the FILL. These parameters are boundary conditions for the thermal hydraulics of the ATHLET model. The use of this special ATHLET-junction for the coupling leads to the following strategy of interfacial data handling. The pressure at the bottom and at the top of the core and the enthalpy at the bottom of the core are calculated by ATHLET. The interface routine transfers them to DYN3D as boundary condition for the next DYN3D time step. Having finished the DYN3D calculation for one time step, the interface routine transfers the mass flow rates at the core inlet and core outlet and the enthalpy at the core outlet to ATHLET. These parameters are now boundary conditions for the next ATHLET time step.

The interface routine also coordinates the separate time step control in both parts of the program. DYN3D calculates as many time steps until the current DYN3D time is greater than the current ATHLET time. Before the data are transferred they are interpolated to the current ATHLET time. For that reason, the DYN3D time steps can be larger as well as smaller than the ATHLET time steps. Therefore the time step size can be controlled by both codes independently adopted to the needs of the codes.

The splitting of the thermalhydraulics into two independent submodels in external coupling caused stability problems in the coupled calculations. These difficulties were caused by numer-

ical reasons but not by physical compatibility of the models. The coupling of the two thermal-hydraulic parts is done explicitly and very small time steps are necessary for stable calculations. Test calculations showed that the numerical solution was stable for a maximum time step of about 0.01 s. The pressure drop over the core and the core mass flow rates oscillate in a random manner caused by numerical effects. This oscillations can be damped by interconnecting a low pass filter of first order for the pressure drop representing the boundary condition for the DYN3D calculation. This low pass filter does not alter the vector of solution but only the time dependent boundary conditions.

The well known differential equation for a low pass filter of first order is:

$$y(t) + \tau \cdot \frac{dy(t)}{dt} = x(t) \quad (11.1)$$

where t is the time constant of the filter, $x(t)$ is the input and $y(t)$ is the output. If DP_{ATHLET} is the pressure drop over the core calculated by ATHLET, DP_{old} is the pressure drop given as boundary condition to DYN3D at the last ATHLET time step and DP_{new} is the pressure drop given to DYN3D as boundary condition for the current time step, the equation (11.1) applied to the pressure drops can be written as follows:

$$DP_{new} + \tau \cdot \frac{DP_{new} - DP_{old}}{DT} = DP_{ATHLET} \quad (11.2a)$$

That leads to:

$$DP_{new} = \frac{1}{1 + \tau/DT} \cdot DP_{ATHLET} + \left(1 - \frac{1}{1 + \tau/DT}\right) \cdot DP_{old} \quad (11.2b)$$

The difference between DP_{ATHLET} and DP_{new} is split up to the absolute pressures at the bottom and the top of the core:

$$\begin{aligned} P_{DYN,in} &= P_{ATHLET,in} - (DP_{ATHLET} - DP_{new}) / 2 \\ P_{DYN,out} &= P_{ATHLET,out} + (DP_{ATHLET} - DP_{new}) / 2 \end{aligned} \quad (11.3)$$

In this way it is possible to solve these difficulties and to get stable calculations even for larger time steps. The calculations are numerically stable for all test cases if time constants of the low pass filter of 1 s or larger are chosen.

The low pass filter has practically no influence on the transients that are to be calculated. It only suppresses oscillations of the pressure drop over the core with high frequencies, caused by random numerical disturbances. There are no distortions even for strong transients, what has been shown by different sample calculations for test cases with fast and large changes of pressure drop over the core (e. g. large break LOCA and ejection of a whole control rod group, both as ATWS) [Gru95a, Gru95b].

11.1.3 Parallel Coupling

Considering the parallel coupling [Gru04], the core thermal hydraulics of ATHLET and DYN3D are calculated parallel. The same code as for the internal coupling is used, but with different input data sets (see paragraph 11.1.1). The thermal hydraulic core boundary conditions as the pressure at the core outlet, the mass flow rates, the coolant temperatures and the boron concentration at the core inlet of the DYN3D model are obtained from ATHLET. The power distribution calculated by DYN3D is transferred to ATHLET. The influence of the core thermal hydraulics on the nuclear power is calculated within the DYN3D model. The DYN3D mapping scheme is used for the mapping between DYN3D fuel assemblies and the DYN3D thermal-hydraulic channels. An additional mapping scheme between the thermalhydraulic DYN3D channels and the ATHLET channels has to be described in the ATHLET input. An iteration between thermalhydraulics and neutron kinetics within DYN3D is possible as in the stand alone version of DYN3D.

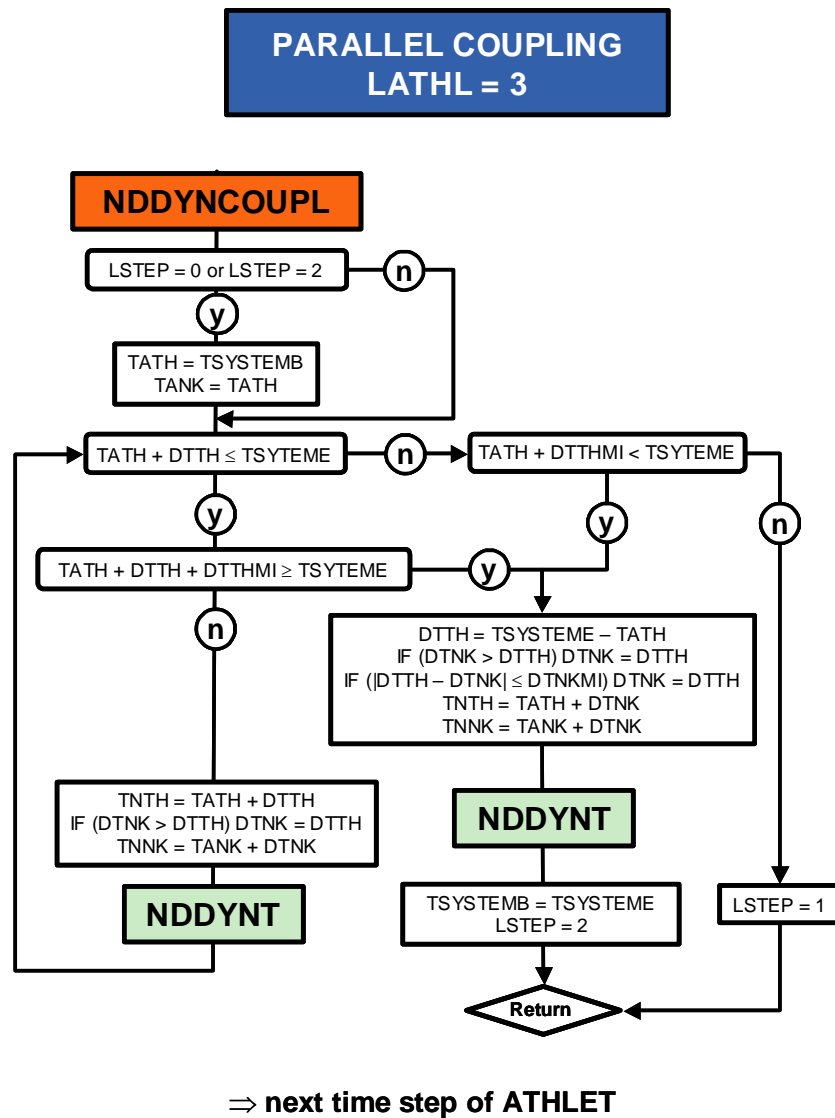


Fig. 11.2: Time step control in DYN3D for parallel coupling

The time step control for parallel coupling differs from the internal coupling (see Fig. 11.2). The thermal-hydraulic step DTTH does not generally agree with the ATHLET time step. If the ATHLET step is greater than the minimum DTTH and greater than current DTTH, several DYN3D steps DTTH are performed until the end of the ATHLET step at TSYSTEME. If the ATHLET step is greater than the minimum DTTH and smaller than current DTTH, the DYN3D step DTTH is changed that the end of the ATHLET step at TSYSTEME is reached. If ATHLET step is smaller than the minimum DTTH, no DYN3D calculation is performed. There is no iteration between ATHLET step and DYN3D calculation.

11.1.4 Use of the Different Types of Coupling

Fig. 11.3 illustrates the parameter exchange between ATHLET and DYN3D in the three different types of coupling.

Both the internal and the external ways of coupling have their specific advantages and disadvantages. Disadvantages of the external coupling are some restrictions of the thermalhydraulic model of DYN3D in comparison with ATHLET. Some situations such as global fluid flow reversal in the core and formation of a mixture level can not be modelled by DYN3D. On the other hand, in the case of the external coupling special models included in DYN3D can be used. For example, in the DYN3D fuel rod model a detailed description of heat transfer through the gas gap between fuel and cladding is given, taking into account the thermo-mechanical behaviour of the rod (see section 6). A special mixing model for the lower plenum of VVER-440 reactors included in the DYN3D code can also be used only in the case of the external coupling (see section 5.5). In the case of a 1:1 assignment of coolant channels to fuel assemblies (large number of parallel coolant channels in the core), the computation is more stable and requires much less computation time in the case of external coupling. The input data sets are simpler than in the case of internal coupling. The most serious disadvantage in the external coupling are the stability problems. Although the problems were solved by introducing the low pass filter, it cannot be shown in general, that this solution is practicable in all possible situations.

The parallel coupling has been developed to combine the advantages of the internal and the external type of coupling. Due to the fact, that the thermalhydraulics of the whole system including the core is calculated within the ATHLET code as a whole, the numerical stability is improved. On the other hand, the whole core (thermalhydraulic and neutron kinetic parts) is calculated by DYN3D with the boundary conditions from the ATHLET model. So, the core thermalhydraulics can be calculated very effectively but also having the possibility to resolve the fuel elements of the full core 1:1.

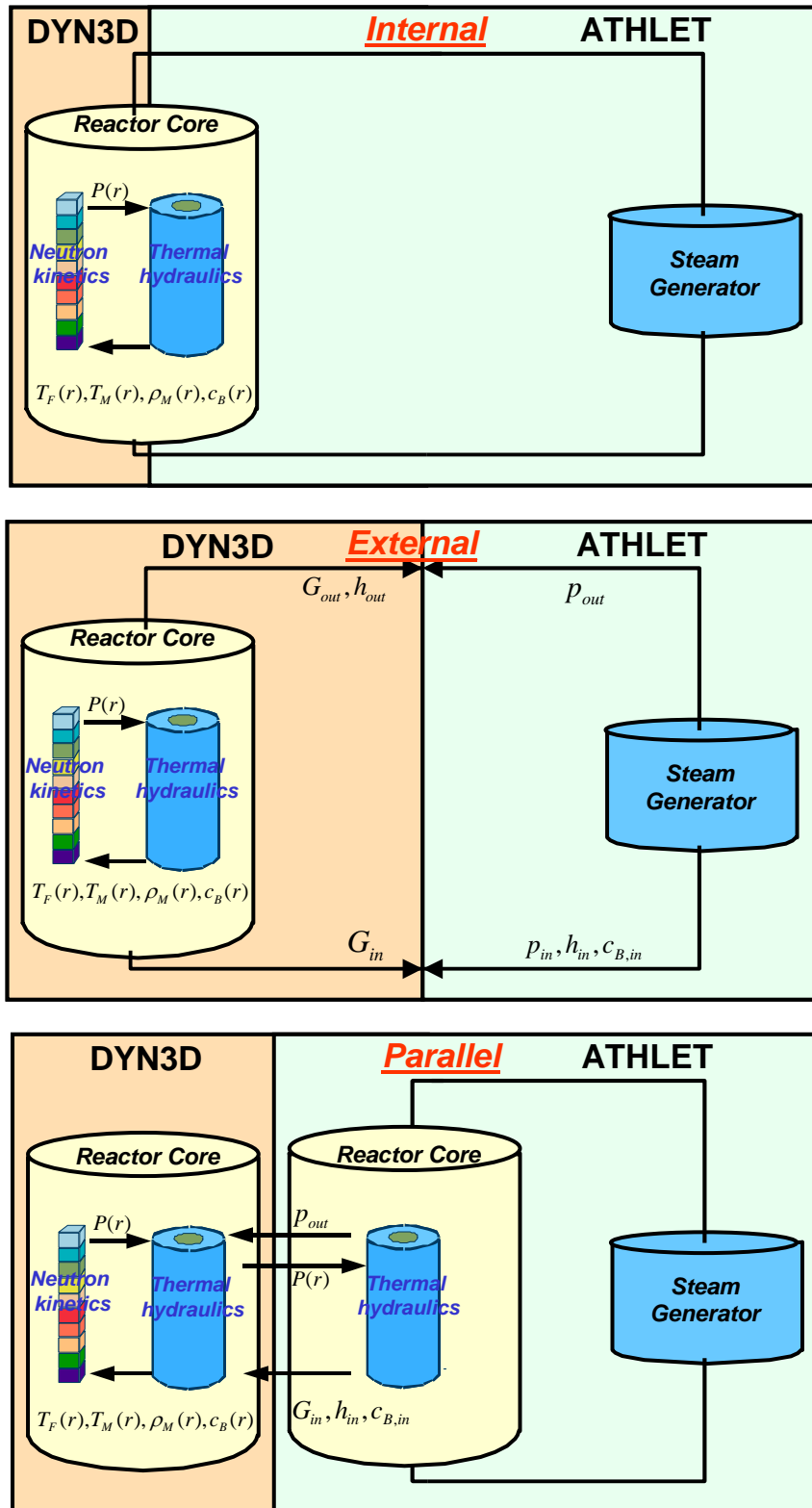


Fig. 11.3: Parameter exchange for the three ways of coupling DYN3D to ATHLET

11.2 Coupling DYN3D - RELAP5

The RELAP5/MOD3 is used worldwide for best-estimate transient simulations of LWR coolant systems. In the NRC versions the reactor power is computed using the point kinetics approximation with thermohydraulic feedback, neglecting space dependent effects on the neutron flux distribution.

The internal coupling approach has been used to perform the coupling of DYN3D with RELAP5 code system [Koz01]. The basic principles of internal coupling are described in section 8.1. The following code system organisation has been realised at the procedure of DYN3D-RELAP5 internal coupling:

Input / Output Organisation

Separate DYN3D and RELAP5 input/output decks are used. The output frequency of the DYN3D dynamic variables is determined by the frequencies of RELAP5 minor and major edits. Required modifications of RELAP5 and DYN3D input decks were minimised.

Restart Organisation

Separate DYN3D and RELAP5 binary restart files are used. Operations of reading/writing data from/to restart files of DYN3D and RELAP5 are completely synchronised. It means that calculations can be started from any of available synchronised restart data blocks stored in restart files.

Variable Exchanges between DYN3D and RELAP5

The variables calculated by RELAP5 and passed on to DYN3D are:

- (1) coolant densities, boron concentrations, and temperatures from the core hydrodynamic volumes,
- (2) average fuel temperatures from each heat generating node of the core.

The variables calculated by DYN3D and passed on to RELAP5 are:

- (1) averaged value of power generated in a single core node,
- (2) normalized spatial profile of the core power distribution, and
- (3) normalized direct heating coefficients for the core volumes.

For the eigenvalue problems to converge several restart runs of the DYN3D/RELAP5 code system are needed. For the transient neutron flux problems the variable exchange cycle occurs at every time step. After each successful time step RELAP5 passes on its variables to the transient model of DYN3D kinetics in order to update the value of core total power and a power distribution profile. Time step control is provided by corresponding means of RELAP5 code.

References Chapter11

- [Gru95a] U. Grundmann, U. Rohde, S. Mittag, D. Lucas: Weiterentwicklung und Verifikation eines dreidimensionalen Kernmodells für Reaktoren vom Typ WWER und seine Ankopplung an den Störfallcode ATHLET, *Report FZR-84*, Rossendorf, April 1995
- [Gru95b] U. Grundmann, D. Lucas, U. Rohde: Coupling of the Thermohydraulic Code ATHLET with the Neutron Kinetic Core Model DYN3D, *Int. Conf. on Mathematics and Computations, Reactor Physics, and Environmental Analyses*, April 30 - May 4, 1995, Portland, Oregon, Proc. Vol. 1, p. 257
- [Gru95c] U. Grundmann, D. Lucas, U. Rohde: Coupling of the Advanced Thermohydraulic Code ATHLET with the 3D Core Model DYN3D, *Int. Topical Meeting on VVER Safety*, 21.-23.09.95, Prague, Proc. p. 197
- [Gru04] U. Grundmann, S. Kliem, U. Rohde: Analysis of the boiling water reactor turbine trip benchmark with the codes DYN3D and ATHLET/DYN3D, *Nucl. Science and Engineering*, vol. 148, pp. 226-234, (2004)
- [Koz01] Y. Kozmenkov, Y. Orekhov, U. Grundmann, S. Kliem, U. Rohde, A. Seidel: Development and Benchmarking of the DYN3D/RELAP code system, *Annual Meeting of the German Nuclear Society 2001*, Dresden, May 15 - 17, 2001, Proc. p.15
- [Lab96] S. Langenbuch, M. Lizorkin, U. Rohde, K. Velkov: 3D Neutronic Codes coupled with Thermal-Hydraulic System Codes for PWR, BWR and VVER Reactors, *OECD/CSNI Workshop on Transient Thermal-Hydraulic and neutronic Codes requirements*, Annapolis (Maryland, USA), November 5 - 8, 1996
- [Roh99] U. Rohde, S. Langenbuch: Gekoppelte Berechnungen von Thermohydraulik und Neutronenkinetik, *Jahrestagung Kerntechnik 1999, Fachsitzung „Neue Ergebnisse aus F+E zur Fluidodynamik und Reaktorphysik“*, INFORUM Verlagsgesellschaft, Bonn, Juni 1999

12 Verification and Validation of DYN3D and the Coupled Code DYN3D/ATHLET

DYN3D is validated by numerous benchmarks (including experimental results) for the two geometries Cartesian and hexagonal fuel element geometry.

12.1 Steady-State Problems

- 3D IAEA Benchmark (Cartesian) [Gru95, Gru96b, Gru97]
- 2D IAEA benchmarks modified for hexagonal geometry [Gru99a]
- 2D and 3D Seidel benchmark for VVER-440 (hexagonal) [Gru99b, Gru99c]
- 3D Schulz benchmark for VVER-1000 (hexagonal) [Gru99b, Gru99c]
- AER (Atomic Energy Research) benchmark problem concerning control rod worth of VVER-440 reactor (hexagonal) [Mit94, Mit96]
- Comparison of calculated reactor parameters (critical boron concentration, reactivity coefficients, control rod efficiency) with measured data for different VVER-reactors [Gru00]
- Comparison of assembly-averaged and pin-wise neutron flux distribution measured at V-1000 zero power test facility (hexagonal) [Gru03c]

12.2 Transient Problems

- Kinetic experiments at the zero power reactor LR-0 (hexagonal) [Ryp90, Gru91]
- 1st - 3rd Kinetic Benchmarks of AER (Atomic Energy Research) with ejection of asymmetrical control rods in a VVER-440 (hexagonal) [Gru94, Kyr96]
- 4th Kinetic Benchmark of AER (Atomic Energy Research) of a boron dilution transient in a VVER-440 (hexagonal) [Kyr97]
- NEACRP benchmarks on control rod ejections in PWR (Cartesian) [Gru96a, Gru96b, Gru97]
- NEA-NSC benchmarks on uncontrolled withdrawal of control rods at hot zero power in PWR (Cartesian) [Gru97]
- DYN3D/ATHLET calculations of an accident with delayed scram at NPP Greifswald (hexagonal) [Kli98]
- OECD-main steam line break benchmark - exercise 2 (Cartesian) [Gru99d]
- OECD-main steam line break benchmark - exercise 3 analysed with DYN3D/ATHLET (Cartesian) [Iva99, Iva01, Kli00, Gru03a]
- 5th kinetic benchmark of AER on main steam header break in a VVER-440 with DYN3D/ATHLET (hexagonal) [Kli99, Koz01]

- DYN3D/ATHLET calculations of the turning-off one feed water pump from working two in the Balakovo-4 VVER-1000 (hexagonal) [Mit01]
- DYN3D/ATHLET calculations for the load drop down to house load level in one of the two working turbines in Loviisa-1 VVER-440 (hexagonal) [Mit02]
- OECD BWR turbine trip benchmark in the reactor Peach Bottom-2 - Exercise 2 analysed with DYN3D (Cartesian) [Gru99d, Gru01, Gru02, Gru03b]
- OECD BWR turbine trip benchmark in the reactor Peach Bottom-2 - Exercise 3 analysed with DYN3D/ATHLET (Cartesian) [Gru01, Gru04]
- 6th kinetic benchmark of AER on a main steam line break in a VVER-440 with DYN3D/ATHLET (hexagonal) [Kli03]
- DYN3D/ATHLET calculations for drop of a single control rod and power control action in the VVER 440/213 of NPP Bohunice 3 (hexagonal) [Häm03]
- DYN3D/ATHLET calculations for the coast-down of a second main coolant pump (start up test) in the VVER-1000/V-320 of Kozloduy 6 (hexagonal) [Häm03]
- DYN3D Calculations for the V-1000 Test Facility and Comparisons with the Measurements (hexagonal) [Gru03c]
- DYN3D/ATHLET calculations for the main coolant pump switching-on experiment in the VVER-1000/V-320 of Kozloduy 6 (hexagonal) in the frame of the OECD V1000CT-Benchmark [Koz04].

References Chapter 12

- [Gru91] Grundmann, U.; Hádek, J.; „Calculations of Neutron Kinetics Experiments on the LR-0 Reactor with the Three - Dimensional Code DYN3D/M1“. KERNENERGIE 34 (1991) 12.
- [Gru94] Grundmann, U.; „Results of Second Kinetic AER-Benchmark“, Proceedings of 4th Symposium of Atomic Energy Research (AER), Sozopol (Bulgaria), 10.-15. October 1994.
- [Gru95] Grundmann, U. „The Code DYN3DR for Steady-State and Transient Analyses of Light Water Reactor Cores with Cartesian Geometry“, Report FZR-114, Rossendorf, November 1995
- [Gru96a] Grundmann, U.; Rohde, U.; „The Reactor Code DYN3DR - Transient Calculations of NEACRP Benchmarks for PWR and BWR“, Proceedings Jahrestagung Kerntechnik '96, Mannheim (1996)
- [Gru96b] Grundmann, U.; Rohde, U.; „DYN3D - A 3-dimensional Core Model for Steady State and Transient Analysis in Thermal Reactors“, Proceedings of the Interna-

- tional Conference on the Physics of Reactors PHYSOR'96, Mito (Japan), 16-20 Sept. 1996.
- [Gru97] Grundmann, U.; Rohde, U.; „Verification of the Code DYN3DR with the Help of International Benchmarks“, Report FZR-195, Rossendorf, 1997.
- [Gru99a] Grundmann U., Hollstein F., A Two-Dimensional Intranodal Flux Expansion Method for Hexagonal Geometry, Nucl Sci Engng, **133** pp. 201-212, (1999).
- Gru99b U. Grundmann, „3D Nodal Expansion Method HEXNEM for the Solution of Neutron Diffusion Equation in Hexagonal Geometry“, Jahrestagung Kerntechnik'99, Karlsruhe, 18.- 20. Mai, 1999
- [Gru99c] U. Grundmann, „HEXNEM - A Nodal Method for the Solution of the Neutron Diffusion Equation in Hexagonal Geometry“, Proceedings of the M&C'99 - Conference on Mathematics and Computations in Nuclear Applications, pp. 1086-1095, Madrid, September, 27 - 30, 1999.
- [Gru99d] U. Grundmann, S. Kliem and U. Rohde, „Analysis of the Exercise 2 of the OECD - MSLB Benchmark with the Code DYN3D/R“, Proceedings of the M&C'99- Conference on Mathematics and Computations in Nuclear Applications, Madrid, September, 27 - 30, 1999.
- [Gru00] Grundmann, U.; Kliem, S.; Rohde, U.; Seidel, A.; Khalimonchuk, V.; Kuchin, A.; “Beiträge zur Validierung fortgeschrittener Störfallanalysecodes mit 3D Neutronenkinetik - WTZ mit der Ukraine“, Wissenschaftlich-Technische Berichte / Forschungszentrum Rossendorf; FZR-301 Oktober, 2000.
- [Gru01] Grundmann, U.; Kliem, S., “Analyses of the OECD - MSLB Benchmark with the Codes DYN3D and DYN3D/ATHLET“, Transactions of the American Nuclear Society, June 2001, Volume 84, page 23 - 25.
- [Gru02] Grundmann, U.; Rohde, U.; „Analysis of the Boiling Water Reactor Turbine Trip Benchmark with the Code DYN3D“, Proceedings of PHYSOR 2002 International Conference on the New Frontiers of Nuclear Technology: Reactor Physics, Safety and High-Performance Computing, October 7-10, 2002, Seoul, Korea.
- [Gru03a] Grundmann, U.; Kliem, S.; „Analyses of the OECD - Main Steam Line Break Benchmark with the Codes DYN3D and ATHLET“, Nucl. Technol. 142, 146 (2003)
- [Gru03b] Grundmann, U.; Rohde, U.; „Different Simulations of the Phase 2 of the OECD/NRC BWR Turbine Trip Benchmark with the Code DYN3D“, Annual Meeting on Nuclear Technology, Berlin, May 20 - 22, 2003
- [Gru03c] U. Grundmann and S. Mittag, „DYN3D Calculations for the V-1000 Test Facility and Comparisons with the Measurements“, Proceedings of the 13th Symposium of AER, Dresden, September 22-26, 2003.

- [Gru04] Grundmann, U.; Kliem, S.; Rohde, U.; „Analysis of the Boiling Water Reactor Turbine Trip Benchmark with the Codes DYN3D and ATHLET/DYN3D“, Nuclear Science and Engineering, vol. 148, pp. 226-234, (2004)
- [Häm03] A. Hämäläinen, T. Vanttola, F.-P. Weiss, S. Mittag, S. Kliem, S. Langenbuch, A. Keresztúri, J. Hádek, C. Strmensky, S. Stefanova, A. Kuchin, P. Hlbocky, D. Siko, S. Danilin, „Validation of Coupled Codes in EU/VALCO WP1 Using Measured VVER Data“, Proceedings of the 13th Symposium of AER, Dresden, September 22-26, 2003.
- [Iva99] K. Ivanov, T. Beam, A. Baratta, A. Irani and N. Trikouros, „Pressurized Water Reactor Main Steam Line Break (MSLB) Benchmark - Volume I: Final Specifications“, NEA/NSC/DOC (99) 8, US Nuclear Regulatory Commission, OECD Nuclear Energy Agency, (April 1999).
- [Iva01] K. Ivanov, A. Baratta, E. Sartori, „OECD/NRC MSLB Benchmark – A Systematic Approach to Validate Best-Estimate Coupled Codes Using a Multi-Level Methodology“, Proceedings of the workshop on 'Advanced Thermal-hydraulic and Neutronic Codes: Current and Future Applications', Barcelona, April 2001, NEA/CSNI/R(2001)2.
- [Kli98] S. Kliem, „Analysis and Calculation of an Accident with Delayed Scram at NPP Greifswald Using the Coupled Code DYN3D/ATHLET“, Proc. International Conference on the Physics of Nuclear Science and Technology, pp. 485-491, ANS, La Grange Park, IL (1998)
- [Kli99] S. Kliem, S. Danilin, R. Kyrki-Rajamäki, J. Hádek, A. Kereszturi, P. Siltanen: „A Benchmark for Coupled 3D Neutron Kinetics/Thermohydraulics System Codes - Main Steam Header Break in a NPP with VVER-440 Reactor“, Proc. International Conference on Mathematics and Computation, Reactor Physics and Environmental Analysis in Nuclear Applications (MC '99), Vol. 1, pp. 359-368, Senda Editorial, S.A. Madrid (Spain)
- [Kli00] S. Kliem, U. Grundmann, and U. Rohde: „Analysis of the OECD MSLB Benchmark Using the Coupled Code DYN3D/ATHLET“, Proceedings of the 8th International Conference on Nuclear Engineering (ICONE 8), Baltimore (USA), April, 2 - 6, 2000.
- [Kli03] S. Kliem: „Comparison of the updated solutions of the 6th dynamic AER benchmark - main steam line break in a NPP with VVER-440“, Proc. 13th Symposium of AER, pp. 413-444, Dresden, September 22-26, 2003.
- [Koz01] Kozmenkov, Y.; Orekhov, Y.; Grundmann, U.; Kliem, S.; Rohde, U.; Seidel, A., “Development and Benchmarking of the DYN3D/RELAP5 Code System“, Proceedings of Jahrestagung Kerntechnik 2001, Dresden, 15 - 17 Mai 2001, pp. 15-18.
- [Koz04] Kozmenkov, Y.; Grundmann, U.; Kliem, S.; Rohde, U.; Weiss, F.-P., “V1000CT-1 benchmark analyses with the DYN3D/RELAP5 and DYN3D/ATHLET coupled

- code systems“, Proc. 11th International Topical Meeting on Nuclear Reactor Thermal Hydraulics NURETH-11 (CD-ROM), 03.-07.October, 2005.
- [Kyr96] Kyrki-Rajamäki, R., U. Grundmann, A. Kereszturi: „Results of Three-Dimensional Hexagonal Dynamic Benchmark Problems for VVER Type Reactors“, Proceedings of the Int. Conf. on the Physics of Reactors PHYSOR'96, pp. J229 - J238, Mito (Japan), 16. - 20. 09. 1996.
- [Kyr97] R. Kyrki-Rajamäki, „Comparison of the first results of the 4th hexagonal dynamic AER benchmark - boron dilution in core“, Proceedings of the 7th Symposium of AER, 23.-26.09.1997, Hörnitz near Zittau (Germany), Vol. I, pp. 321-350.
- [Mit94] Mittag, S.; „Solution of AER Benchmark Problem on Control Rod Worth of VVER-440 Reactor“, Proceedings of 4th Symposium of Atomic Energy Research (AER), Sozopol (Bulgaria), 10.-15. October 1994.
- [Mit96] Mittag, S.; „Burnup and Rod Worth Calculations for Paks-2 Using the Code DYN3D with Two Different Group Data Libraries“, Proceedings of 6th Symposium of Atomic Energy Research (AER), Kirkkonummi (Finland), 23.-26. September 1996.
- [Mit01] S. Mittag, S. Kliem, F.-P. Weiß, R. Kyrki-Rajamäki, A. Hämäläinen, S. Langenbuch, S. Danilin, J. Hadek, G. Hegyi, A. Kuchin, D. Panayotov, „Validation of Coupled Neutron Kinetic / Thermal-Hydraulic Codes. Part 1: Analysis of a VVER-1000 Transient (Balakovo-4)“, Annals of Nuclear Energy 28, pp. 857-873 (2001).
- [Mit02] A. Hämäläinen, R. Kyrki-Rajamäki, S. Mittag, S. Kliem, F.-P. Weiß, S. Langenbuch, S. Danilin, J. Hadek, G. Hegyi, „Validation of Coupled Neutron-Kinetic / Thermal-Hydraulic Codes. Part 2: Analysis of a VVER-440 Transient (Loviisa-1)“, Annals of Nuclear Energy 29, pp. 255-269 (2002).
- [Ryp90] Rypar, V.; Racek, J.; Fährmann, K.- H.; Grundmann, U.; „Neutron Kinetics Investigations at the LR-0 Zero Power Reactor“, Nucl Sci Engng, 105, (1990) 218.

List of Variables in Neutron Kinetics

Latin Symbols:

A_s, A_c :	vectors of the coefficients $a_{s,k}$ and $a_{c,k}$ of the exponential functions of the hexagonal plane, respectively
A^u :	vectors of the coefficients a_1^u, a_2^u of the exponential functions of one of the directions $u \in x, y, z$
a :	length of a node in one of the directions $u \in x, y, z$
a_u^n :	length of sides of the rectangular node n in one of the directions $u \in x, y, z$
a_z^n :	length of the hexagonal node n in the axial direction z
$a_{s,k}, a_{c,k}$:	expansion coefficients of the exponential functions of the flux expansion in the hexagonal plane
a_1^u, a_2^u :	expansion coefficients of the exponential functions of the flux expansion in one of the directions $u \in x, y, z$
$a_{s,i}^f, a_{c,i}^f$:	Coefficients of sin and cos (sinh and cosh) of the fundamental mode of the flux reconstruction
$a_{c,i}^t, a_{s,i}^t$:	Coefficients of sinh and cosh of the transient mode of the flux reconstruction
BU :	Burnup of fuel at time of shut down in MWd/kg _{Uranium}
B', B'' :	buckling of any energy group g calculated by $\sqrt{\frac{\Sigma'}{D'}}$ or $\sqrt{\frac{\Sigma''}{D''}}$, respectively
$B_{z,g}^n$:	Axial buckling of the node n and energy group g
B_i^f, B_i^t :	Buckling of the fundamental and transient solution of the two-dimensional two-group diffusion equation solved for flux reconstruction
$C_j^n(\mathbf{r}, t)$:	precursor density of precursor group j in the node n at time t
$\bar{C}_j^n(t)$:	node averaged precursor density of precursor group j in the node n at time t
$\bar{C}_j(t)$:	core averaged precursor density of precursor group j at time t
$c_{pre,j,i}^n(t)$:	coefficient i of the polynomial expansion of the precursor density of delayed neutron group j in the node n at time t (radial plane of hexagonal geometry)
$c_{pre,j,i}^{u,n}(t)$:	coefficient i of the polynomial expansion of the precursor density of delayed neutron group j in the node n at time t for any of the directions $u \in x, y, z$

$C^{[(k)]}, C^{*[(k)]}$:	vectors of the coefficients c_i of the polynomials of the hexagonal plane (iteration step k , updated (*))
$C^{u[(k)]}, C^{t^*[(k)]}$:	vectors of the coefficients c_i^u of the polynomials of one of the directions $u \in x, y, z$ (iteration step k , updated (*))
c_i :	expansion coefficients of the polynomials of the hexagonal plane
$c_{[g], i}^{u, [n]}([t])$:	expansion coefficients of the polynomials of the flux expansion in one of the directions $u \in x, y, z$ (energy group g , node n , time t)
c_I :	concentration of ^{135}I of the the node n
c_{Pm} :	concentration of ^{149}Pm of the the node n
c_{Sm} :	concentration of ^{149}Sm of the the node n
c_{Xe} :	concentration of ^{135}X of the the node n
$D_g^n(t)$:	diffusion coefficient of the energy group g in the node n
D'_g, D''_g :	dimensionles diffusion coefficients of the energy group g by division with $\frac{d}{2}$ or one of the $a \in a_x, a_y, a_z$, respectively
d :	diameter of the hexagonal nodes (distance between the parallel sides)
e_0 :	Initial enrichment of ^{235}U
E_{Np} :	the average decay heat of ^{239}Np
E_U :	the average decay heat of ^{239}U
$e^{n, m}$:	unit vector perpendicular from node n to node m perpendicular the the interface
$e_{s, k}$:	unit vector from the center of a hexagon to the center of side k
$e_{c, k}$:	unit vector from the center of a hexagon to the corner k
F_{hex} :	cross-section of the hexagonal assemblies
$F^{n, m}$:	area of the interface between the nodes m and n
$F_g(\mathbf{r})$:	fission source term of fast energy group or scattering source term of thermal group in a node of steady-state diffusion equation
$\hat{F}_g(x, y)$:	fission source term of fast energy group or scattering source term of thermal group in a node of steady-state diffusion equation of hexagonal plane
$\hat{F}'_g(x', y')$:	dimensionless fission source term of $\hat{F}_g(x, y)$ of the dimensionless variables $x' = 2\frac{x}{d}$, $y' = 2\frac{y}{d}$

$\hat{F}_g(u)$:	fission source term of fast energy group or scattering source term of thermal group in a node of the one-dimensional steady-state diffusion equation for one of the directions $u \in x, y, z$
$\hat{F}''_g(u'')$:	dimensionless fission source term $\hat{F}_g(u)$ for one of the dimensionless co-ordinates $u'' \in x'', y'', z''$
$f^s, f^s(i)$:	assembly discontinuity factor (ADF) at any neutron energy group at any radial side of the assembly i
$f^c(i)$:	assembly discontinuity factor (ADF) at any neutron energy group at any radial corner point of the hexagonal assembly i
$f_{r,p}^{z_k}$:	radial power peak factor of the flux reconstruction in the assembly
H_s, H_c :	matrices for updating the polynomial coefficients of the flux expansion in the hexagonal plane at the end of inner iteration
H^u :	matrices for updating the polynomial coefficients of the flux expansion in one of the directions $u \in x, y, z$ at the end of inner iteration
$h_i(x', y')$:	polynomials of the hexagonal plane
$h_i(u'')$:	polynomials of one of the co-ordinates $u'' \in x'', y'', z''$
$J_g^n(\mathbf{r}, t)$:	neutron current of energy group g in the node n
$J_{s,k}^\pm$:	partial currents at the sides of the radial plane
$J_{s,k}^{\dagger \pm}$:	partial currents of adjoint flux at the sides of the radial plane
$J_{c,k}^\pm$:	partial currents at the corner points of the hexagonal plane
J_s^\pm :	vector of the side averaged partial currents of the hexagonal nodes
J_c^\pm :	vector of the corner point partial currents of the hexagonal nodes
$J_{u_0}^\pm, J_{u_1}^\pm$:	averaged partial currents at the sides of the rectangular node for the directions $u \in x, y, z$
$J_{g,l}^{\pm n(k)}$:	side averaged partial currents of the node n , energy group g , side l , outer iteration step k
$J_{c,i,g}^\pm$:	partial current of energy group g at the corner point i of the hexagon at the outer boundary
K_1, K_2 :	auxiliary constants defined in the relations for the corner point boundary conditions of hexagonal geometry
K_3, K_4 :	auxiliary constants defined in the equations for flux reconstruction
$k_{eff}, k_{eff}^{(k)}$:	steady-state eigenvalue of neutron kinetics (at outer iteration step k)
$k_{r,\infty}$:	radial multiplication factor defined in the flux reconstruction method

$\hat{L}_g(x, y, [t]) :$	transversal leakage of the energy group g in a node of steady-state diffusion equation of hexagonal plane, steady-state or at time t
$\hat{L}'_g(x', y') :$	dimensionless transversal leakage of $\hat{L}_g(x, y)$ of the dimensionless variables $x' = 2\frac{x}{d}$, $y' = 2\frac{y}{d}$
$\hat{L}_g(u) :$	transversal leakage of the energy group g in a node of the one-dimensional steady-state diffusion equation for one of the directions $u \in x, y, z$
$\hat{L}''_g(u'') :$	dimensionless transversal leakage $\hat{L}_g(u)$ for one of the dimensionless co-ordinates $u'' \in x'', y'', z''$
$L_0 :$	averaged value of the transversal leakage in the hexagonal plane
$L_0^z :$	averaged value of the transversal leakage in the axial direction z
$L_{z_l}, L_{z_u} :$	approximations of the transversal leakage at the six sides at lower and upper side of the hexagonal node
$L_k :$	approximations of the transversal leakage at the six sides of the hexagon
$l :$	prompt neutron life time
$l_i([t]) :$	coefficients of the polynomials $h_i(x', y')$ for the transversal leakage in the hexagonal plane (time t)
$l_{[g], i}^{u[n]}([t]) :$	coefficients of the polynomials $h_i(u'')$ for the transversal leakage of one of the co-ordinates $u'' \in x'', y'', z''$ (energy group g , node n , time t)
$N_i :$	normalization factors of the polynomials $h_i(x', y')$
$P_s^\pm, P_c^\pm :$	matrices of the equations for the partial currents in the hexagonal plane in relation to the polynomial expansion
$P^{u^\pm} :$	matrices of the equations for the partial currents for one of the directions $u \in x, y, z$ in relation to the polynomial expansion
$\frac{P_i^n(t)}{Q_i} :$	fission rate of isotope i in the node n (depends on the initial enrichment e_0 and the burnup b)
$\frac{P_k^n}{Q} = \sum_{i=1}^4 \frac{P_{i,k}^n}{Q_i} :$	the total fission rate in the node n in the time interval T_k of power history
$\frac{P_{i,k}^n}{Q_i} :$	the rate of fissions of the isotopes i in the node n in the time interval T_k of power history
$P_r^n(\mathbf{r}_{xy}), \bar{P}_r^n :$	reconstructed radial power distribution in the node n and averaged value

$\mathcal{Q}_{ss}^{\pm}, \mathcal{Q}_{sc}^{\pm}, \mathcal{Q}_{cs}^{\pm}, \mathcal{Q}_{cc}^{\pm}$:	matrices of the equations for the partial currents in the hexagonal plane in relation to the exponential functions
$\mathcal{Q}^{u\pm}$:	matrices of the equations for the partial currents for one of the directions $u \in x, y, z$ in relation to the exponential functions
Q_i :	energy per fission of a nucleus of isotope i
$Q_g(x, y)$:	total source term (fission and transversal leakage) of energy group g in a node of steady-state diffusion equation of hexagonal plane
$Q'_g(x', y')$:	dimensionless total source term $Q_g(x, y)$ of the dimensionless variables $x' = 2\frac{x}{d}, y' = 2\frac{y}{d}$
$Q_g(u)$:	total source term (fission and transversal leakage) of energy group g in a node of the one-dimensional steady-state diffusion equation for one of the directions $u \in x, y, z$
$Q''_g(u'')$:	dimensionless total source term $Q_g(u)$ for one of the dimensionless coordinates $u'' \in x'', y'', z''$
q_i :	expansion coefficients of the polynomials $h_i(x', y')$ for the sources in the hexagonal plane
q_i^u :	expansion coefficients of the polynomials $h_i(u'')$ for the sources in one of the directions $u'' \in x'', y'', z''$
R :	the ratio of neutron capture rate to total fission rate at the end of power operation
\mathbf{r} :	position vector
\mathbf{r}_{xy} :	radial position vector for flux reconstruction
$\mathbf{r}'_{x,y}$:	vector of position in the dimensionless hexagon
$R_{gg'}^s$:	albedos for incoming partial currents of energy group g depending on outgoing partial currents of energy group g' of the node faces at the outer boundary
$R_{gg'}^{c, tij}$:	albedos for incoming partial currents of energy group g depending on outgoing partial currents of energy group g' of the corners of the hexagonal nodes at the outer boundary of radial direction
\bar{S} :	core averaged external external source
$S_{ext}^n(\mathbf{r})$:	external source of fast neutrons in the node n
$S_g^n(\mathbf{r}, t)$:	neutron source of energy group g in the node n at time t for the time integration over the step Δt

$S_g^n(t)$:	node averaged neutron source of energy group g in the node n at time t for the time integration over the step Δt
$\hat{S}_g(u)$:	fission source of the fast energy group or scattering source of the thermal group in a node of the one-dimensional steady-state diffusion equation for one of the directions $u \in x, y, z$
$S^{(k)}(x', y')$:	expansion of the fission source with the polynomials $h_i(x', y')$ (hexagonal plane) at the iteration step k
$S^{(k)}(u'')$:	expansion of the fission source with the polynomials $h_i(u'')$ for one of the directions $u'' \in x'', y'', z''$ at the iteration step k
$s_i^{(k)}$:	polynomial coefficients of the fission source of the outer iteration step k of radial direction of the hexagonal plane
$s_i^{u(k)}$:	polynomial coefficients of the fission source of the outer iteration step k for any of the directions $u \in x, y, z$
$u' \in x', y'$:	dimensionless co-ordinates in a node of the hexagonal plane $x' = 2\frac{x}{d}$, $y' = 2\frac{y}{d}$
$u'' \in x'', y'', z''$:	dimensionless co-ordinates of one of the three directions in a node $x'' = \frac{x}{a_x}$, $y'' = \frac{y}{a_y}$, $z'' = \frac{z}{a_z}$
V^n :	volume of the node n
V_s, V_c :	matrices of the equations for the outgoing partial currents in the hexagonal plane in relation to the polynomial expansion
V^u :	matrices of the equations for the outgoing partial currents for one of the directions $u \in x, y, z$ in relation to the polynomial expansion
$W_{ss}, W_{sc}, W_{cs}, W_{cc}$:	matrices of the equations for the outgoing partial currents for one of the directions $u \in x, y, z$ in relation to the incoming partial currents
W^u :	matrices of the equations for the outgoing partial currents in the hexagonal plane in relation to the incoming partial currents
v_g^n :	average neutron velocity of the energy group g in the node n
$w^n(t)$:	total decay heat power from power history and the transients
$w_{fp}^n(t)$:	decay heat power from fission products of the four fissile isotopes ^{235}U , ^{238}U , ^{239}Pu and ^{241}Pu
$w_{s,ij}^n(t)$:	decay heat power from fission products group j of the fissile isotope i from power history

$w_{t,ij}^n(t)$:	decay heat power from fission products group j of the fissile isotope i from the transient
$w_{239U}^n(t)$:	decay heat power from neutron capture in ^{239}U
$w_{239Np}^n(t)$:	decay heat power from neutron capture in ^{239}Np
$w_{cap}^n(t)$:	decay heat power from neutron capture by fission products except ^{239}U , ^{239}Np and actinides
$w_{act}^n(t)$:	decay heat power from neutron capture by other actinides

Greek Symbols:

α :	effective fraction of delayed neutrons divided by prompt neutron life time
α_{ij}^d :	fraction of decay heat power originating from decay group j for a fission of the isotope i
$\beta_{g,j}^n$:	yield of precursors of group j from a fission by a neutron of energy group g in the node n
β_g^n :	yield of all precursors from a fission by a neutron of energy group g in the node n
$\beta_{eff,j}$:	core averaged yield of precursors of group j
β_{eff} :	core averaged total yield of precursors
γ_I^n :	fission yield of ^{135}I in the node n
γ_{Pm}^n :	fission yield of ^{149}Pm in the node n
γ_{Xe}^n :	fission yield of ^{135}Xe in the node n
δ_j^n :	auxiliary variable for the time integration of precursors of group j in the node n
ε_g^n :	thermal energy release from a fission initiated by a neutron of energy group g in the node n
$\Phi_g^n(\mathbf{r}, [t])$:	neutron flux of energy group g in the node n
$\Phi_g^{\dagger n}(\mathbf{r})$:	adjoint neutron flux of energy group g in the node n at the steady state
$\bar{\Phi}_g^n([t])$:	average neutron flux of energy group g in the node n
$\bar{\Phi}_g^{n*(k)}$:	average neutron flux of energy group g in the node n in the iteration step k (updated (*))

$\hat{\Phi}_g(x, y, [t]):$	neutron flux of energy group g of a node two-dimensional steady-state diffusion equation in the hexagonal plane
$\Phi_{r,g}^n(x, y, t):$	neutron flux of energy group g of a flux reconstruction in the radial plane
$\hat{\Phi}_g(u, [t]):$	neutron flux of energy group g of a node of the one-dimensional steady-state diffusion equation for one of the directions $u \in x, y, z$
$\bar{\Phi}_{het}^s:$	side averaged neutron flux of any energy group g of the solution of heterogeneous neutron transport problem
$\bar{\Phi}_{hom}^s:$	side averaged neutron flux of any energy group g of the solution of homogeneous neutron transport problem
$\Phi_c(i), \Phi_c:$	reconstructed corner point fluxes of the assembly and the average value
$\Psi_g^n(\mathbf{r}, [t]):$	shape function of the neutron flux of energy group g in the node n
$\lambda_j^n:$	decay constant of precursors group j of delayed neutrons in the node n
$\bar{\lambda}_j:$	node averaged decay constant of precursors group j of delayed neutrons
$\lambda_{ij}^d:$	decay constant of fission product of decay group j from fission of isotope i
$\lambda_I:$	decay constant of ^{135}I to ^{135}X
$\lambda_{Pm}:$	decay constant of ^{149}Pm to ^{149}Sm
$\lambda_{Xe}:$	decay constant of ^{135}Xe to ^{135}Cs
$\Sigma_a^n(t):$	macroscopic removal cross section of the thermal energy group of the isotope i in the node n . It is the sum of capture and fission section of the second energy group: $\Sigma_a = \Sigma_{c,2} + \Sigma_{f,2}$
$\nu\Sigma_{f,g}^n(t):$	total macroscopic fission cross section for neutrons of energy group g in the node n multiplied by the number of fission neutrons ν
$\nu\Sigma_{f,g}^{n*}:$	modified macroscopic fission cross section for neutrons of energy group g in the node n multiplied by the number of fission neutrons ν for flux reconstruction in the radial plane
$\Sigma_{f,g}^n(t):$	total macroscopic fission cross section for neutrons of energy group g in the node n
$\Sigma_{f,g,i}^n(t):$	macroscopic fission cross section of the isotope i for neutrons of energy group g in the node n
$\tilde{\Sigma}_g^n(t):$	modified total macroscopic cross section in the time integration over the time step Δt

$\Sigma_r^n(t)$:	macroscopic removal cross section of the fast energy group of the isotope i in the node n . It is the sum of capture, fission and scattering cross section of the first energy group: $\Sigma_r = \Sigma_{c,1} + \Sigma_{f,1} + \Sigma_s$
$\Sigma_s^n(t)$:	macroscopic scattering cross section of the fast energy group to thermal energy group in the node n
$\Sigma_{c,g}^{n,pois}$:	total macroscopic capture cross section with poisons (energy group g , node n)
Σ_g :	total cross section of the energy group g in a node
Σ'_g, Σ''_g :	dimensionless total cross section of the energy group g in a node by multiplication with $\frac{d}{2}$ or one of the $a \in a_x, a_y, a_z$, respectively
$\rho(t)$:	dynamical reactivity
$\Theta^s(ij)$:	auxiliary constant regarding the ADF
$\Theta^c(i)$:	auxiliary constant regarding the corner point ADF of hexagonal assemblies
λ_U :	the average decay heat of ^{239}U
λ_{Np} :	the average decay heat of ^{239}Np
$\sigma_{Xe,g}^n$:	microscopic absorption cross section of ^{135}Xe of energy group g in the node n
$\sigma_{Sm,g}^n$:	microscopic absorption cross section of ^{149}Sm of energy group g in the node n
Ω^n :	exponent of the exponential transformation in the node n

List of Variables in Thermal Hydraulics

Latin symbols

A, A_{flow}	cross section; flow cross section	
A_n , a_{nm}	coefficients in the mixing model	
C	coefficients in heat transfer correlations	
c_b	boron (acid) concentration	
D	diameter	
D_{heat}	equivalent heated diameter	$D_{heat} = \frac{4 \cdot A_{flow}}{P_{heat}}$
D_{hyd}	equivalent hydraulic diameter	$D_{hyd} = \frac{4 \cdot A_{flow}}{P_{wet}}$
F	form factor	
E	elasticity module	
f	empirical function	
G	mass flow density	
g	gravity acceleration	
H	height; hardness	
h	specific enthalpy	
L	characteristic length; wave length	
\dot{m}	mass flow rate	
P_{heat}	heated perimeter	
P_{wet}	wetted perimeter	
p	pressure	
q“	heat flux	
q““	volume density of heat	
R	radius; friction factor	

r	radius; evaporation heat
S	phase slip ratio
T	temperature
t	time
u	velocity
v	specific volume; velocity
\dot{x}	vapour mass fraction
z	axial co-ordinate

Greek symbols

α	heat transfer coefficient
β	vapour volumetric flow ratio
β_{ij}, γ_i	angles
δ	gap width
ε	deformation, strain
φ	volume void fraction
λ	friction coefficient; heat conductivity
μ	evaporation / condensation rate
ρ	density
ν	kinematic viscosity
η	dynamic viscosity
σ	surface tension; mechanical stress
Θ	mixing scalar; dimensionless temperature
ζ	hydraulic resistance coefficient
Φ	two-phase friction multiplier

Subscripts

<i>f</i>	fluid
<i>v</i>	vapour
<i>sat</i>	saturation
<i>boil</i>	boiling
<i>conv</i>	convective
<i>crit</i>	critical
<i>sub</i>	subcooled
<i>lam</i>	laminar
<i>turb</i>	turbulent
<i>fric</i>	friction
<i>w</i>	wall
<i>cl</i>	cladding
<i>k</i>	coolant channel index
<i>i</i>	mesh index

Superscripts

<i>n</i>	time step index
<i>(k)</i>	iteration index
	thermodynamic parameters π :
π'	saturated liquid
π''	saturated steam

Dimensionless scaling numbers

Re Reynolds number

Nu Nusselt number

Fr Froude number

Ra Rayleigh number

We Weber number